



Ricardo Pinto Enes Martinho

Licenciado em Química Aplicada – *Perfil de Química Orgânica*

Development and application of NMR techniques to study water-in-CO₂ microemulsions

Dissertação para obtenção do Grau de Mestre em
Química Bioorgânica

Orientador: Professor Doutor Eurico José da Silva Cabrita,
Professor Auxiliar, FCT/UNL
Co-orientador: César António Tonicha Laia,
Investigador Assistente, FCT/UNL

Júri:

Presidente: Prof. Doutora Paula Cristina de Sérgio Branco
Arguente: Prof. Doutor Pedro Lúcio Maia Marques de Almeida
Vogal: Prof. Doutor Eurico José da Silva Cabrita



FACULDADE DE
CIÊNCIAS E TECNOLOGIA
UNIVERSIDADE NOVA DE LISBOA

Setembro 2015

Ricardo Pinto Enes Martinho

Licenciado em Química Aplicada – *Perfil de Química Orgânica*

**Development and application of NMR
techniques to study water-in-CO₂
microemulsions**

Dissertação para obtenção do Grau de Mestre em
Química Bioorgânica

Orientador: Professor Doutor Eurico José da Silva Cabrita,
Professor Auxiliar, FCT/UNL
Co-orientador: Doutor César António Tonicha Laia,
Investigador Assistente, FCT/UNL

Development and application of NMR techniques to study water-in-CO₂ microemulsions.

“Copyright”

Ricardo Pinto Enes Martinho

Eu, Ricardo Pinto Enes Martinho, declaro que a Faculdade de Ciências e Tecnologia e a Universidade Nova de Lisboa têm o direito, perpétuo e sem limites geográficos, de arquivar e publicar esta dissertação através de exemplares impressos reproduzidos em papel ou de forma digital, ou por qualquer outro meio conhecido ou que venha a ser inventado, e de a divulgar através de repositórios científicos e de admitir a sua cópia e distribuição com objectivos educacionais ou de investigação, não comerciais, desde que seja dado crédito ao autor e editor.

ACKNOWLEDGEMENTS

São muitas as pessoas que me ajudaram muito durante o tempo deste trabalho, tanto em termos académicos como pessoais. Vou tentar não me esquecer de muitas.

Desde logo quero agradecer ao Prof. Eurico. Nestes dois anos e meio em que tenho sido seu aluno aprendi muito, foi uma experiência exigente mas muito interessante e proveitosa. Obrigado pelo tempo dispensado comigo e pelas oportunidades.

Quero também agradecer ao Dr. César Laia, com quem já trabalho desde o meu segundo ano de licenciatura e com quem aprendi muito. Obrigado pela orientação ao longo destes anos

Não posso também deixar de agradecer à Dra. Marta Corvo, pelo auxílio indispensável com os ensaios de alta pressão, mas também pelas conversas muito úteis sobre o meu trabalho.

E claro, quero agradecer a todos do grupo MSI NMR. Aos postdocs, que sempre estiveram dispostos a ajudar, a Dra. Ana Sofia, o Dr. Ângelo e a Dra. Filipa. E aos meus colegas, que foram uma grande companhia e apoio ao longo deste ano, mesmo que durante algum tempo à distância, à Ana, à Carmen, à Helena, à Inês, ao João, ao Micael, à Sílvia, ao Tiago, e ao Wagner, um muito obrigado!

I was also lucky to have stayed for four months at Georgetown University as a visiting student of Prof. Richard Weiss. I would like to thank you for the time and enthusiasm you dedicated to me. I really learned a lot with this stay, obrigado!

And to my colleagues at the Weiss group: Dr. Ajay, Jingjing, Louis, Maria Victoria, Mike, Mohan, Teresa, Theresa, Trevor and Yan. I wish you all the best, it was a really enriching experience getting to know you and work alongside you.

To my DC family, everyone at the International Student House, you guys were invaluable for me to keep my sanity. Thank you so much for being great people and amazing friends.

Aos meus amigos, muito obrigado pelo carinho, sobretudo quando estava fora. O vosso contributo foi muito importante.

Aos meus pais, e à minha família, muito obrigado, pelo apoio nesta aventura, por estarem sempre presentes quando era necessário, mesmo quando não o estavam fisicamente.

À Patrícia, por em todos estes anos me aturares, por continuares a aturar-me, por estares sempre ao meu lado: muito muito obrigado por tudo!

This work was financed as part of the Marie Curie International Research Staff Exchange Scheme Fellowship within the 7th European Community Framework Programme (Contract grant number: PIRSES-GA-2012-318930 – InTechSE).

The author would like to thank Fundação para a Ciência e Tecnologia (FCT) and Ministério da Educação (UID/Multi/04378/2013CQFB). The NMR spectrometers are part of the National NMR Network (RNRMN) and are funded by FCT (project RECI/BBB-BQB/0230/2012).

RESUMO

A auto-organização (*self-assembly*) é um fenómeno que ocorre frequentemente no universo. Neste trabalho dois sistemas que o fazem foram estudados: a formação de micelas reversa em isooctane e em dióxido de carbono supercrítico (scCO₂), e a formação de géis em solventes orgânicos. O propósito foi o estudo físico-químico destes sistemas e o desenvolvimento de metodologias de RMN para os estudar.

Neste trabalho, AOT é utilizado como uma molécula modelo para estudar extensivamente um sistema vastamente investigado, água/AOT/isooctano com diferentes concentrações de água e para avaliar a agregação em dióxido de carbono supercrítico em diferentes pressões. Para o fazer, uma metodologia de RMN foi desenvolvida, na qual foi possível determinar com exatidão o raio hidrodinâmico da micela (de acordo com as medidas de DLS) utilizando DOSY, a estabilidade micelar e a sua dinâmica. Isto foi essencialmente determinado através de estudos de relaxação de RMN de ¹H, que permitiram determinar tempos de correlação e o tamanho de moléculas de água correlacionadas, que estão de acordo com o tamanho da esfera que interage com a membrana micelar. A encapsulação de carboidratos de diferentes tamanhos permitiu a compreensão da dinâmica e estabilidade dos agregados nestas condições.

Microemulsões de água em CO₂ foram preparadas utilizando AOT e água em dióxido carbono supercrítico, com etanol como cossurfactante. O comportamento dos diferentes componentes do sistema foi avaliado e é provável que acima de 130 bar se tenham obtido microemulsões reversas. A homogeneidade do sistema foi determinada por RMN.

A formação de uma rede de gel através de dois agentes gelificantes moleculares em tolueno-d₈ foi estudado através de DOSY. Uma metodologia empregando One-shot DOSY para adquirir estes espectros foi desenvolvida e aplicada com sucesso. Isto permitiu uma compreensão sobre o papel do solvente e da molécula gelificante no processo de agregação, bem como uma estimativa do tempo de gelificação.

Palavras chave: surfactantes; microemulsões; CO₂ supercrítico; espectroscopia de RMN; géis; LMOGs; carboidratos; agregação.

ABSTRACT

Self-assembly is a phenomenon that occurs frequently throughout the universe. In this work, two *self-assembling* systems were studied: the formation of reverse micelles in isooctane and in supercritical CO₂ (scCO₂), and the formation of gels in organic solvents. The goal was the physicochemical study of these systems and the development of an NMR methodology to study them.

In this work, AOT was used as a model molecule both to comprehensively study a widely researched system water/AOT/isooctane at different water concentrations and to assess its aggregation in supercritical carbon dioxide at different pressures. In order to do so an NMR methodology was devised, in which it was possible to accurately determine hydrodynamic radius of the micelle (in agreement with DLS measurements) using diffusion ordered spectroscopy (DOSY), the micellar stability and its dynamics. This was mostly assessed by ¹H NMR relaxation studies, which allowed to determine correlation times and size of correlating water molecules, which are in agreement with the size of the shell that interacts with the micellar layer. The encapsulation of differently-sized carbohydrates was also studied and allowed to understand the dynamics and stability of the aggregates in such conditions.

A W/CO₂ microemulsion was prepared using AOT and water in scCO₂, with ethanol as cosurfactant. The behaviour of the components of the system at different pressures was assessed and it is likely that above 130 bar reverse microemulsions were achieved. The homogeneity of the system was also determined by NMR.

The formation of the gel network by two small molecular organogelators in toluene-d₈ was studied by DOSY. A methodology using One-shot DOSY to perform the spectra was designed and applied with success. This yielded an understanding about the role of the solvent and gelator in the aggregation process, as an estimation of the time of gelation.

Keywords: surfactants; microemulsions; supercritical CO₂; NMR spectroscopy; gels; LMOGs; carboidratos; agregação.

TABLE OF CONTENTS

ACKNOWLEDGEMENTS	vii
RESUMO.....	ix
ABSTRACT	xi
LIST OF FIGURES.....	xv
LIST OF TABLES	xix
TABLE OF ABBREVIATIONS AND NOMENCLATURE	xxi
1. INTRODUCTION	1
1.1. Supercritical CO ₂ and the solubilization of polar molecules	1
1.1.1. Surfactants and micellar systems.....	3
1.1.2. Characterization of RMs through NMR spectroscopy	7
1.1.3. Applications to NMR spectroscopy.....	10
1.2. Molecular gels.....	11
1.2.1. Structural studies of molecular gels.....	12
1.3. Thesis outline and objectives	14
2. CHARACTERIZATION AND DYNAMICS OF REVERSE MICROEMULSIONS IN ORDINARY AND SUPERCRITICAL SOLVENTS	15
2.1. Development of a NMR methodology to characterize W/O reverse micelles	15
2.1.1. Size determination of RMs	17
2.1.1.1. Dynamic Light Scattering determination.....	17
2.1.1.2. Application of a NMR methodology	19
2.1.1.3. Comparison of methods	21
2.1.2. Dynamics of AOT RMs in isooctane.....	22
2.1.2.1. Stability of AOT W/O microemulsions	24
2.1.2.2. Confined water dynamics	25
2.1.3. Encapsulation of carbohydrate molecules in AOT RMs.....	31
2.2. Application of the NMR methodology to W/CO ₂ microemulsions.....	38
2.2.1. Influence of CO ₂ in AOT aggregation	39
2.2.2. Assessment of W/CO ₂ microemulsions using NMR spectroscopy	41
2.2.2.1. Homogeneity assessment of W/CO ₂ microemulsions	45
2.2.2.2. Diffusion of W/CO ₂ microemulsions	48

2.2.2.3.	Dynamics of RMs in scCO ₂ studied by NMR.....	50
2.3.	Experimental section	52
2.3.1.	Chemicals	52
2.3.2.	Synthetic procedures	52
2.3.3.	Physicochemical studies of W/O microemulsions	53
2.3.3.1.	DLS measurements	54
2.3.3.2.	NMR experiments	54
2.3.4.	Physicochemical studies of W/CO ₂ microemulsions	55
2.3.4.1.	HP fluorescence experiments.....	55
2.3.4.2.	HP NMR experiments	56
3.	NMR STUDIES OF THE PROCESS OF GELATION OF LMOGS	57
3.1.	Proof of concept NMR studies to follow the formation of LMOG-based gels	57
3.2.	Experimental section	62
3.2.1.	Chemicals	62
3.2.2.	NMR experiments	62
4.	CONCLUSIONS AND FUTURE PERSPECTIVES	65
A)	APPENDIX.....	67
5.	REFERENCES	73

LIST OF FIGURES

Fig. 1.1 Phase diagram of carbon dioxide, highlighting its critical point. Image taken from ref 6..	1
Fig. 1.2 i) Dipoles present in water (A) and carbon dioxide (B) molecules. ii) Interactions established between CO ₂ and carbonyl compounds. Adapted from Raveendran et al. ⁸	2
Fig. 1.3 Aggregation model of a water-in-oil reverse micelle. Figure adapted from Kilikian et al. ³²	3
Fig. 1.4 Molecular structure of AOT.	4
Fig. 1.5 Correlation between P_{trans} (Pressure of phase transition, through cloud point measurements) and surface tension at the CMC. Image taken from Eastoe et al. ¹⁸	5
Fig. 1.6 Relation between γ_{CMC} and the surfactant concentration. The point in which the CMC is reached is highlighted. Figure adapted from Czajka et al. ¹⁹	8
Fig. 1.7 Measurements of AOT reverse micelles through several techniques compared with diffusion ordered NMR spectroscopy technique. Figure credits are due to Law et al. ⁶² PGSTE refers to Pulsed-gradient stimulated-echo (DOSY NMR technique); SAXS is Small angle X-Ray scattering; FCS corresponds to Fluorescence correlation spectroscopy.	9
Fig. 1.8 Representation of the relaxation between the R_1 and R_2 relaxation rates and the correlation time. Figure withdrawn from Kowalewski et al. ⁶⁹	10
Fig. 1.9 Molecular weight dependence of correlation time for encapsulated proteins in different nonpolar solvents, and comparison with water. Figure withdrawn from Nucci et al. ⁷³	11
Fig. 1.10 Molecular structure of HSA.	12
Fig. 1.11 HSA fibrillar or ribbonlike aggregates in organic solvents. Image removed from Terech et al. ⁸¹	12
Fig. 1.12 Correlation between the diffusion of gelatin and temperature for both heating and cooling processes. Figure withdrawn from Brand et al. ⁸⁴	13
Fig. 2.1 Water/AOT/isooctane phase diagram. Figure taken from De et al. ⁹³	15
Fig. 2.2 Pictorial representation of the coated model of water droplets dispersed in isooctane. Adapted from Rička et al. ⁹⁴ r_w is the water core radius; δ is the thickness of the the surfactant layer; r_h is the hydrodynamic radius of the droplet. Also displayed are the optical dielectric constants of the surfactant (ϵ_s), oil (ϵ_o) and water (ϵ_w) phases, which correspond to the square of the respective refractive indexes.	15
Fig. 2.3 Assigned ¹ H NMR spectrum of a 0.1M AOT in isooctane with water ($\omega_0=40$)	16
Fig. 2.4 Correlation between r_h and ω_0 determined experimentally by DLS (expt.) and by the coated droplet model (cdm)	19
Fig. 2.5 DOSY plot of AOT RM in isooctane with water, $\omega_0=50$. In the figure, the regions pertaining to the different components is identified.	20
Fig. 2.6 Relation between the hydrodynamic radii measured by DOSY (for the water and the H3 proton in AOT) and the amount of water dispersed in isooctane. Also shown are the hydrodynamic radii determined through equation (2).	21
Fig. 2.7 Relation between the diffusion coefficients measured through DLS and from the water protons with DOSY. Correlation equation (10) is obtained with R^2 of 0.985.	22

Fig. 2.8 Relation between the chemical shift displacements of water (left y axis) and AOT H1 proton (right y axis) and ω_0	23
Fig. 2.9 Plot between the H ₂ O chemical shift and the microviscosity inside the AOT W/O droplets. A linear fitting discarding $\omega_0=20$ was obtained, as depicted, with a $R^2=0.97$ and a slope of -0.187	24
Fig. 2.10 Plot between water diffusion coefficient and time allowed for diffusion in the AOT W/O solution with $\omega_0=50$. The error bars belong to the error of the fitting.	25
Fig. 2.11 Activity of water dependence with the increase of ω_0 . The figure was withdrawn from Luisi et al. ³⁴	26
Fig. 2.12 Plot between T_1 relaxation times for H ₂ O (left y axis) and AOT H3 (right y axis) protons and ω_0 . The error bars result from the error associated with the exponential fitting.	27
Fig. 2.13 Plot between T_2 relaxation times for H ₂ O (left y axis) and AOT H3 (right y axis) protons and ω_0 . The error bars result from the error associated with the exponential fitting.	28
Fig. 2.14 Relation between τ_c (correlation time) of water and AOT H3 protons of W/O AOT reverse micelles and ω_0	29
Fig. 2.15 Relation between a^{rn} (radius of the relaxing nucleus) of water determined by the microviscosity inside the RM for AOT reverse micelles and ω_0	31
Fig. 2.16 Structure of D-(+)-Glucose and intramolecular distances determined from molecular mechanics using Chem3D Pro 14.0. $a=6.864$ Å; $b=5.034$ Å.....	32
Fig. 2.17 ¹ H water suppressed NMR spectrum of D-(+)-Glucose with the respective assignment, highlighting the proton bound to the anomeric carbon and the suppressed water peak.	34
Fig. 2.18 Plots between the chemical shifts of AOT H1' protons, i) and half height line width in $\omega_0=60$ AOT W/O RMs, ii) with the evolution of the molecular weight for each carbohydrate molecule dissolved. In ii) the left y axis refers to H1' and the right y axis refers to An.	34
Fig. 2.19 Diffusion coefficients of different protons in $\omega_0=60$ AOT W/O RMs with three different-sized carbohydrates. This was assessed using a ledbpgps2s pulse sequence. ¹²¹ The error bars belong to the error of the fitting.	35
Fig. 2.20 Relation between the hydrodynamic radii from the water diffusion coefficients in $\omega_0=20$ and $\omega_0=60$ AOT W/O RMs with three different-sized carbohydrates and without solute.....	36
Fig. 2.21 Plot between water diffusion coefficient and time allowed for diffusion in the AOT W/O solution with $\omega_0=60$ and D-(+)-Glucose as a solute, studied by dstebgp3s. The error bars belong to the error of the fitting.	37
Fig. 2.22 Spin-lattice relaxation times of the anomeric protons of three different-sized carbohydrates in $\omega_0=20$ and $\omega_0=60$ AOT W/O RMs.	38
Fig. 2.23 Emission (emi.) and excitation (exc.) spectra at 25° C (i) and at 40° C (ii) of Nile red in water, and aqueous solutions of AOT, 8mM and 30 mM. Excitation spectra were followed at the maximum emission wavelength. Right y axis – spectra in water; left y axis – remaining samples.....	39
Fig. 2.24 Fluorescence spectra of Nile red in aqueous 30 mM AOT solutions with increasing pressure.....	40
Fig. 2.25 Variation of the intensity of emission of an aqueous AOT nile red solution with an increase in pressure.	40

Fig. 2.26 ¹ H NMR spectrum of AOT, H ₂ O and ethanol in scCO ₂ (T=40.0° C and P=142.0 bar) with the assignment of the components.	42
Fig. 2.27 ¹ H, ¹ H-NOESY spectrum of the AOT mixture in scCO ₂ (T=40.0° C; P=118.6 bar). The cross relaxation line of the ethanol methylene peak is highlighted.	42
Fig. 2.28 1D projection (extracted from Fig. 2.27) of the NOE spectrum excited at the methylene peak of ethanol.	43
Fig. 2.29 Relation between half-height linewidth (i), chemical shift displacement, using the lowest pressure point as a zero (ii) and the pressure of the system bearing AOT and water, at 40.0° C. The methyl group of ethanol was used as a chemical shift reference and is therefore not depicted. In ii) the right y axis corresponds to AOT, whereas the left y axis corresponds to the remainder nuclei.	44
Fig. 2.30 Schematic representation of the NMR slice selection procedure.	46
Fig. 2.31 ¹ H (i) and ¹³ C, displaying only the CO ₂ signal (ii) slice selective spectra for a solution of AOT with ethanol and water in 93.7 bar of CO ₂ at 40.0° C.	46
Fig. 2.32 ¹ H (i) and ¹³ C, displaying only the CO ₂ signal (ii) slice selective spectra for a solution of AOT with ethanol and water in 151.7 bar of CO ₂ at 40.0° C.	47
Fig. 2.33 Plot between diffusion coefficients of the components in the AOT, ethanol, water in scCO ₂ mixture, at 40.0° C. The error bars belong to the error of the fitting.	48
Fig. 2.34 Relation between the spin-lattice relaxation time of the mixture components at 40° C and different pressures. The right y axis is the AOT scale, whereas the left one is used for the remainder of the protons. The error bars belong to the error of the fitting.	50
Fig. 2.35 ¹ H NMR spectrum of a saturated D-(+)-Glucose solution in a solution of AOT, ethanol and water dispersed in supercritical carbon dioxide at 141.4 bar at 40.0 °C.	51
Fig. 3.1 Chemical structure of Ni(DODA) ₂	57
Fig. 3.2 ¹ H NMR spectrum of Ni(DODA) ₂ in toluene-d ₈ , 5.0 wt%.	58
Fig. 3.3 ¹ H DOSY spectra of Ni(DODA) ₂ (5.0 wt% in toluene-d ₈). t=48 min (i); Center: t=78 min (ii); Right: t=infinite (iii).	58
Fig. 3.4 Representation of the diffusion coefficient of Ni(DODA) ₂ (5 wt% in toluene-d ₈) over time. The error bars belong to the error of the fitting.	59
Fig. 3.5 Representation of ratio between the diffusion coefficients of Ni(DODA) ₂ (5 wt%) and toluene-d ₈ over time. The error bars belong to the error of the fittings on this ratio.	59
Fig. 3.6 Diffusion coefficients plotted over time for HSA, 2.0 wt% in toluene-d ₈ . The error bars belong to the error of the fitting.	60
Fig. 3.7 DOSY spectra of HSA (1 wt% in toluene-d ₈). t=5 minutes and 35 seconds (i); t=54 minutes and 20 seconds (ii).	61
Fig. 3.8 Diffusion coefficients plotted over time for HSA, 1.0 wt%, in toluene-d ₈ . The error bars belong to the error of the fitting.	61
Fig. 3.9 Representation of ratio between the diffusion coefficients of HSA (1.0 wt%) and toluene-d ₈ over time. The error bars belong to the error of the fittings on this ratio.	61
Fig. A.1 ¹ H NMR spectrum of isooctane in CDCl ₃	67

Fig. A.2 Relation between a (radius of the relaxing nucleus) of water protons of W/O AOT reverse micelles and ω_0 68

Fig. A.3 Plot between microviscosity and ω_0 in AOT W/O RMs with data from Rafiq et al,¹⁰⁷ which was fitted to obtain (24) with $R^2=0.991$ 68

Fig. A.4 Molecular mechanics structure of D-(+)-Glucose obtained using Chem3D Pro 14.0..... 69

Fig. A.5 Molecular mechanics structure of D-(+)-Cellobiose obtained using Chem3D Pro 14.0.. 69

Fig. A.6 Molecular mechanics structure of D-(+)-Cellotriose obtained using Chem3D Pro 14.0.. 70

Fig. A.7 Structure of D-(+)-Cellobiose and intramolecular distances determined from molecular mechanics using Chem3D Pro 14.0. $a=10.278$ Å; $b=10.385$ Å..... 70

Fig. A.8 Structure of D-(+)-Cellotriose and intramolecular distances determined from molecular mechanics using Chem3D Pro 14.0. $a=14.581$ Å; $b=13.738$ Å..... 70

Fig. A.9 Diffusion coefficients of water in carbon dioxide at 35° C at different pressures. Data extracted from Xu et al.¹⁴³ The equation for the trendline of the exponential fitting is (25) and was obtained with a $R^2=0.98$ 71

Fig. A.10 Solvent suppressed ¹H NMR spectrum of saturated D-(+)-Glucose diluted in a D₂O volume similar to the one in the HP tube..... 72

LIST OF TABLES

<i>Table 1.1 Data for surfactants developed for scCO₂. All data were obtained at the water-air interface Data attained at; a) 35° C. b) 25° C. c) 24° C.</i>	6
<i>Table 2.1 Properties for the components of water/AOT/isooctane ternary mixtures. δ is the thickness of the surfactant layer; v_w is the volume of water; v_s is the volume of AOT; n are the refractive indices of the respective molecules; η corresponds to viscosity.</i>	16
<i>Table 2.2 DLS determined sizes of water droplets at different ω_0. Experimental (expt.) r_h and polydispersity indexes (ρ) are presented. The coated droplet model (cdm) r_h is also determined and the diffusion coefficient (D) of the droplets is inferred from it. The error for the DLS measurement was determined by the standard deviation of the several measurements conducted. The diffusion coefficient was determined by using (3), employing the viscosity of isooctane present in Table 2.1.</i>	18
<i>Table 2.3 Diffusion coefficients (D) and hydrodynamic radii (r_h) taken from DOSY data for the H₂O and AOT H3 protons. The r_h was determined using (3) and the viscosity in Table 2.1.</i>	20
<i>Table 2.4 Data obtained from chemical shift measurements of different protons in the solutions.</i>	22
<i>Table 2.5 Relaxation times (spin-lattice and spin-spin) for the W/O AOT RM solutions.</i>	27
<i>Table 2.6 NMR relaxation determined correlation times and sizes (a) of the aggregates responsible for the relaxation for AOT W/O RM solutions. The sizes were obtained from the viscosity of isooctane present in Table 2.1 (a^η) and for water it was also attempted to use the microviscosity defined previously to determine the size (a^{η}).</i>	30
<i>Table 2.7 Summary of the maximum distances (r_{max}) measured through MM for the carbohydrates used in this study and the respective molecular weights (MW).</i>	32
<i>Table 2.8 Data obtained from water suppressed ¹H spectra: chemical shifts ($\Delta\delta$) and half-height line width ($v_{1/2}$) for solutions of carbohydrates in AOT W/O RMs.</i>	33
<i>Table 2.9 Data obtained from the relaxation and diffusion ordered NMR spectroscopy studies for solutions of carbohydrates in AOT W/O RMs. T₁ was assessed by t1iresgp; T₂ was assessed by presaturated CPMG for $\omega_0=60$ and CPMG for $\omega_0=20$; DOSY was acquired with ledbpgpes2s for $\omega_0=60$ and with dstebpgp3s for $\omega_0=20$. Diffusion coefficients (D) is displayed in m² s⁻¹.</i>	35
<i>Table 2.10 Diffusional data for water in carbohydrate solutions in AOT W/O RMs. This was obtained using a dstebgp3s pulse sequence to determine the hydrodynamic radius, employing the viscosity described in Table 2.1.</i>	36
<i>Table 2.11 λ_{max} for the emission of the different samples with [NR] = 2X10⁻⁶ M in study at 25° C and 40° C.</i>	40
<i>Table 2.12 Density and viscosity data for the different CO₂ pressures at 313.15 K used during this work. Mass of carbon dioxide determined from the Peng-Robinson equation.¹³³ Remaining information determined using NIST online tool.¹³⁴</i>	41
<i>Table 2.13 Observables (obs) taken from 1D ¹H NMR spectra for the AOT mixture in scCO₂, at 40° C at different pressures. The methyl group of ethanol has a constant chemical shift displacement because it was used as a reference.</i>	43

Table 2.14 Diffusional data obtained from W/CO ₂ microemulsions at different pressures of carbon dioxide. The diffusion coefficient of ethanol is the average between the diffusion coefficients of its methyl and methylene proton peaks and the error corresponds to its standard deviation.	48
Table 2.15 Spin-lattice relaxation data for the mixture of AOT, H ₂ O and ethanol in scCO ₂ at 40° C and at different pressures.	50
Table 2.16 Experimental amounts of the solution of AOT in isooctane and water added to prepare the different solutions used in this study.	53
Table A.1 Variation of microviscosity ($\mu\eta$) with ω_0 for AOT W/O RMs, taken from Rafiq et al ¹⁰⁷ and (24).	69
Table A.2 ¹ H NMR chemical shift, line width and relaxation data summary obtained for a D-(+)-Glucose 50mM solution in D ₂ O. An is the proton adjacent to the anomeric carbon in the sugar molecule.	71

TABLE OF ABBREVIATIONS AND NOMENCLATURE

Acronym	Meaning
1D	1 dimensional
2D	2 dimensional
AcN	Acetonitrile
AOT	Sodium 1,4-bis(2-ethylhexyl) sulfosuccinate
approx.	Approximately
cdm	Coated droplet model
CMC	Critical micelle concentration
CP-MAS	Cross Polarization Magic Angle Spinning
CPMG	Carr-Purcell-Meiboom-Gill
<i>D</i>	Diffusion coefficient
<i>d</i>	Doublet (NMR spectra)
DLS	Dynamic Light Scattering
DOSY	Diffusion ordered spectroscopy
EOR	Enhanced oil recovery
EtOH	Ethanol
expt.	Experimental
g	Grams
G	Gauss
HP	High pressure
HSA	(R)-12-hydroxystearic acid
Hz	Hertz
K	Kelvin
<i>k_B</i>	Boltzmann constant
Lit.	Literature
LMOG	Low molecular-mass organogelators
m	Meter
m	Multiplet (NMR spectra)
M	Molar
mmol	Milimol
ms	milisecond
MW	Molecular weight
ND	Not determined
Ni(DODA) ₂	Nickel di(9,10-dioxooctadecanoate)
NMR	Nuclear Magnetic Resonance
NOE	Nuclear Overhauser Effect
NOESY	Nuclear Overhauser Effect Spectroscopy

° C	Degree Celsius
PFG	Pulsed field gradient
p-TSA	p-toluenesulfonic acid
Ref.	Reference
r_h	Hydrodynamic radius
RM	Reverse micelle
s	Second
s	Singlet (NMR spectra)
SANS	Small Angle Neutron Scattering
scCO ₂	Supercritical carbon dioxide
SCF	Supercritical fluid
t	Time
T	Tesla
T_1	Spin-lattice relaxation
T_2	Spin-spin relaxation
T_g	Temperature of gelation
TLC	Thin layer chromatography
TMS	Tetramethylsilane
W/CO ₂	Water-in-carbon dioxide
W/O	Water-in-oil
wt%	Weight percent

*There is nothing that nuclear spins will not do for you,
as long as you treat them as human beings*

Erwin Hahn, 1949

1. INTRODUCTION

Over the course of this thesis, two main themes will be approached, both related to the formation of supramolecular aggregates from small molecular amphiphiles. The main subject is the development and characterization of reverse micelles in scCO₂. This is done through NMR and spectrophotometric techniques. The second one is the development of a novel NMR methodology for the characterization of the dynamics of formation of organogels formed by low molecular-mass organogelators (LMOGs). In this introduction, I will explore the state of the art for these two subjects and devise an outline for the whole thesis.

1.1. Supercritical CO₂ and the solubilization of polar molecules

Carbon dioxide is an abundant atmospheric gas (approximately 400 ppm¹) that results from several natural and man caused activities, ranging from respiration to combustion. It is considered a greenhouse gas and its concentration has been steadily growing for several decades.¹ Hence the reduction of its presence in the atmosphere is a major goal worldwide. Research and development using this molecule have been of major relevance ranging from methodologies for its capture², to the employment of this as a substrate for chemical synthesis³ or as an industrial solvent.⁴ This might be done by compressing CO₂ into a liquid or a supercritical fluid. I will focus on the latter, which is obtained at temperatures and pressures above its critical point: 30.97° C and 73.74 bar (CO₂ phase diagram is presented in Fig. 1.1).⁵

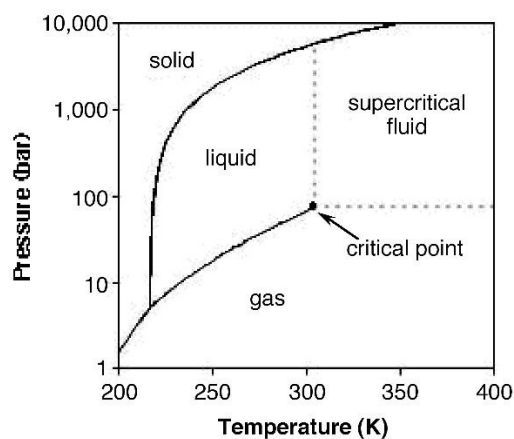


Fig. 1.1 Phase diagram of carbon dioxide, highlighting its critical point. Image taken from ref 6.

scCO₂ is considered a green solvent, while comparing it to ordinary organic solvents^a, due to being nontoxic. It also possesses the advantage of being obtained at mild temperature conditions, which are biologically compatible, thus making it promising for bioengineering or preparation of pharmaceutically active compounds or formulations.⁷ It is simple to control its properties by altering the pressure and/or

^a When in this thesis ordinary, regular or normal solvents are mentioned, these refer to common organic solvents, such as n-hexane, dichloromethane or pyridine. These terms are used in opposition to supercritical fluids.

the temperature of the system, which makes it a solvent tuneable for a wide range applications. Due to being in a physical state between liquid and gas it has low viscosity while also having liquid-like solvent densities.⁸

Turning now to carbon dioxide as a molecule, one can easily understand it has a zero dipole moment.⁸ This is due to the fact that it has two dipoles that cancel each other out, having though an overall quadrupolar moment (Fig. 1.2 i) (A)). It also has a low dielectric constant, being approx. 1.0, varying with density.⁹ All of these considerations would let us to guess that, as a solvent, CO₂ would behave as an alkane-like liquid. However, hydrocarbon molecules are not highly soluble in scCO₂.^{10,11} Indeed, the described CO₂-philic molecules range from fluorocarbons (the main CO₂-philic¹¹) to carbonyl containing molecules,¹² but also others such as amines,¹³ poly- or oligoethylene oxides,¹⁴ or sugar acetates.¹⁵ scCO₂ is considered a nondipolar solvent and its properties actually make it resemble with solvents such as benzene or hexafluorobenzene, also quadrupolar molecules.¹⁶ In fact, its net dipole moment is zero, however it is a charge separated molecule bearing several nonzero dipole moments.⁸ In a microscopic level, this allows CO₂ to have mainly quadrupolar dipolar solvent-solute specific interactions, having the ability to act as a weak Lewis acid or as a Lewis base.⁸ It can establish hydrogen bonding interactions, which account, per example, for its strong interactions with carbonyl groups¹², but also for its reasonably high solubility (while comparing to carbon monoxide⁸) in water (Fig. 1.2 ii).¹⁷ One example that shows how CO₂ behaves alike a polar molecule is its strong solubility of fluorinated compounds. Even though there is not a consensus on why this happens, it has been shown that CO₂ interacts more strongly with more polar fluorinated molecules, rather than with those with lower or no polarity.¹⁰

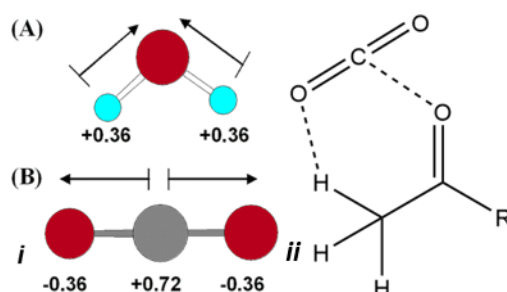


Fig. 1.2 i) Dipoles present in water (A) and carbon dioxide (B) molecules. ii) Interactions established between CO₂ and carbonyl compounds. Adapted from Raveendran et al.⁸

Despite being considered as a polar molecule, the solubility of water in CO₂ is low (approx. 0.14% at 15° C and 450 bar¹⁸), and to take advantage of the properties of this solvent with polar molecules strategies have been devised for it to solubilize water. Even though molecular interactions (demonstrated through the difference in dipole moments in Fig. 1.2 i)) may account for a part of this behaviour, surface tension (γ) plays a significant role. This is a property that arises from the fact that at the liquid-air interface, the last layer of molecules do not have more neighbours and due to that are attracted to the bulk. This results in an energy imbalance at the surface relative to the bulk, which is surface free energy.¹⁹ Liquids organize themselves to have the minimum exposure to the surface thus minimizing this interaction. Water has a particularly high surface tension (71.99 mN m⁻¹ at 25° C²⁰), which is an issue for it to solubilize in CO₂.¹⁹ To solve these issues a self-assembling species may be

added to the mixture, in order to form a microemulsion (these are usually tensioactive molecules that adsorb to the interface and result in a reduction of the surface tension¹⁹), usually a reverse micelle.¹⁸ This might be done employing amphiphilic polymers^{21–23} or surfactants (these might be single^{24,25}, di-^{25,26} or tri-chain²⁵ surfactants or even dendritic surfactants²⁷). It is also worth to add that such microemulsions might be formed in surfactant free conditions, either adding acetone²⁸ or functionalized bi-wetting particles.²⁹ In this work, the main focus will be on surfactant formed reverse microemulsions and this will be further discussed in 1.1.1.

1.1.1. Surfactants and micellar systems

When two solvents are put together they can mix into a homogeneous phase if these are mutually soluble. If immiscible, the two liquids can form two phases or they might form an emulsion, depending on the phase volumes.³⁰ An emulsion is a colloidal system in which droplets are dispersed in a liquid.³¹ These might be classified according to composition, and the simplest ones rely on the existence of an oil and an aqueous phase. Depending on which is dispersed in the other these might be oil-in water or water-in-oil emulsions. In this work, we will focus on the latter. In order to form these droplets there is an increase in interfacial tension, hence work is needed to form an emulsion. The amount will depend on the characteristics of each system however, this might be dropped by the addition of an emulsifying agent that will adsorb to the surface and lower the energy of formation and stable droplets are more easily formed.³⁰ As it was already introduced in 1.1, these substances are tensioactive and are known as surfactants. While these might be useful for several applications ranging from detergents to inks, passing by enhanced oil recovery, in this work we will focus on their role as de-emulsifiers.³⁰ Indeed, while added to water dispersed in oil phase, these avoid the formation of a nonhomogeneous phase and yield microemulsions, which are thermodynamically stable, forming small droplets (usually up to 10 nm radius) that usually are spontaneously formed. The structures formed are commonly reverse micelles (as depicted in Fig. 1.3), monolayer aggregates that are commonly monodisperse in these conditions.³⁰

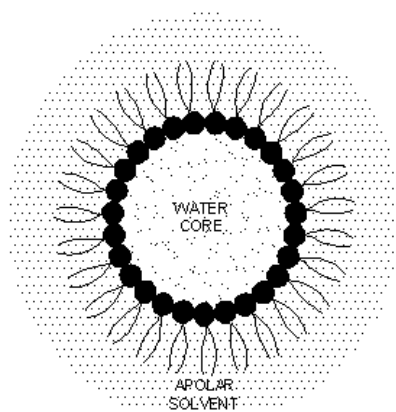


Fig. 1.3 Aggregation model of a water-in-oil reverse micelle. Figure adapted from Kilikian et al.³²

It is characteristic of surface active molecules to be amphiphilic, having a polar *head* and a nonpolar *tail*. These structures can yield an array of aggregates, i.e. bicelles, which are bilayer assemblies or

micelles, which are monolayer assemblies. Structure-wise hydrophilic and lyophilic (here named reverse) micelles are alike. However, as shown in Fig. 1.3, reverse micelles have the polar *heads* turned inside, towards the water pool. Surfactants that may allow these type of aggregates can be either ionic (such as AOT) or non-ionic (i.e. Span or Tween).³³ These have been widely studied and several concepts around it are fairly well known.

Critical micelle concentration (CMC= is the minimum concentration in which the aggregates are obtained, although its value is not easily attainable due to the nature of the mixture.³³ Although, it is noted that the CMC may depend on the amount of water present in the system (ω_0). It is considered that the concentration might range between 10^{-5} and 10^{-2} M.³³ The shape of reverse micelles is usually considered as spherical, due to steric interactions, though in oil phases it is described that ellipsoid shapes, among others can also easily occur.³³ This also may depend on the counterion, when considering ionic surfactants, the size and interactions may have an important role on the aggregation process. One shall also describe the system employing a ratio between the concentrations of water and surfactant (ω_0):

$$\omega_0 = \frac{[H_2O]}{[Surfactant]} \quad (1)$$

This allows to understand the amount of water dispersed in the oil phase and furthermore will relate to some properties of the micelles, mainly its size. This is well documented for AOT (the main molecule studied throughout this thesis, which is depicted in Fig. 1.4), that has a linear relation between its hydrodynamic radius (r_h) and ω_0 (shown in (2) in Å).³⁴

$$r_h = 15 + 1.75\omega_0 \quad (2)$$

Through AOT reverse micelles it is possible to achieve $\omega_0=60$,³⁵ which, applying (2) corresponds to a hydrodynamic radius of 12.0 nm. This allows to encapsulate reasonably large molecules, such as biopolymers like proteins. This has been a relevant application for these reverse micelles.³⁴

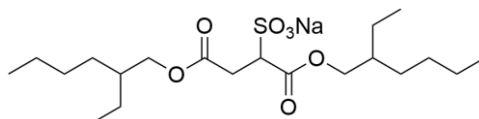


Fig. 1.4 Molecular structure of AOT.

Even though colloid scientists have already properly described the properties of W/O microemulsions, the case when the oil phase is a supercritical fluid gains further complexity. It is necessary to lower the surface tension of water, which is the same valid for the regular microemulsions however, it is also necessary that surfactant is soluble in scCO₂. This is a difficulty because, as it has been stated earlier on, hydrocarbons do not have high solubility in CO₂, and most surfactants have hydrocarbon *tails*. Let us take the case of AOT. This surfactant has been shown to be able to form stable reverse micelles in supercritical alkanes.³⁶ Despite that, it shows no solubility in scCO₂.³⁷ To be able to

achieve reverse micelles of AOT it is necessary to add a co-surfactants, such as ethanol or propanol.^{38–40} And the aggregation of AOT in isooctane is also influenced by the addition of carbon dioxide, which results in the reduction of its CMC.⁴¹ Hence, AOT certainly has some characteristics that allow it to interact with CO₂ and researchers have found that a while ago.⁴² Some of those derivatives are presented in Table 1.1 with the data for its surface tension at the water-air interface. This has been described as a good reporter for the CO₂-*philicity* of tensioactives, as represented in Fig. 1.5.¹⁸ Furthermore this figure demonstrates that more highly fluorinated molecules are more soluble in CO₂. This, as mentioned before in this introduction, has been a subject of major discussion. In Table 1.1 it is possible to confirm precisely that fluorocarbon surfactants are clearly better than hydrocarbon ones, looking at entries 1, 2 and 3, which are among the best surfactants for CO₂ described in the literature. This, as entry 2 demonstrates, is not only valid for AOT derivatives. In this case this is a fluorinated sugar derivative. Sugar molecules can also be a template for other surfactant development endeavours such as Cássio *et al.*⁴³ suggested. Also, if a fluorocarbon phosphate is employed, instead of a sulfonate molecule, good scCO₂ solubility may also be achieved.⁴⁴

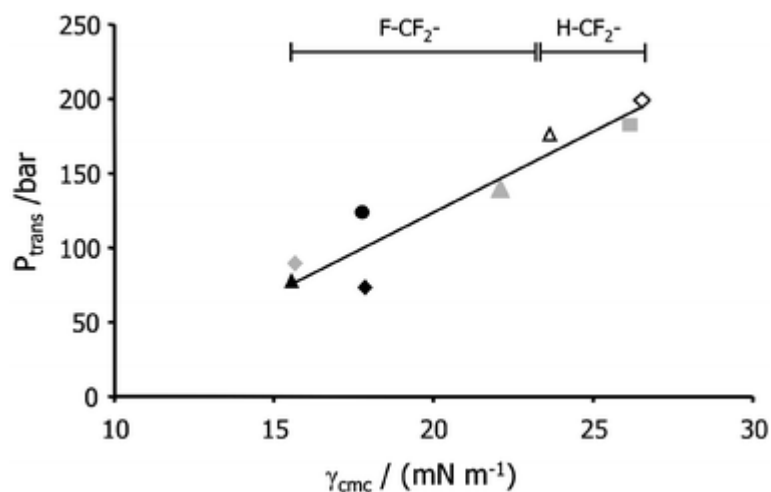
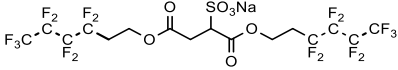
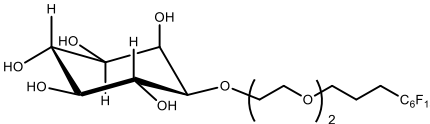
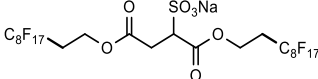
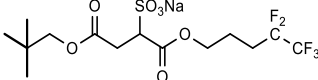
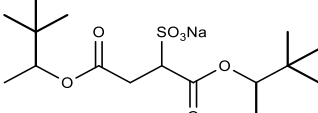
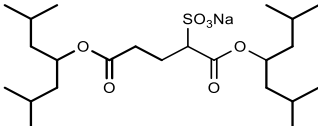
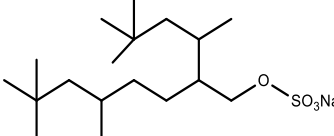
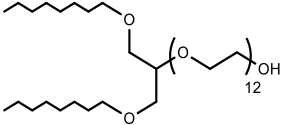
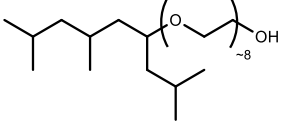
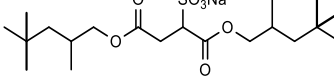
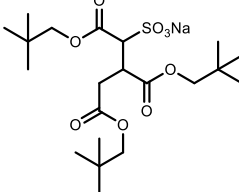
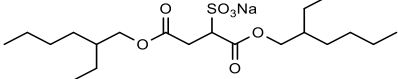


Fig. 1.5 Correlation between P_{trans} (Pressure of phase transition, through cloud point measurements) and surface tension at the CMC. Image taken from Eastoe *et al.*¹⁸

Using fluorinated surfactants instead of hydrocarbon ones is both more expensive, which make them industrially less desirable, and health hazardous. Therefore several researchers, mostly the groups of Eastoe and Sagisaka, have tried to reach CO₂-*philic* hydrocarbon surfactants. The strategy is to get close to the surface tension of hexane, which is 17.89 mN m⁻¹ at 25° C.²⁰ Hexane has such a low (comparing to other solvents) surface tension due to the close packing of its alkyl chains. Hence, using AOT as a template is interesting because it allows for the molecule to have two chains reasonably close to each other. However, AOT itself does not allow for tight packing, hence researchers have started to use more highly branched derivatives, such as entries 5, 6 or 10 in Table 1.1. Branching has been shown to enhance *tail* solvation, and to significantly increase the adsorption of the surfactant to the surface, hence minimizing the interactions between the two phases.⁴⁵ Nevertheless, the effect is not linear, there must be a reasonable amount of branching, neither too high nor too low, since it influences the surfactant area and how the chains interact between each other.⁴⁶ Earlier on, it was mentioned that

Table 1.1 Data for surfactants developed for scCO₂. All data were obtained at the water-air interface Data attained at; a) 35° C. b) 25° C. c) 24° C.

Entry	Surfactant	γ_{cmc} (mN m ⁻¹)	CMC (M)	Ref.
1		17	4.3x10 ⁻⁴	47 a)
2		17.4	3.9x10 ⁻⁴	48 b)
3		20	2.7x10 ⁻⁴	49 a)
4		22.5	4.7x10 ⁻²	26 b)
5		23.8	1.62x10 ⁻²	46 a)
6		24.0	6.31x10 ⁻⁴	46 a)
7		25	1.5x10 ⁻³	24 a)
8		25.6	1.7x10 ⁻⁴	50 c)
9		26	8.8x10 ⁻⁴	49 a)
10		27	-	42
11		27.0	2.2x10 ⁻²	25 b)
12		30.8;31.8	2.5x10 ⁻³	25 b)

carbonyl functional groups interact favourably with CO₂, these are indeed found in the sulfosuccinate moieties of AOT derivatives, but it has been already attempted to insert these in the side chain, as it is the case of AOK.⁵¹ This approach has shown also to be a promising one towards the design of surfactants. To even improve this effort, it has been attempted to combine alkyl and fluorinated chains (one in each ester group of the sulfosuccinate moiety), to obtain *hybrid* surfactants.^{52,53} This has shown to be successful, as entry 4 demonstrates. This molecule is highly CO₂-*philic*, having only 5 fluorine atoms. This is a compromise between fluorine content, CO₂ solubility and water incorporation, which has been approximately reached. Despite the progress made, research is still far from the goal to reach the surface tension of hexane. Other goals can be found if one looks at the surface tensions of different organic solvents. One of those is diethyl ether ($\gamma=16.65$ mN m⁻¹ at 25° C²⁰) that has a lower surface tension than even water with fluorocarbon surfactants. Indeed, researchers have been using from earlier on surfactants bearing oxyethylene moieties, which are ethers and might also help lowering the surface tension.⁵⁴ Entries 2, 8 and 9 have this moiety and prove to be good efforts. This approach has not been fully explored though. One other solvent that has a low surface tension is trimethylamine ($\gamma=13.41$ mN m⁻¹ at 25° C²⁰). The fact that it is an amine is also interesting in the CO₂ context, since amines (mostly primary and secondary ones) react with CO₂ to yield carbamates. Smith *et al.*¹³ have described several tertiary amine esters that lower the surface tension of CO₂-in-water microemulsion, but are not so suitable for water-in-CO₂ reverse micelles, due to electrostatic repulsion

The understanding of how surfactants work at the carbon dioxide interface is crucial for the design of novel effective surfactants. Molecular dynamics studies have been done to compare two phosphate surfactant analogues, one fluorinated and the other having an alkyl chain instead.⁵⁵ These hinted that the hydrocarbon amphiphile has a higher penetration of both water and CO₂ in the surfactant layer relative to the fluorocarbon one. This will result in a higher surface tension thus having the opposite effect of what is desired. Although this goes to show that more favourable interactions with fluorine atoms are not directly responsible for its higher solubility and hydrocarbon surfactants that have a lower penetration in the micellar layer, perhaps through branching as suggested, will be more CO₂-*philic*.

1.1.2. Characterization of RMs through NMR spectroscopy

In order to understand if stable water pools are obtained, as the properties and spatial organizations of these, it is necessary to employ different characterization techniques. In general, to analyse microemulsions in the scCO₂ phase is not much different from what is done in regular oil phase reverse micelles. The major difference is that it has to be conducted in a high pressure apparatus. One measurement that allows to understand whether or not a stable microemulsion is formed is the observation of the cloud point, the maximum pressure (or temperature) at which a visible emulsion is observed. This can be aided by spectrophotometric techniques. One thing that can also be easily done is to put into the mixture a water soluble dye that will only show either absorption or emission if incorporated in a reverse micelle.⁵⁶ Light scattering techniques are commonly employed to characterize the dynamics of reverse micelles, since these disperse light.³⁰ In the case of DLS, it is possible to obtain the autocorrelation function from the dispersion of light over time. Assuming Brownian motion of molecules, it is possible to obtain the diffusion coefficient of the particles and therein the hydrodynamic

radius of the micelle (through the Stokes-Einstein equation, (3), in which k_b is the Boltzmann constant, T , the temperature, η is the viscosity of the medium and r_h is the hydrodynamic radius of the diffusing species).

$$D = \frac{k_b T}{6\pi\eta r_h} \quad (3)$$

Although this is a common procedure for characterizing reverse micelles in organic solvents, it has only recently been adapted to W/CO₂ microemulsions.⁵⁶ In this study, this technique was used as a size-controlling aid, which is a matter of relevance for applications.

Many techniques can be employed to determine whether or not an aggregate is obtained. Tensiometric measurements are extremely powerful, because these allow to determine the CMC, since a plateau is reached from the CMC on to higher concentrations (Fig. 1.6). As it was discussed earlier on, surface tension at the water-air interface is a relevant indicator of CO₂-philicity, however interfacial tension in scCO₂ can also be measured and is an indicator of the stability of the mixture.⁵⁷

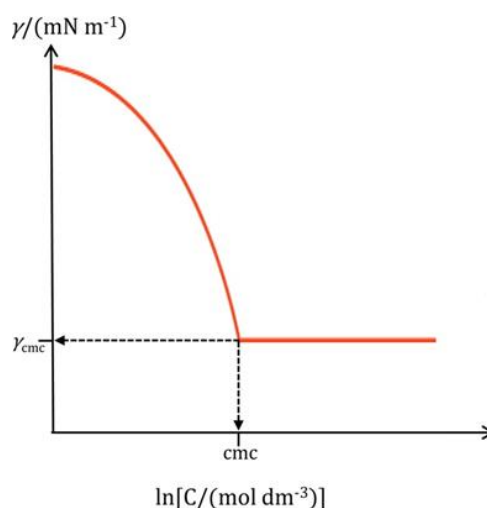


Fig. 1.6 Relation between γ_{CMC} and the surfactant concentration. The point in which the CMC is reached is highlighted. Figure adapted from Czajka et al.¹⁹

The techniques previously described are useful to assess the existence of aggregates, but not so much the dynamics and structure of the networks formed (on the exception of DLS). For that one can use other spectrophotometric approaches, such as fluorescence anisotropy or vibrational spectroscopy (IR and Raman spectroscopies).⁵⁸ Other than that, SANS is probably the most efficient reporter of size, and dynamics of the aggregates in scCO₂, from which it is possible to obtain the scattering from the different components of the mixture and thus assessing its shape and stability.²² Nevertheless, in this work the focus will be directed towards NMR spectroscopy. NMR is a widely used technique to determine structure and dynamics from the behaviour of nuclear spins. NMR can be used in both atmospheric and high pressure conditions, indeed it has been widely used to characterize different systems in supercritical CO₂.⁵⁹

The characterization of reverse micellar behaviour through solution state NMR has been significantly exploited and different observables are taken into account. First of all, some information about aggregation may be withdrawn from simple one-dimensional spectra observables, such as chemical shift and line width. Getting from a state of free dissolved molecules to aggregates, a change in both of these is expected. The chemical shift is not only affected by the intramolecular environment but also by its surroundings. Stahla *et al.*⁶⁰ have shown that for the case of reverse micelles of AOT having different counterions, the chemical shifts are different, as is the line broadening. Chemical shift can even be used to estimate the size of the water droplets in W/O AOT reverse micelles.⁶¹ There is though a more efficient way to perform this through NMR spectroscopy. Alike what is done through DLS, the diffusion coefficient can be measured through diffusion ordered spectroscopy (DOSY). This is done by the measurement of the signal attenuation in a gradient stimulated spin echo. By obtaining the diffusion coefficient, D , it is possible, through (3), to obtain the hydrodynamic radius. This has already been described for W/O AOT reverse micelles and it shows a good relation with data obtained from other techniques, even though there is a size overestimation (Fig. 1.7).⁶²

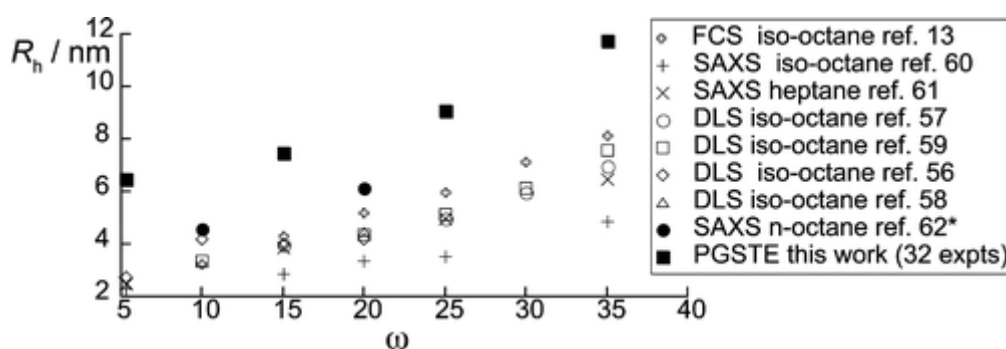


Fig. 1.7 Measurements of AOT reverse micelles through several techniques compared with diffusion ordered NMR spectroscopy technique. Figure credits are due to Law *et al.*⁶² PGSTE refers to Pulsed-gradient stimulated-echo (DOSY NMR technique); SAXS is Small angle X-Ray scattering; FCS corresponds to Fluorescence correlation spectroscopy.

DOSY is a way of studying translational motions that occur in the ms to s timescale. However, it is also possible to study through NMR quicker rotational motions (sensitive to motions of ns or ps) through spin-lattice (or longitudinal, T_1) or spin-spin (or transverse, T_2) relaxation measurements. The dynamics of water entrapped in AOT-based RMs has already been studied through these techniques and it was possible to conclude that water is confined in small water pools.⁶³ These techniques have also been employed to observe the phenomenon of percolation and different properties associated to it.⁶⁴

These techniques are powerful and have already been applied to study W/CO₂ aggregates. The acquisition of DOSY and relaxation spectra throughout different pressures allowed to assess the water droplet size evolution or the specific motions existent in a certain surfactant.^{22,65,66} Thurecht *et al.*⁶⁶ were able to achieve significant site-specific differences in relaxation spectra, which was a way to observed the kinetics of self-assembling. Rotating frame imaging has also been done for a system alike the ones described and it gave rise to observe the uniform dispersion of a salt throughout the sample, which indicates homogeneity.⁶⁷ Fremgen *et al.*⁶⁷ have also conducted NOE studies to assess specific

interactions. More recently, ¹²⁹Xe NMR has been applied to a W/CO₂ microemulsion. This nucleus is highly sensitive to the change in molecular environment and just by measuring its chemical shifts it was possible to witness aggregation occurring.⁶⁸

1.1.3. Applications to NMR spectroscopy

Setting aside characterization, reverse micelles can also be useful media for NMR studies. One of the main issues in NMR spectroscopy is sensitivity. One of the problems underlying this is the loss of signal due to relaxation (spin-spin relaxation). To avoid this modern NMR experiments employ deuterated solvents. Since deuterium is a quadrupolar nucleus, relaxation processes of ¹H nuclei through it are significantly lower than with other ¹H nuclei. This is mainly an issue for large molecules which have slow tumbling, such as proteins. This is due to R₂ (the rate that leads to transverse relaxation) being directly proportional to the correlation time (τ_c) of the nucleus (Fig. 1.8). In its turn, τ_c is directly related with molecular size, thus macromolecules have short relaxation times.⁶⁹

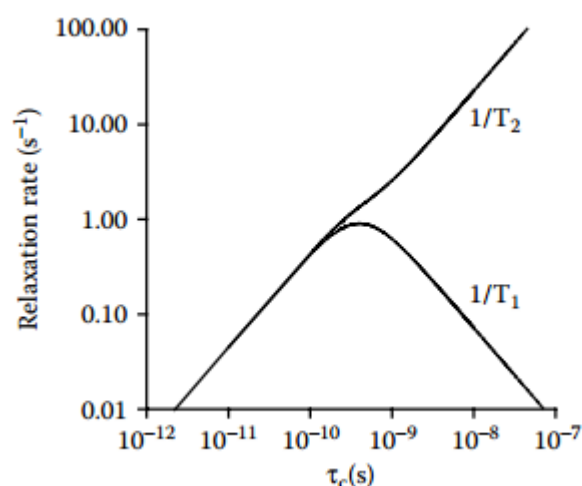


Fig. 1.8 Representation of the relaxation between the R₁ and R₂ relaxation rates and the correlation time. Figure withdrawn from Kowalewski *et al.*⁶⁹

To avoid this phenomenon, a strategy that has been devised is to encapsulate proteins inside reverse micelles that are dispersed in low viscosity fluids, such as alkanes.⁷⁰ The desired effect can be confirmed in Fig. 1.9. Since scCO₂ is even less viscous than common organic solvents, it might be even more advantageous to employ it in these studies. This is easily verifiable by observing the behaviour for compressed ethane. Valentine *et al.*⁷¹ have also shown that it is possible to use RMs as a medium for the use of dynamic nuclear polarization (DNP), which is a spin polarization technique. This allied to the avoidance of signal loss through spin-spin relaxation by RM encapsulation leads to a great increase of sensitivity that is essential to study larger proteins. These systems can also have the advantage of being effective in emulating cellular molecular crowding, therefore being useful for bio-mimetic structural and dynamic studies of proteins through NMR spectroscopy.⁷²

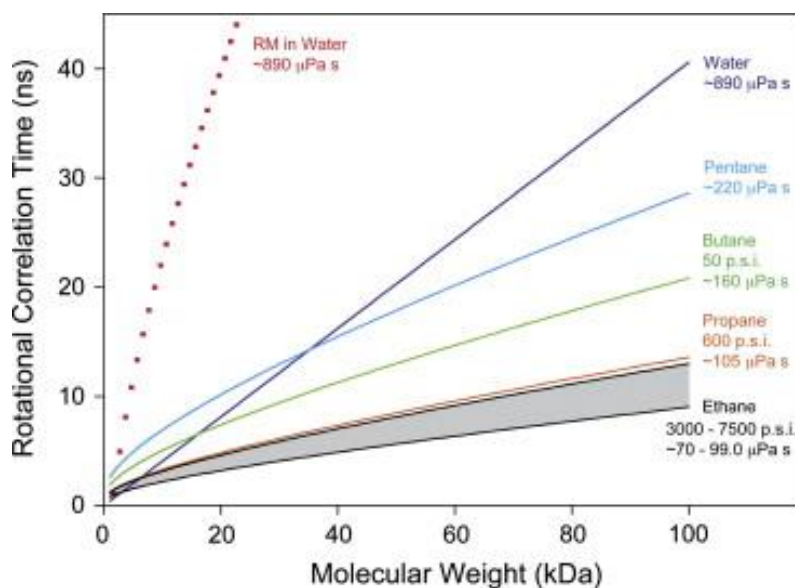


Fig. 1.9 Molecular weight dependence of correlation time for encapsulated proteins in different nonpolar solvents, and comparison with water. Figure withdrawn from Nucci et al.⁷³

1.2. Molecular gels

Gels are dispersions with such strong attractive interactions between the gelator molecules that these form a rigid network.³⁰ A gel has a continuous structure with macroscopic dimensions that is permanent on the time scale of an analytical experiment and, rheologically it is solid-like below a certain stress limit, behaving as viscoelastic materials.⁷⁴ Alike what was discussed in section 1.1, these might be formed from polymeric or small amphiphilic molecules. Even though some differences exist, those rely mostly on the forces holding the aggregates together being stronger in gels rather than in micelles. A surfactant that forms micelles in certain conditions can form gels in favourable circumstances.³⁰ Alike what is seen in surfactants, there is a critical gelator concentration (CGC), the minimum concentration to achieve a gel phase. To have the formation of this dispersion it is necessary to have an impulse. This might be the addition of a catalyst that triggers a reaction, it might be a light stimulus that provides an isomerization or an increase in temperature that allows the system to surpass an energetic barrier. In this work molecular gels will be employed to achieve these aggregates. These molecules immobilize their liquid component macroscopically, by surface tension and capillary forces. Despite that, the liquid still presents mobility within the networks.⁷⁴

A gel might be classified according to its solvent, thus there are organogels and hydrogels, but also due to its gelator, which can be polymeric, an organic molecule or an organometallic one. In this work will focus on molecular gels, formed by LMOGs (the latter two types of molecules fit in this category). These are usually formed at a low concentration (usually below 2 wt%).⁷⁵ These molecules self-assemble through highly specific interaction forming commonly fibers or strands, often having a crystalline structure. The forces that might give rise to these assemblies are H-bonding, π - π stacking or even London dispersion forces.⁷⁵ Different kinds of structural assemblies can give rise to gels. Molecules bearing aromatic moieties have been thoroughly employed.⁷⁴ In this work we will focus on an amphiphilic

aliphatic molecule and derivatives, which have been widely studied by the Weiss group, (R)-12-hydroxystearic acid (HSA,).⁷⁶⁻⁷⁸

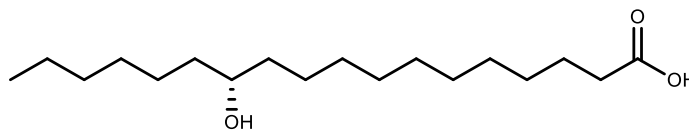


Fig. 1.10 Molecular structure of HSA.

HSA is a chiral molecule that under solution conditions forms a micelle, but as a gel it forms a left-handed chiral mesophase, which yield helically twisted fibers (Fig. 1.11).^{79,80} These are held together by dipolar interactions among the polar carboxylic groups and unidirectional hydrogen bonds through the hydroxyl group at C₁₂.⁸¹ It forms a gel in several solvents, such as n-hexane, carbon tetrachloride or toluene. In this solvent, it forms a clear gel, with a T_g of 44-45° C.⁷⁶

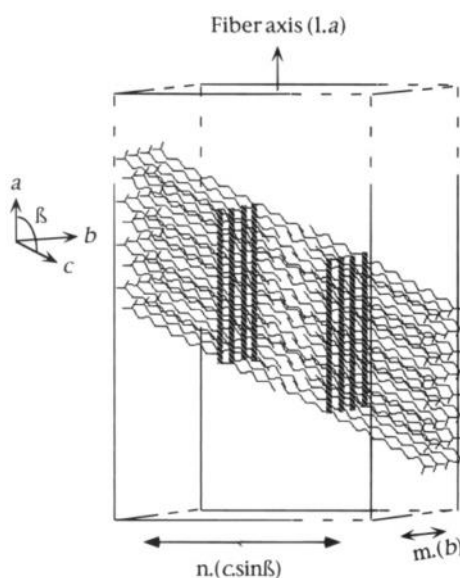


Fig. 1.11 HSA fibrillar or ribbonlike aggregates in organic solvents. Image removed from Terech et al.⁸¹

1.2.1. Structural studies of molecular gels

The purpose of this section of the work is to understand the dynamics of formation of tridimensional gel networks. Alike what was mentioned in the case of reverse micelles, a plethora of techniques can be used for this purpose. One can follow the formation through microscopy or through spectrophotometric technique or even through SANS. Different approaches may be taken. However, in this work the focus will be on NMR spectroscopy, because it allows to follow both the kinetics of formation and the structure of the network being formed, which is the main advantage. The principles behind the experiments have been presented in section 1.1.2, so only applications and results will be referred from now on. NMR spectroscopy has been widely applied to study gels, both polymeric gels and LMOGs.⁸² Aggregation and behaviour can be followed by chemical shift and line broadening and interactions can be assessed through NOE. Additionally, if a solid-like state is achieved Magic Angle

Spinning techniques like CP-MAS must be used.⁸² However, since the goal is the dynamics of formation, two major techniques will be employed, DOSY and relaxation (both T_1 and T_2).

DOSY is widely described as being an effective technique to differentiate molecules according to their size, without any actual separation process.⁸³ This is true for complex mixtures of different compounds but it can also be applied to the case of aggregating molecules, in which differently-sized assemblies can exist. The gelation point of gelatin was first presented by DOSY NMR by Brand *et al.*⁸⁴ The sample was heated and cooled, as shown in Fig. 1.12, and a minimum in D was obtained at approximately 25° C, which was considered the T_g . This is a counterintuitive result, the gel phase has an increase in diffusion coefficient comparing to T_g . This might be due to the fact that larger aggregates are attached to the gel phase thus NMR invisible, by having a quick relaxation process. By decreasing the temperature, only smaller aggregates will be in the solution phase. A similar result was observed by Nonappa *et al.*⁸⁵ that performed a titration with a cholic acid derivative. A similar decrease in D was achieved while nearing CGC and then an increase in the gel phase was obtained. A diffusion coefficient increase in the gel phase was not observed for other gel systems,^{86–88} which is a hint that it is possible to assess different types of packing through DOSY. The time of gelation has also been assessed through DOSY for a concentrated casein suspension.⁸⁹ The data obtained in the mentioned works made it possible to understand the dynamics of the gelation processes. A similar work can be done, and has been done, through relaxation measurements, which are also useful in determining the gelation point and the dynamics of gel structures, that in this case related to rotational motions.^{90,91} A combination of these two types of techniques is ideal for the NMR characterization of gels. García-Aparicio *et al.*⁹² followed the elution of molecules in chitosan gel phases through slice selective NMR. This is a promising result that might allow to use gel phases as chromatographic phases for NMR studies.

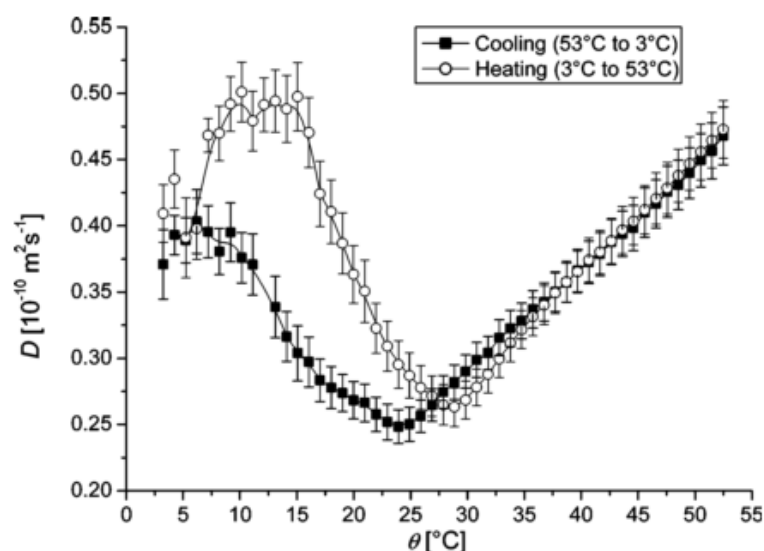


Fig. 1.12 Correlation between the diffusion of gelatin and temperature for both heating and cooling processes. Figure withdrawn from Brand *et al.*⁸⁴

1.3. Thesis outline and objectives

The work conducted throughout this thesis has two different parts that are however connected by the study of molecular assemblies formed by small amphiphilic molecules and the use and development of NMR methodology to study these systems. One of the major objectives is to develop and to apply a concise NMR approach towards observing motions and study what implications these have for the behaviour of materials and to understand how we can use them to improve spectroscopic studies.

The core subject of this work deals with reverse micelles both in a nonpolar solvent as in scCO₂. In this work, AOT will be used as a model molecule to develop the application of NMR techniques such as DOSY and relaxation measurements. One purpose of this work is to understand how polar molecules behave inside water droplets dispersed in low viscosity fluids. This has the long term purpose to achieve a more effective system to perform NMR spectroscopy of biomacromolecules. Another aim is to develop new surfactant for W/CO₂ microemulsions to develop these NMR studies. To make it more affordable to use these systems, fluorinated surfactants are avoided. This is meant as a proof of concept study thus only preliminary studies are conducted.

Part of the work (4 months) was conducted at Georgetown University, at Prof. Richard Weiss' group, as part of the InTechSE project. In this framework, a collaboration was developed to study molecular gels through NMR. More specifically, this work aims to demonstrate that DOSY NMR is a technique that can study the dynamics of gelation and assess the time of gelation in gels formed by LMOGs. This work is based in HSA and derivatives.

Overall, this work is intended to improve the application of NMR techniques towards the understanding of self-assemblies.

2. CHARACTERIZATION AND DYNAMICS OF REVERSE MICROEMULSIONS IN ORDINARY AND SUPERCRITICAL SOLVENTS

In this chapter, I will unravel the path undertaken from the analysis of AOT RMs in isooctane by DLS and NMR to the application of an identical methodology to a W/CO₂ microemulsion. The main aspect of this work is to develop an NMR methodology to determine size, aggregational behaviour and study dynamics of micellar assemblies in scCO₂ environment.

2.1. Development of a NMR methodology to characterize W/O reverse micelles

In order to develop the methodology to study W/CO₂ microemulsions through HP-NMR, a model system of AOT-based W/O microemulsions was utilized. This is a fairly well-known system and it was simply necessary to ensure that the conditions used would lead to stable RMs. The phase diagram for this ternary mixture is described in the literature (Fig. 2.1).⁹³ If the AOT concentration is too high, other types of phases will be formed. However, in reasonably low concentrations of AOT and small amounts of water dispersed in the oil phase, it is possible to obtain stable RMs. In this work, a 0.1 M concentration of AOT in isooctane and ω_0 up to 60 were employed.

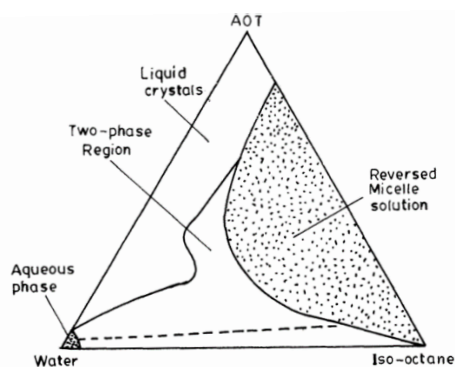


Fig. 2.1 Water/AOT/isooctane phase diagram. Figure taken from De et al.⁹³

In the devised system, water droplets are dispersed in the oil, coated with a surfactant monolayer, as displayed in Fig. 2.2. These are properties inherent to the system and therefore are listed in Table 2.1.

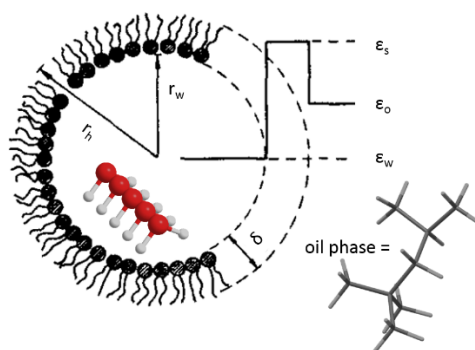


Fig. 2.2 Pictorial representation of the coated model of water droplets dispersed in isooctane. Adapted from Rička et al.⁹⁴ r_w is the water core radius; δ is the thickness of the surfactant layer; r_h is the hydrodynamic radius

of the droplet. Also displayed are the optical dielectric constants of the surfactant (ϵ_s), oil (ϵ_o) and water (ϵ_w) phases, which correspond to the square of the respective refractive indexes.

Table 2.1 Properties for the components of water/AOT/isooctane ternary mixtures. δ is the thickness of the surfactant layer; v_w is the volume of water; v_s is the volume of AOT; n are the refractive indices of the respective molecules; η corresponds to viscosity.

Property	Value	Ref.
MW (g mol ⁻¹)	444.56	
δ (nm)	1.1	95
v_w (nm ³)	0.03	94
v_s (nm ³)	0.63	94
n (AOT)	1.463	94
n (water)	1.3325029	96
n (isooctane)	1.3914	
η (isooctane) (cP)	0.474	97

The core section of this work is to develop and apply an NMR methodology. Therefore, first of all, the assignment for the ¹H NMR spectrum of AOT in isooctane with encapsulated water is necessary. This is presented in Fig. 2.3, where the methyl groups of the surfactant and most of isooctane (its ¹H NMR spectrum can be found in Fig. A.1) are not identified, due to being overlapped thus difficult to study through the NMR approaches used. This is mostly due to isooctane not being deuterated, which was considered unnecessary since the signals of water and surfactant *heads* are further downfield.

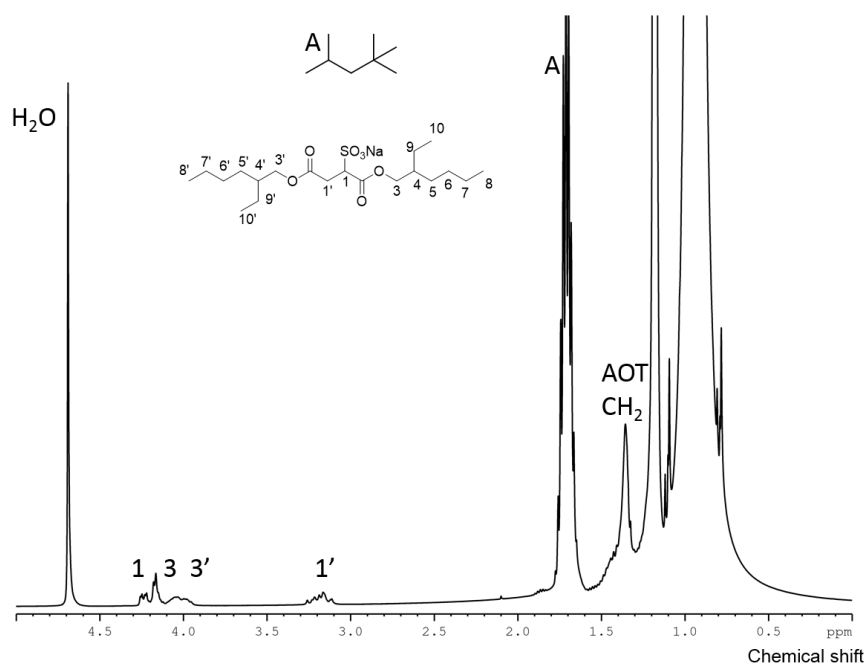


Fig. 2.3 Assigned ¹H NMR spectrum of a 0.1M AOT in isooctane with water ($w_0=40$).

NMR spectroscopy has been vastly employed in studying microemulsions and more specifically W/O AOT RMs. In this section of the work, several previously used techniques will be employed to shed

a new light on a vastly researched system, still with several mysteries. Frank *et al*⁹⁸ said, in the first work of the sort that “proton magnetic resonance measurements offer those interested in the complex equilibria associated with micellar solubilization of water an excellent tool for study, particularly if higher degrees of resolution and peak detection can be utilized”. NMR spectroscopy has certainly come a long way since 1968, and in this work we will approach the same target, but with new *tricks*. In order to develop methodology, from now the NMR and DLS studies with different concentrations of water in the solution are presented.

2.1.1. Size determination of RMs

One of the most relevant parameters of RMs is its size. If one wishes to encapsulate polar molecules in these, one must pay attention to the relation of size between the solute and the aggregate. In the case of AOT, as aforementioned, the size of W/O microemulsions depends on the amount of water dispersed in the hydrophobic phase (2).

2.1.1.1. Dynamic Light Scattering determination

A water droplet dispersed in an oil phase scatters light. If the scattered light intensity is followed over time and it has a Brownian motion, it is possible to obtain its diffusion coefficient and employing (3) its hydrodynamic radius. This is essentially the principle of DLS. This technique has been vastly employed to study W/O reverse micellar systems and more specifically employing AOT as the tensioactive agent.^{95,99,100} Since water droplets are dispersed in an oil phase, several refractive indices are involved (as can be confirmed by Table 2.1). This results in the optical polarizability not having the same evolution as in other scattering systems. The diffusion coefficients determined by DLS do not evolve linearly with the size of the droplets dispersed in the oil phase, having even a point at which the scattering intensity approaches zero due to optical matching of the water and the continuous phase.⁹⁴ Therefore, a model has been devised, the coated droplet model, which allows for a more accurate size determination. The following equations are employed to obtain the hydrodynamic radius of the aggregate:

$$r_h = 3\delta \frac{\omega_0}{y} \frac{1 + 3\gamma}{1 + 2\gamma} \frac{A}{B - \left(\frac{2}{9}\right) \left(\frac{y}{\omega}\right) C} \quad (4)$$

$$A = \frac{(1 + 5\gamma)(1 + 4\gamma)}{(1 + 2\gamma)(1 + 2\gamma)} \left(\frac{\omega_0}{y}\right)^2 + 2\nu \frac{1 + 4\gamma}{1 + 2\gamma} \frac{\omega_0}{y} + \nu^2 \quad (5)$$

$$B = \frac{(1 + 4\gamma)(1 + 3\gamma)}{(1 + 2\gamma)(1 + 2\gamma)} \left(\frac{\omega_0}{y}\right)^2 + 2\nu \frac{1 + 3\gamma}{1 + 2\gamma} \frac{\omega_0}{y} + \nu^2 \quad (6)$$

$$C = \frac{(1 + 3\gamma)}{(1 + 2\gamma)} \left(\frac{\omega_0}{y} \right)^2 + 2v \frac{\omega_0}{y} + v^2 \quad (7)$$

In which γ is the polydispersity (which corresponds to the square of the polydispersity index, p). y is the ratio between the volumes of surfactant and water molecules ($y = v_s/v_w$). Finally, v can be found in (8). All of these parameters have been previously described in either Fig. 2.1 or Table 2.1.

$$v = \frac{\frac{\epsilon_s - \epsilon_o}{\epsilon_s - 2\epsilon_o}}{\frac{\epsilon_w - \epsilon_o}{\epsilon_w - 2\epsilon_o}} \quad (8)$$

For each ω_0 several experiments were conducted, in order to obtain an average of the hydrodynamic radius determined. In order to apply the coated droplet model, the experimental data necessary is the polydispersity index. Due to optical matching, this observable gets high near $\omega_0=20$ (in this case this is especially true for $\omega_0=30$), as it can be verified in Table 2.2. Hence, an average of all the remaining polydispersity indices (all but the two mentioned conditions) was used in the determination of each hydrodynamic radius ($p_{\text{average}}=0.189$). For droplets with small water pools (below $\omega_0=10$) this model was not applied due to the low scattering intensity they provide. A summary of the experimental data obtained through DLS is shown in Table 2.2.

Table 2.2 DLS determined sizes of water droplets at different ω_0 . Experimental (expt.) r_h and polydispersity indexes (p) are presented. The coated droplet model (cdm) r_h is also determined and the diffusion coefficient (D) of the droplets is inferred from it. The error for the DLS measurement was determined by the standard deviation of the several measurements conducted. The diffusion coefficient was determined by using (3), employing the viscosity of isoctane present in Table 2.1.

ω_0	r_h (nm), expt	p	r_h (nm), cdm	D (m ² s ⁻¹)
1	2.23±0.03	0.376	-	-
5	3.08±0.03	0.198	-	-
10	3.98±0.03	0.181	3.04	1.51 x10 ⁻¹⁰
20	5.33±0.12	0.188	4.02	1.15 x10 ⁻¹⁰
30	9.45±0.25	0.963	6.12	7.53 x10 ⁻¹¹
40	11.15±0.53	0.057	8.87	5.20 x10 ⁻¹¹
50	11.73±0.35	0.138	10.45	4.41x10 ⁻¹¹

The hydrodynamic radii obtained in this study using DLS are in agreement with the literature, as is the evolution with the amount of water dispersed in the continuous oil phase (Fig. 2.4).⁹⁵ Hence this is useful to compare with the NMR measured data, which are presented in 2.1.1.2.

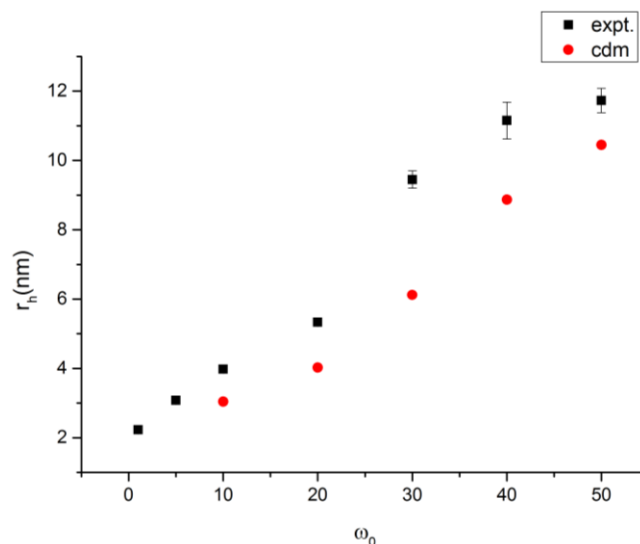


Fig. 2.4 Correlation between r_h and ω_0 determined experimentally by DLS (expt.) and by the coated droplet model (cdm).

2.1.1.2. Application of a NMR methodology

To the best of my knowledge, the first approach taken to determine droplet sizes for this system through NMR was done by Maitra that employs an approach based on chemical shift.⁶¹ This is an approach that requires the employment of several empirically determined parameters and is based on the observation of different chemical shifts for free and bound water nuclei. In this work, it was not possible to observe two distinct chemical shifts for water, therefore this was not a feasible option. Diffusion ordered NMR spectroscopy (DOSY) experiments were then conducted. This was already done for this system with interesting results.^{62,101} In the simplest pulse sequence that can be used, a pulsed field gradient (PFG) is applied (for a δ time) after a 90° pulse, hence causing spatial phase encoding.¹⁰² Then a 180° pulse creates an echo that removes chemical shift contribution and finally, a PFG with the same magnitude (g) is applied a time to allow for diffusion (Δ). Due to diffusion, after the application of the second gradient, the spins will not be in the same location thus these will present attenuation. By varying the gradient strength this will give rise to a decay that can be described by the Stejskal-Tanner equation (9).¹⁰²

$$I(g) = I_0 e^{-D\gamma g \delta^2 (\Delta - \frac{\delta}{3})} \quad (9)$$

Since a low viscosity fluid was employed, two pulse sequences to obtain diffusion ordered spectroscopy were compared: ledbpgp2s¹⁰³ and dstebgp3s.¹⁰⁴ The main difference between both is that the latter features a double stimulated echo for convection compensation, which in this case is extremely useful because of the low viscosity of the solvent. An example of the DOSY plots obtained can be found in Fig. 2.5.

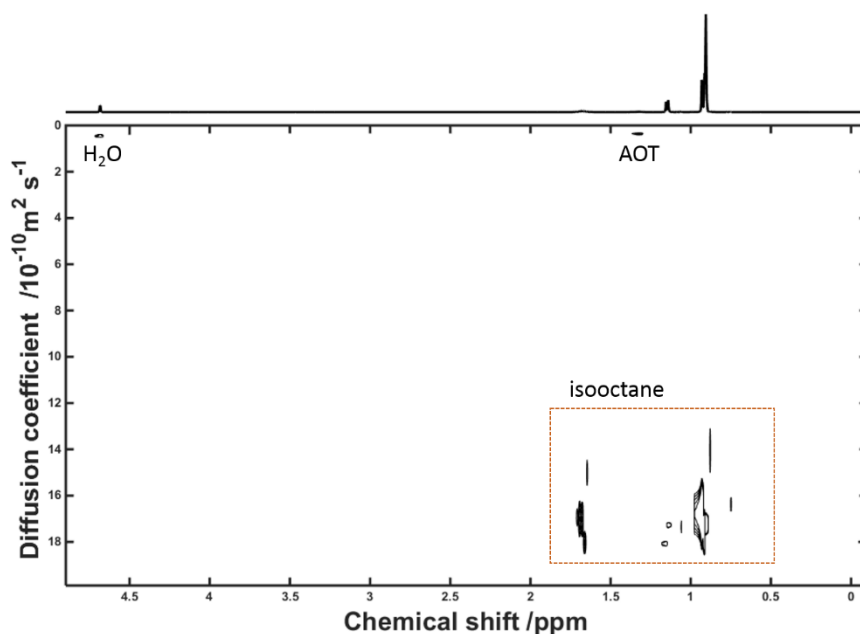


Fig. 2.5 DOSY plot of AOT RM in isooctane with water, $\omega_0=50$. In the figure, the regions pertaining to the different components is identified.

The DOSY experiments conducted revealed a diffusion coefficient different for the nuclei of encapsulated molecules and for those belonging to the solvent. Isooctane is less viscous and it is not aggregated, as are the micelles. This is reflected in the diffusion coefficients determined, AOT and water have a clearly smaller one than isooctane (Fig. 2.5). This is actually a way to tell that these are indeed aggregated and behave more like a macromolecule than as a small molecule. The overall data obtained for the determination of aggregate size can be seen in Table 2.3.

Table 2.3 Diffusion coefficients (D) and hydrodynamic radii (r_h) taken from DOSY data for the H₂O and AOT H3 protons. The r_h was determined using (3) and the viscosity in Table 2.1.

ω_0 \ DOSY data	D_{H_2O} (m ² s ⁻¹)	r_h (nm), H ₂ O	D_{H3} (m ² s ⁻¹)	r_h (nm), H3
10	1.35×10^{-10}	3.4	9.70×10^{-11}	4.7
20	1.11×10^{-10}	4.2	9.22×10^{-11}	5.0
30	6.84×10^{-11}	6.7	5.44×10^{-11}	8.5
40	5.72×10^{-11}	8.0	4.20×10^{-11}	11.0
50	4.56×10^{-11}	10.1	3.59×10^{-11}	12.8
60	3.18×10^{-11}	14.5	2.48×10^{-11}	18.6

While increasing the amount of water dispersed in the oil phase, the size of the micelles also increases, in an approx. linear fashion. This is observed in Table 2.3, through the decrease of the diffusion coefficient of the protons, which is due to the aggregation.

More significantly, that is seen for both water and AOT protons, which reveals that there should be a homogeneous system, in which both of these molecules have a diffusion that is governed by the viscosity of the continuous phase. It is also possible to observe that AOT has a lower diffusion coefficient than that of water. This may be due to the fact that this experiment reveals for AOT the diffusion

alongside its solvation shell, which would correspond to a larger aggregate, whereas for water the equivalent to a solvation shell is the surfactant monolayer. Geiger *et al*⁶¹ tried to bypass this sort of observation by taking into consideration the exchange of AOT between a monomer dissolved in isooctane and an aggregated micelle and this subject will be further addressed in section 2.1.2.1, but as it will be shown later this hypothesis was assessed and there is no evidence of exchange by the water protons. Therefore, this determination of size is deemed as valid. The relationship with ω_0 is depicted in Fig. 2.6.

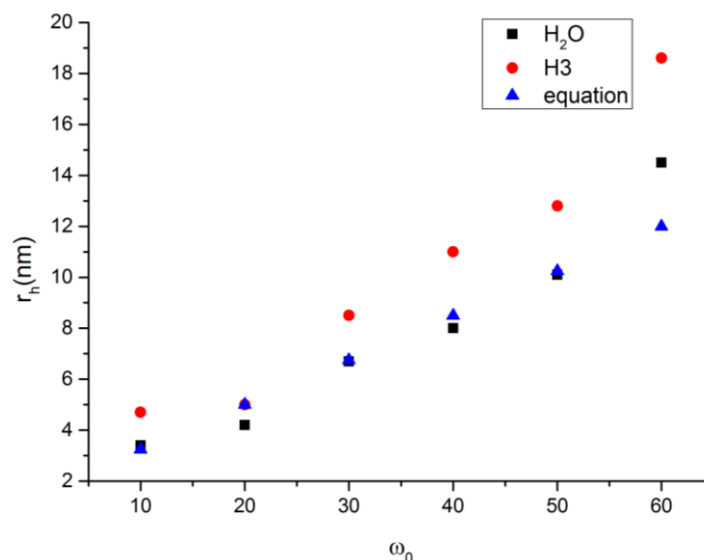


Fig. 2.6 Relation between the hydrodynamic radii measured by DOSY (for the water and the H3 proton in AOT) and the amount of water dispersed in isooctane. Also shown are the hydrodynamic radii determined through equation (2).

Both water and AOT H3 proton's diffusion rates evolve in a linear fashion with ω_0 , which is in agreement with the literature.⁶² In that work, there was an overestimation of the size of the droplets while measuring surfactant diffusion rates. The same was obtained here. However, the water diffusion appears to be a more accurate way to estimate the size of the RMs, overlapping in most points. The aforementioned work takes an approach to scale the data obtained by NMR by dividing the experimental radii by an empirical number of surfactants. In this work, the endeavour was to determine a relation with one other experimental technique, DLS, as will be shown in section 2.1.1.3.

2.1.1.3. Comparison of methods

Law *et al*⁶² had already shown that DOSY data yield smaller diffusion coefficients than those obtained through DLS. The data previously presented confirm that, but what these also confirm is that there is a more accurate estimation of the sizes of RMs by measuring the diffusion from the water protons. Therefore these diffusion coefficients were plotted against the ones taken from DLS data, as represented in Fig. 2.7.

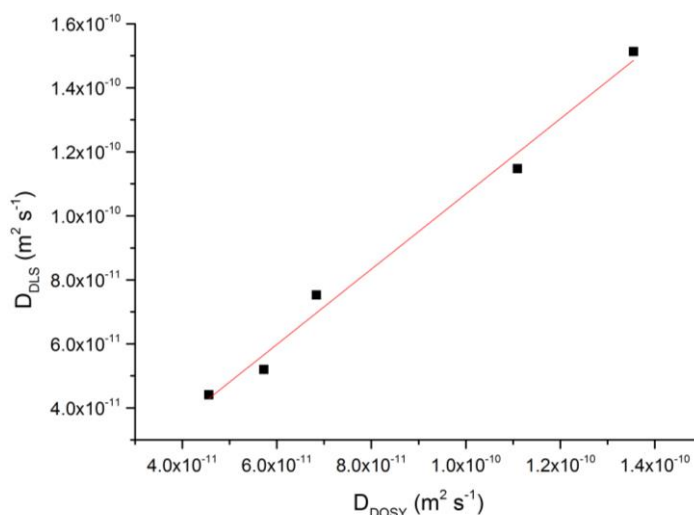


Fig. 2.7 Relation between the diffusion coefficients measured through DLS and from the water protons with DOSY. Correlation equation (10) is obtained with R^2 of 0.985.

Since the ultimate goal is to develop an NMR methodology to assess the properties of microemulsions under a scCO₂ environment and we do not have the sort of equipment necessary to conduct DLS experiments under the necessary pressured conditions, the obtained correlation between the diffusion coefficients obtained through DOSY to the more accurate ones obtained by DLS is presented in (10) and can be applied to study these systems in high pressure conditions.

$$D_{DLS} = 1.1758D_{DOSY} - 1.07469 \times 10^{-11} \quad (10)$$

2.1.2. Dynamics of AOT RMs in isooctane

The first principle approach towards studying the dynamics of any system using NMR spectroscopy is to study how its chemical shift evolves either through time, concentration or temperature. In this work the change that occurs is in the concentration of water dispersed in isooctane, already studied by Maitra and Frank *et al.*^{61,105} In order to determine chemical shift displacements, all spectra were internally calibrated to peak A from isooctane (Fig. 2.3). It is therefore assumed that no significant modification occurs on the solvent, which has already been reported.¹⁰¹ The chemical shift determined is represented as $\Delta\delta$ and can be found in Table 2.4.

Table 2.4 Data obtained from chemical shift measurements of different protons in the solutions.

$\omega_0 \setminus \Delta\delta$	$\Delta\delta_{H_2O}$ (ppm)	$\Delta\delta_{H1}$ (ppm)	$\Delta\delta_{H3}$ (ppm)	$\Delta\delta_{H1'}$ (ppm)	$\Delta\delta_{CH_2,AOT}$ (ppm)
10	4.418	4.272	4.164	3.190	1.355
20	4.523	4.258	4.165	3.189	1.356
30	4.643	4.246	4.166	3.188	1.358
40	4.690	4.239	4.165	3.188	1.356
50	4.729	4.236	4.166	3.189	1.359
60	4.748	4.234	4.166	3.188	1.359

From the data in Table 2.4 it is possible to observe different trends in the behaviour of the studied nuclei. Water and the protons belonging to the *tail* (H3) of the surfactant move downfield with the increase of ω_0 , whereas the protons from the AOT *head* (H1 and H1') have the opposite evolution, becoming more shielded.

It is expected that with a higher amount of water content, a more significant interaction exists with the surfactant layer. This might partially justify the deshielding of water and certainly the shielding of the AOT *head*. Additionally, and probably more significantly, with the increase of the amount of water dispersed, the water molecules should behave more alike bulk water, which also makes it a good way to estimate the size of the aggregates. These correlations are displayed in Fig. 2.8 for H1 and H₂O, which in the case of H₂O is in agreement with the literature.⁶¹ No description for the AOT proton has been found.

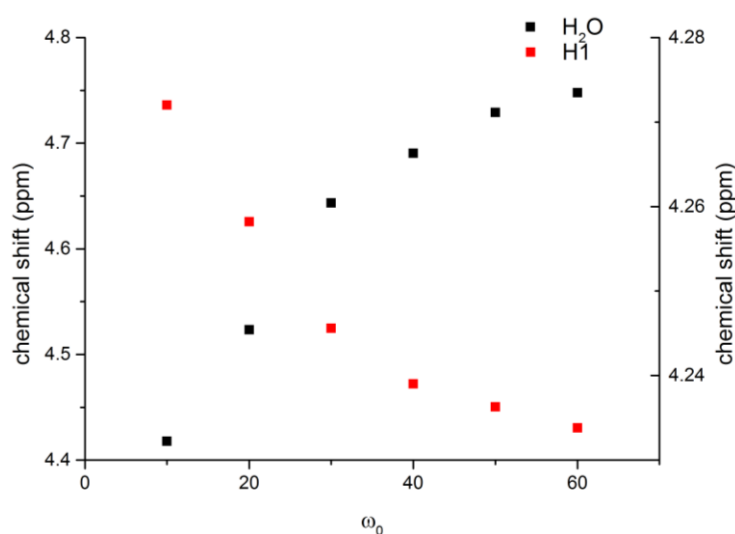


Fig. 2.8 Relation between the chemical shift displacements of water (left y axis) and AOT H1 proton (right y axis) and ω_0 .

One factor that can affect the properties in a solution is viscosity. So far in this work it has been considered that the system is mainly affected by the isooctane viscosity, which has been considered to remain constant at different amounts of encapsulated water. However, several studies conducted to study microviscosity ($\mu\eta$) inside AOT reverse micelles have proven it changes with ω_0 .^{106,107} These data are obtained by fluorescence measurements of a probe that is located at the surfactant layer. In order to account for the changes in microviscosity the data taken from Rafiq *et al*¹⁰⁷ were extrapolated for higher water concentrations as demonstrated in (24), Fig. A.3 and Table A.1. This approach necessarily involves some errors, however, the goal was to have an estimate of such values to study its possible influence on the NMR parameters.

The correlation of the water chemical shifts with the different microviscosities inside the droplets is depicted in Fig. 2.9.

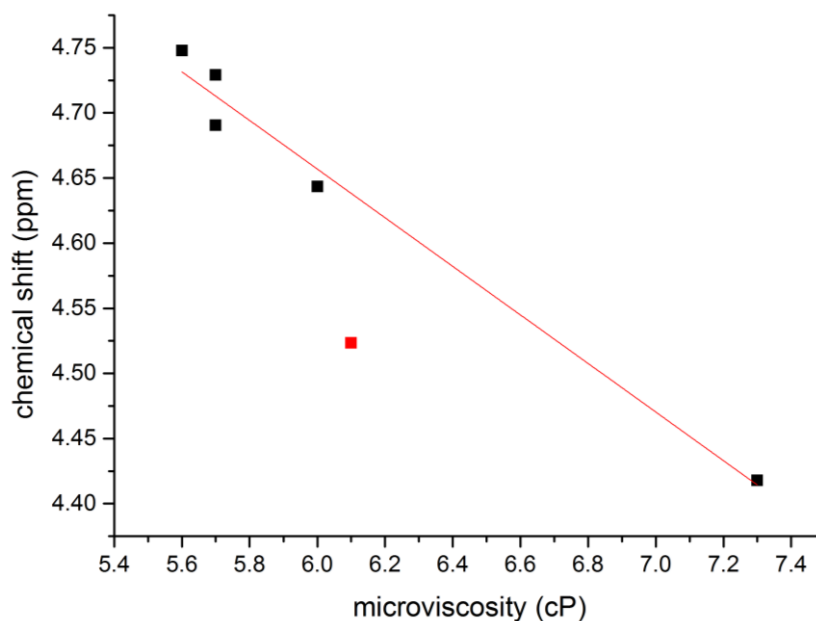


Fig. 2.9 Plot between the H₂O chemical shift and the microviscosity inside the AOT W/O droplets. A linear fitting discarding $\omega_0=20$ was obtained, as depicted, with a $R^2=0.97$ and a slope of -0.187 .

The plot describes a reasonable correlation, mostly if $\omega_0=20$ is taken out, then a $R^2=0.97$ is attained. This shows that viscosity inside the droplets greatly influences the behaviour of water. If it is taken into account that these measurements are done near the micellar interface, it indicates that even though different water chemical shift are not observed, the influence of the confinement, therefore in the state of bound and free water is relevant for the overall dynamics. This indicates that the residence times were not long enough to differentiate chemical shifts, which are in general low,¹⁰⁸ but an influence in chemical shift clearly exists.

2.1.2.1. Stability of AOT W/O microemulsions

It has been widely described that AOT forms stable reverse micelles in a hydrophobic solvent. As previously mentioned, the residence times of bound and free water are not large enough to allow to differentiate both in terms of chemical shift, under these conditions the exchange between free and bound water is in the fast regime time scale ($\Delta\delta \ll k_{\text{exchange}}$) and only one peak is observed in the NMR spectrum for both forms.

In this section, the chemical exchange will be studied. There are several mechanisms that can be taken into account, however assuming that free and bound waters are associated with different diffusion coefficients this can be explored by determining the diffusion coefficient of water using different diffusion times. Under the correct relation between, k_{exchange} and diffusion time, the water diffusion will be modulated by the lifetime of the water in the different environments, which can be varied in different diffusion experiments by changing the total time allowed for the molecules to diffuse, the diffusion time. This influence of exchange in diffusion can then be detected by plotting the different diffusion coefficients against the diffusion times.¹⁰⁹ If this yields a constant diffusion coefficient, then no exchange is taking place or the limit of very fast diffusion exchange has already been reached. If there is a slope then there

is an indication that diffusion exchange is occurring and a mechanism can be studied. The data were plotted for the system with $\omega_0=50$ (Fig. 2.10).

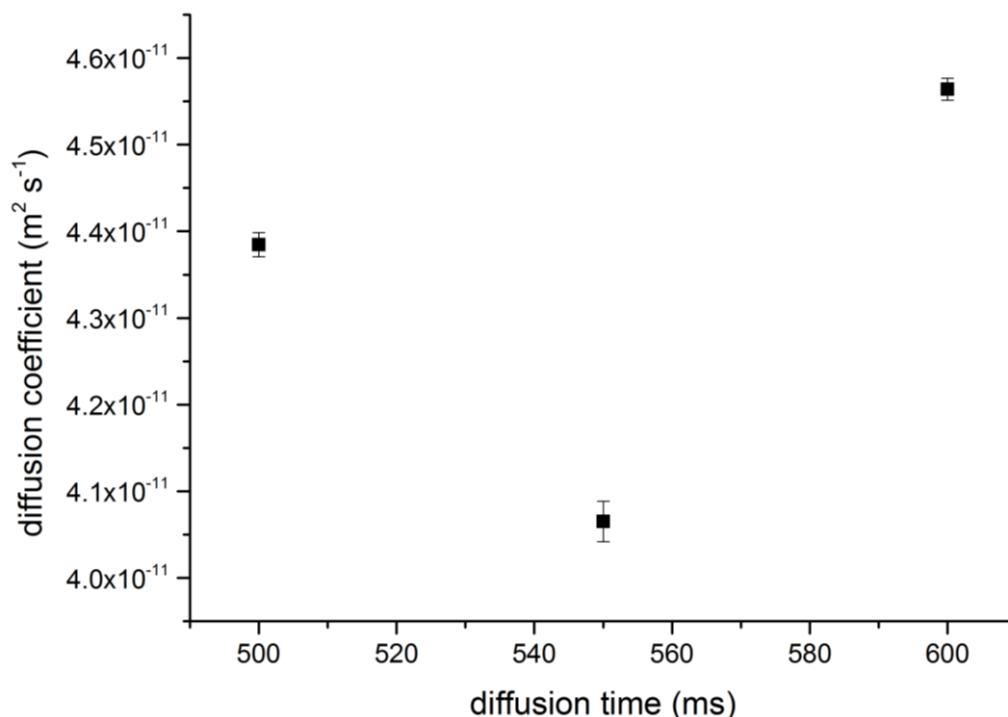


Fig. 2.10 Plot between water diffusion coefficient and time allowed for diffusion in the AOT W/O solution with $\omega_0=50$. The error bars belong to the error of the fitting.

The amount of water that is bound ought to be significantly smaller than that of free water. If the sample is in a regimen of slow exchange then it would be expected that an equilibrium would be observed. By having a larger diffusion time the exchange time is larger comparing to the observation time thus a higher diffusion coefficient would be observed. There is also another state of water that can be taken into account, which is water diffusing in isooctane. All of these situations would lead to a trend. Therefore it is considered that no diffusion exchange occurs, comparing to the timescale observed.

2.1.2.2. Confined water dynamics

Confinement significantly affects the dynamics of water and dissolved molecules.¹¹⁰ This phenomenon has already been studied by different techniques in AOT W/O reverse micellar systems.³⁴ Hauser *et al*¹¹¹ suggested that each AOT molecule affects 13 water molecules, being two directly bound to the Na⁺ ion while the others remain weakly associated. Previously data always demonstrated that the activity of water inside the droplets gets larger with the amount of water dispersed and starts resembling bulk water (Fig. 2.11).³⁴

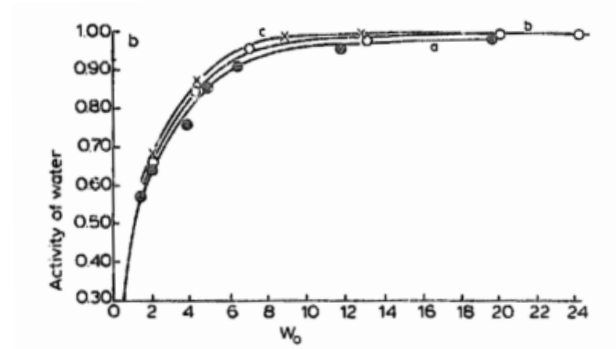


Fig. 2.11 Activity of water dependence with the increase of w_0 . The figure was withdrawn from Luisi et al.³⁴

It has already been shown that the translational diffusion coefficient of water has a clear relationship to that of the micelle itself. Water inside the droplet has therefore its self-diffusion restricted by the nanoenvironment it is in. If however we consider a quicker and smaller scale motion, rotational diffusion, this might be affected differently by the encapsulation. Therefore, in this work this will be studied using spin-lattice (T_1) and spin-spin (T_2) NMR relaxation measurements.

As previously demonstrated, these NMR observables are directly influenced by the correlation time, T_2 varies linearly, whereas T_1 has a minimum, and two different sorts of behaviours, depending on the correlation time and thus the molecular size (Fig. 1.8).

T_1 is the time frame for the process of reestablishment of thermal equilibrium population in the z axis that is given by (11), in which M_z corresponds to the z magnetization.

$$M_z(\tau) = M_z(0) \left(1 - 2e^{-\frac{\tau}{T_1}}\right) \quad (11)$$

Experimentally to determine T_1 an inversion recovery pulse sequence is used, which consists of a 180° pulse, which is followed by a delay and a 90° pulse. By varying the delay, different magnetization intensities are obtained and the data can be fitted to (11).

Using the previously described methodology, the spin-lattice relaxation times for this system were determined and presented in Table 2.5 and in Fig. 2.12, where the evolution with water dispersion in isooctane is depicted for the case of water and the AOT H3 protons.

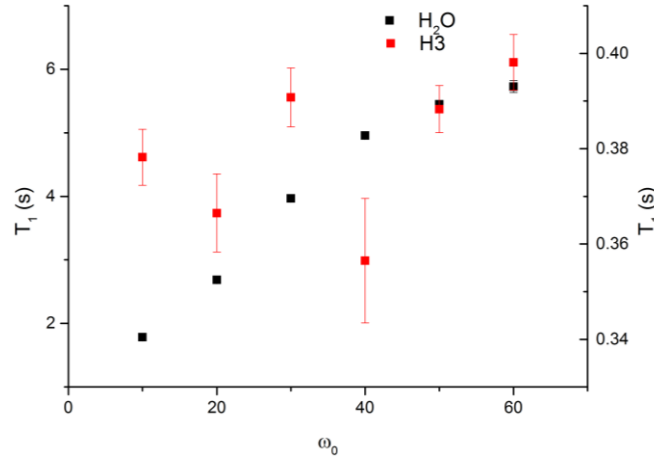


Fig. 2.12 Plot between T_1 relaxation times for H₂O (left y axis) and AOT H3 (right y axis) protons and ω_0 . The error bars result from the error associated with the exponential fitting.

The water relaxation time has a clear evolution with the amount of water inside the micelle. It is likely that at low concentrations of water a larger portion of it has ion-dipole interactions with the surfactant layer, more specifically the Na⁺ ions, as previously suggested.⁶³ AOT nuclei do not appear to be significantly affected by the increase in encapsulated water.

T_2 is related to the loss of magnetization in xy plane, and all mechanism leading to T_1 relaxation also lead to T_2 , but T_2 is also affected by spin-spin interactions, such as J coupling or solvent mediated relaxation, and therefore it is usually lower than T_1 . Spin-spin relaxation has also a direct influence on line broadening.

$$M_{xy}(\tau) = M_{xy}(0)e^{-\frac{\tau}{T_2}} \quad (12)$$

To assess T_2 , a Carr-Purcell-Meiboom-Gill pulse sequence was employed, which consists of a 90° pulse, which is followed by a delay and a 180° pulse. By varying the delay, different magnetization intensities are obtained and the data can be fitted to (12).

The same procedure as previously described was conducted for T_2 relaxation times, which can be found in Table 2.5 and Fig. 2.13.

Table 2.5 Relaxation times (spin-lattice and spin-spin) for the W/O AOT RM solutions.

$\omega_0 \backslash$ $T_1; T_2$	H ₂ O		AOT H1		AOT H3		AOT H1'		Isooctane A	
	T_1 (s)	T_2 (s)	T_1 (s)	T_2 (s)	T_1 (s)	T_2 (s)	T_1 (s)	T_2 (s)	T_1 (s)	T_2 (s)
10	1.78	0.20	1.08	ND	0.38	0.017	0.41	ND	3.42	0.60
20	2.68	0.32	1.08	9.4X10 ⁻³	0.37	0.047	0.38	ND	3.66	0.55
30	3.97	0.34	1.03	ND	0.39	0.024	0.40	ND	3.43	0.93
40	4.96	0.32	0.71	ND	0.36	0.033	ND	ND	3.54	0.50
50	5.45	0.56	0.82	ND	0.39	0.033	0.38	ND	3.39	0.50
60	5.73	0.74	0.83	ND	0.40	0.024	ND	ND	3.44	0.69

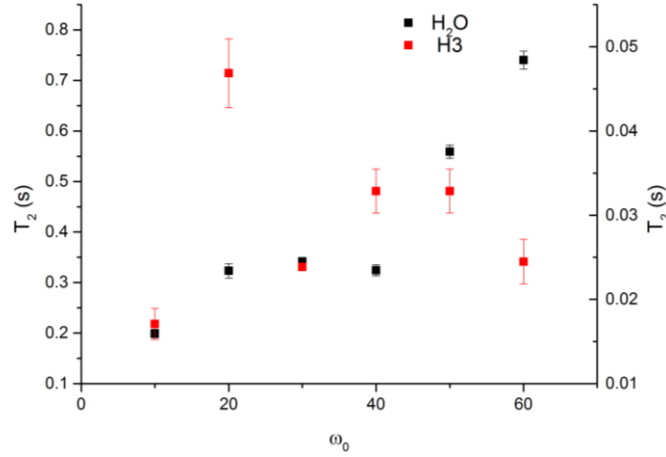


Fig. 2.13 Plot between T_2 relaxation times for H₂O (left y axis) and AOT H3 (right y axis) protons and ω_0 . The error bars result from the error associated with the exponential fitting.

It is possible to observe that water has an increase in its spin-spin relaxation times, being stopped by a plateau at ω_0 30 and 40, but then retaken. This might be due to a different sort of structure occurring, that shifts at higher concentrations in which water behaves more alike bulk water. This is in agreement with what was reported by Wong *et al.*⁶³ In the case of AOT, if $\omega_0=20$ is excluded (which might or not be accurate) there is an increase of the relaxation time up to the higher concentrations in which it decreases. This might be due to the sort of aggregation taking place, since there is no sequential evolution, which could be expected from a linear increase in size of the micelles. However, the T_2 values are rather short and the variation might not even be significant.

By obtaining relaxation times it is possible to differentiate mechanisms of aggregation by understanding the process of rotational diffusion. This is possible by determining the correlation time, τ_c , which corresponds to the Brownian rotational diffusion of a molecule. This can be obtained from the autocorrelation function, G , which is related to the spectral density function that is related with T_1 and T_2 .⁶⁹

$$G(\tau) = G(0)e^{-\frac{\tau}{\tau_c}} \quad (13)$$

If one assumes that relaxation occurs through a mechanism of *random reorienting field* that simply takes into account a random molecular tumbling, independent of other interactions, the following relationships between the relaxation times and τ_c are obtained (in which γ is the gyromagnetic ratio; b is a local magnetic field with a constant magnitude; ω_0 is the frequency of the nucleus measured)⁶⁹:

$$T_1^{-1} = 4\gamma^2 b^2 \left(\frac{\tau_c}{1 + \omega_0^2 \tau_c^2} \right) \quad (14)$$

$$T_2^{-1} = 2\gamma^2 b^2 \left(\frac{\tau_c}{1 + \omega_0^2 \tau_c^2} + \tau_c \right) \quad (15)$$

Even though these models can be employed, they assume physically unrealistic mechanisms. The possible mechanisms occur through dipolar or quadrupolar interactions or can be manifested as chemical shift anisotropy (CSA). In this work only ¹H relaxation times were measured, thus quadrupolar mechanisms need not be taken into account. CSA is not significant for ¹H nuclei. Therefore in this work the data will be interpreted as dipolar relaxation. This depends on the distance of the dipolarly coupled nuclei. To eliminate the distance dependence from the equations in order to determine the correlation time, τ_c , the ratio between the relaxation rates is used as demonstrated in (16).¹¹²

$$\frac{T_1}{T_2} = \frac{\frac{2}{1 + \omega_0^2 \tau_c^2} + \frac{8}{1 + 4\omega_0^2 \tau_c^2}}{3 + \frac{5}{1 + \omega_0^2 \tau_c^2} + \frac{2}{1 + 4\omega_0^2 \tau_c^2}} \quad (16)$$

In order to simplify this process, Carper *et al*¹¹² suggested that this may be calculated using a polynomial equation. In this work, the equation that corresponds to ¹H-¹H relaxation at a 9.4 T magnetic field, with T_1/T_2 in the range of 1.1-20 is used, (17).^b

$$\tau_c (ns) = -0.180407 + 0.295565 \frac{T_1}{T_2} - 0.022874 \left(\frac{T_1}{T_2} \right)^2 + 0.000993 \left(\frac{T_1}{T_2} \right)^3 - 0.000016 \left(\frac{T_1}{T_2} \right)^4 \quad (17)$$

Using this methodology, the correlation times for AOT H3 protons, water and isoctane were determined and the results are presented in Table 2.6 and Fig. 2.14.

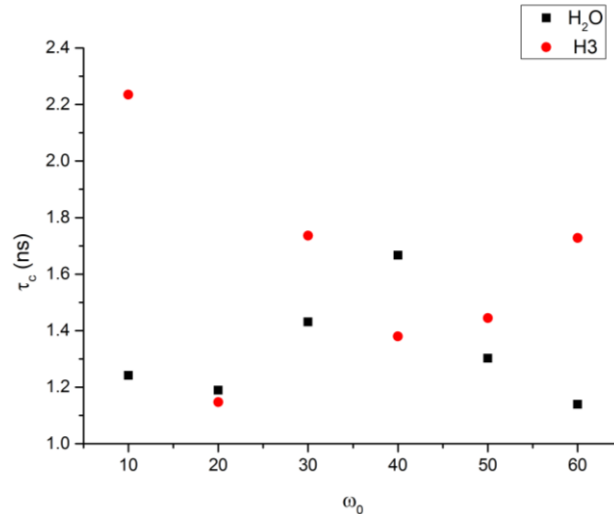


Fig. 2.14 Relation between τ_c (correlation time) of water and AOT H3 protons of W/O AOT reverse micelles and ω_0 .

^b AOT proton H3, with $\omega_0=10$, is in the ratio of 20-1200, therefore (23) was employed.¹¹²

If, yet again, $\omega_0=20$ is excluded from the plot, there is an increase of the correlation time of water until $\omega_0=40$, which is natural since a structure more alike a large molecule is obtained by an increase in size. However at higher concentrations there is a decrease. The exact opposite is observed for AOT. Comparing to a previous study, the variation of the water correlation time with ω_0 obtained in the present study is significantly different.⁶³ One possible reason is that in the paper mentioned a fixed distance for the relaxation process is utilized. It is also possible that the variation is random and just reflects experimental errors and the actual correlation time is a measure of the above. But the changes are significant, given that correlation times are commonly in the ps range. The correlation time for the water molecule in a 50 mM solution of D-(+)-Glucose is 1.92 ns (Table A.2). It is clear that the correlation times while entrapped in RMs are smaller, which may be due to that the fact that the droplets are dispersed in a less viscous solvent, which not only modifies its translational motion but also its rotational diffusion.

Being aware that a dipolar relaxation mechanism likely takes place, it would be possible to estimate the correlation time for the rotational motion, based on the viscosity of the medium, temperature and volume of the relaxing molecules (having in consideration the radius, a)⁶⁹:

$$\tau_c = \frac{4\pi\eta a^3}{3k_B T} \quad (18)$$

Since τ_c is an experimental result, (18) was used to estimate the radius of the aggregate water that leads to the rotational motion (Fig. A.2). This was also determined for the other nuclei, as depicted in Table 2.6.

Table 2.6 NMR relaxation determined correlation times and sizes (a) of the aggregates responsible for the relaxation for AOT W/O RM solutions. The sizes were obtained from the viscosity of isooctane present in Table 2.1(a^n) and for water it was also attempted to use the microviscosity defined previously to determine the size (a^m).

$\omega_0 \setminus \tau_c; a$	H ₂ O			AOT H3		isooctane A	
	τ_c (ns)	a^n (Å)	a^m (Å)	τ_c (ns)	a^n (Å)	τ_c (ns)	a^n (Å)
10	1.24	13.7	5.5	2.23	16.7	0.93	12.5
20	1.19	13.5	5.8	1.15	13.3	1.03	12.9
30	1.43	14.4	6.2	1.74	15.3	0.64	11.0
40	1.67	15.1	6.6	1.38	14.2	1.08	13.1
50	1.30	13.9	6.1	1.44	14.4	1.05	13.0
60	1.14	13.3	5.8	1.73	15.3	0.84	12.0

This demonstrates that at $\omega_0=40$ there is a maximum size of aggregated water molecules, 15.1 Å, ranging from 13.3 Å. There is an issue though, which viscosity should be considered? The one inside or outside the micelle? The microviscosity data previously addressed (Table A.1) have also been used to determine a radius of the water molecules conducting to rotational diffusion as depicted in Table 2.6 as a^m and in Fig. 2.15.

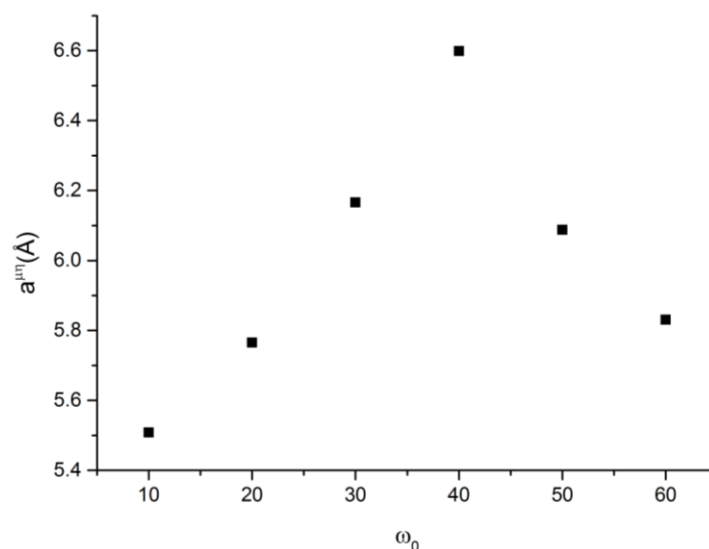


Fig. 2.15 Relation between a^m (radius of the relaxing nucleus) of water determined by the microviscosity inside the RM for AOT reverse micelles and ω_0 .

The evolution with ω_0 is identical to the one just addressed, however the sizes of aggregates are close to 6 Å, which would mean about 3 or 4 molecules. In order to understand which approach is more accurate, there are several literature works that studied the dynamics of confined water in these micelles.^{113–117} In these works, orientational relaxation times are mentioned to be in ps range. The correlation times determined in this work are in the ns range and were performed with a different technique, however former works for other sorts of RMs using NMR and also considering the dipolar relaxation mechanism of specific regions of the molecules determined these in the range of hundreds of ps.¹¹⁸ Since in this case, the considered dipolar relaxation occurs with the bulk, the differences are normal.

Inside reverse micelles there is a water pool that can be deemed as *free*, but there is also one that is bound to the surfactant layer. Piletic *et al*¹⁵ have tested this hypothesis, thinking of a core shell model with a water shell bound to the surfactant. The thickness of this shell has been shown to be 5 Å. This is similar to the radii determined applying the microviscosity at the micellar surface. It is likely that the fact that water molecules are adjacent or in that shell, is the driving force for its rotational behaviour.

2.1.3. Encapsulation of carbohydrate molecules in AOT RMs

In order to further characterize the dynamics of AOT W/O RMs, probe molecules were employed. In this case, sugars were employed, more specifically glucose-based water soluble carbohydrates: D-(+)-Glucose, 1,4 β -D-(+)-Cellobiose and 1,4 β -D-(+)-Cellotriose. These experiments are meant to answer three questions: how do the probe molecules affect micelle dynamics? How do oligomers with different sizes influence aggregation? How are the sugars affected by the encapsulation? In order to answer to these questions, the first approach was to conduct a simple molecular mechanics optimization of the structures, therefore understanding the sizes occupied by each solute. The demonstration of this study

can be found in Fig. 2.16 (the pictorial exemplification of the remaining calculations conducted can be found in Fig. A.7 and Fig. A.8) and the data are gathered in Table 2.7.

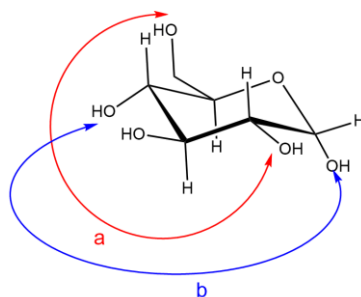
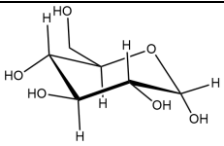
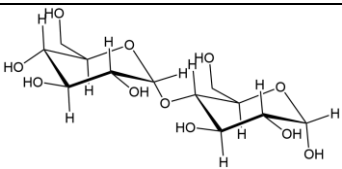
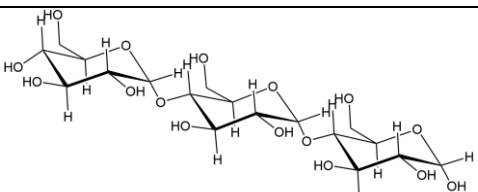


Fig. 2.16 Structure of D-(+)-Glucose and intramolecular distances determined from molecular mechanics using Chem3D Pro 14.0. $a=6.864 \text{ \AA}$; $b=5.034 \text{ \AA}$.

Table 2.7 Summary of the maximum distances (r_{\max}) measured through MM for the carbohydrates used in this study and the respective molecular weights (MW).

Molecule name	Molecular structure	MW (g mol ⁻¹)	r_{\max} (Å)
D-(+)-Glucose		180.16	6.864
D-(+)-Cellobiose		342.30	10.385
D-(+)-Cellotriose		504.44	14.581

These molecules have been widely studied in this group and it is known that these assume linear conformations while in solution. Since the monomer of this molecule is the same, the fact that there is a steady increase in the size of the probe molecules allows to study the effect of the solute size in the encapsulation process. In this work, a solution of D₂O:H₂O (9:1) with a carbohydrate concentration of 50mM has been used to encapsulate in RMs. Only using such conditions it is possible to observe the probe molecule through NMR, since the water is diluted in the isooctane bulk. In order to understand the differences between the dynamics in a large and a smaller water pool, $\omega_0=60$ and $\omega_0=20$ were used. By doing some simple calculations, it is possible to determine that the ratio between sugar and water molecules in this concentration is 0.0009. If we take into account the amount of water per micelle (approx. 350,000 for $\omega_0=60$ solutions and approx. 5,400 for $\omega_0=20$ solutions¹¹⁵), we conclude that approx. 315 molecules of sugar should be encapsulated in the $\omega_0=60$ RM and approx. 4.8 molecules in the $\omega_0=20$ RMs. Even though this implies that a different amount is found per micelle between the two

studies, these conditions guarantee that the water composition is the same thus no alterations in viscosity, surface tension and others are found. The encapsulation of polar molecules in RMs has been already significantly exploited, and studied in terms of kinetics, thermodynamics and location in the droplet.¹¹⁹ These have even been used as a model carbohydrate binding.¹²⁰

In order to study the dynamics of the sugar molecules encapsulated in the water droplets it was necessary to employ solvent-suppression NMR techniques. This is due to isooctane being clearly more abundant than the remainder of the molecules, thus by suppressing its methyl and methylene peaks it was possible to enhance the signal to noise ratio of the other peaks. In Fig. 2.17 the ¹H NMR spectrum of D-(+)-Glucose is presented. In this study, the focus will be on the dynamics of the surfactant, the water inside it and the proton belonging to the anomeric carbon of glucose (deemed as An) and its oligomers. It is both isolated in the spectrum and it is prone to alterations due to conformation, thus it should be more sensitive to eventual structural changes. The samples of this study were analysed in a way identical to the one presented in sections 2.1.1 and 2.1.2. First of all, the observables from ¹H NMR spectra were taken into account and are gathered in Table 2.8 (the chemical shifts are referenced by the isooctane A peak). There are little interferences found in the ¹H NMR spectra, both in the surfactant as in the water molecules that follow the trend of increasing molecular size (which is represented here by molecular weight).

Table 2.8 Data obtained from water suppressed ¹H spectra: chemical shifts ($\Delta\delta$) and half-height line width ($\nu_{1/2}$) for solutions of carbohydrates in AOT W/O RMs.

ω_0	sugar	An		H ₂ O		AOT H1		AOT H3		AOT H1'	
		$\Delta\delta$ (ppm)	$\nu_{1/2}$ (Hz)	$\Delta\delta$ (ppm)	$\nu_{1/2}$ (Hz)	$\Delta\delta$ (ppm)	$\nu_{1/2}$ (Hz)	$\Delta\delta$ (ppm)	$\nu_{1/2}$ (Hz)	$\Delta\delta$ (ppm)	$\nu_{1/2}$ (Hz)
20	Glucose	5.302	8.9	4.593	2.6	4.251	20.4	4.165	9.8	3.191	27.3
	Cellobiose	5.305	51.6	4.559	2.5	4.254	20.2	4.165	9.9	3.191	26.9
	Cellotriose	5.303	7.3	4.591	2.7	4.250	20.4	4.165	9.9	3.190	27.5
60	Glucose	5.288	6.7	4.720	2.6	4.237	21.8	4.165	10.1	3.175	28.1
	Cellobiose	5.284	7.2	4.739	2.3	4.235	22.6	4.166	10.2	3.172	28.3
	Cellotriose	5.288	7.6	4.708	2.4	4.238	20.8	4.165	9.8	3.184	28.5

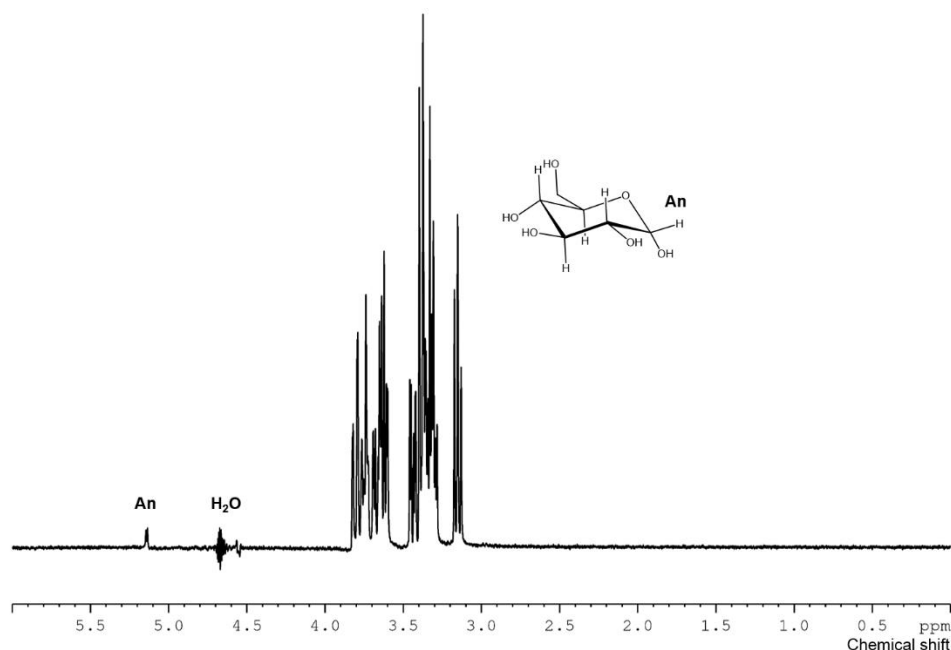


Fig. 2.17 ¹H water suppressed NMR spectrum of D-(+)-Glucose with the respective assignment, highlighting the proton bound to the anomeric carbon and the suppressed water peak.

In Fig. 2.18 the trends in the chemical shift with increasing molecular weight are depicted for AOT and the probe molecule as well as the linewidths at half width (directly related to T_2 and therefore an indication of the variation of τ_c).

As seen in Fig. 2.18, there is a clear difference for AOT chemical shift depending on the size of the micelle, at the two different sizes.

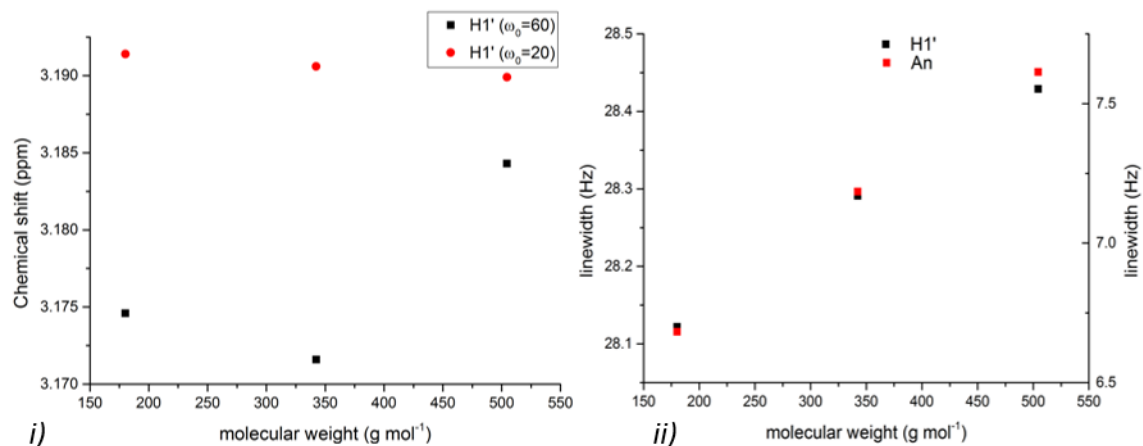


Fig. 2.18 Plots between the chemical shifts of AOT H1' protons, i) and half height line width in $\omega_0=60$ AOT W/O RMs, ii) with the evolution of the molecular weight for each carbohydrate molecule dissolved. In ii) the left y axis refers to H1' and the right y axis refers to An.

While considering $\omega_0=20$, there is a slight decrease in the chemical shift of the H1' proton of AOT, whereas more significant changes, but with no trend are observed in larger sizes micelles.

Comparing the data for the anomeric proton of carbohydrates in reverse micellar solutions and the one of D-(+)-Glucose in water solution (Table A.2), one can observe that there is a significant deshielding

effect due to entrapment. This is more significant in the $\omega_0=20$ micelles, in which there are probably stronger interactions with the negatively charged surfactant molecules. The peaks belonging to the anomeric proton in RM solutions are also broader than those found in the aforementioned aqueous solution of D-(+)-Glucose.

There is indeed a trend between the linewidth of such protons and the size of the carbohydrate in the large micelle conditions (*ii*). An identical one is found in the H1' proton of the AOT polar *head*. This might be due to interactions or perhaps to an alteration in the structure of the aggregates. In order to investigate such hypothesis, NOE studies were conducted, but since the sensitivity is low no specific cross relaxation evidences were found. Therefore, the studies continued towards other experiments, namely relaxation studies and DOSY (the data can be found in Table 2.9). The evolution of the diffusion coefficient of different nuclei is depicted in Fig. 2.19.

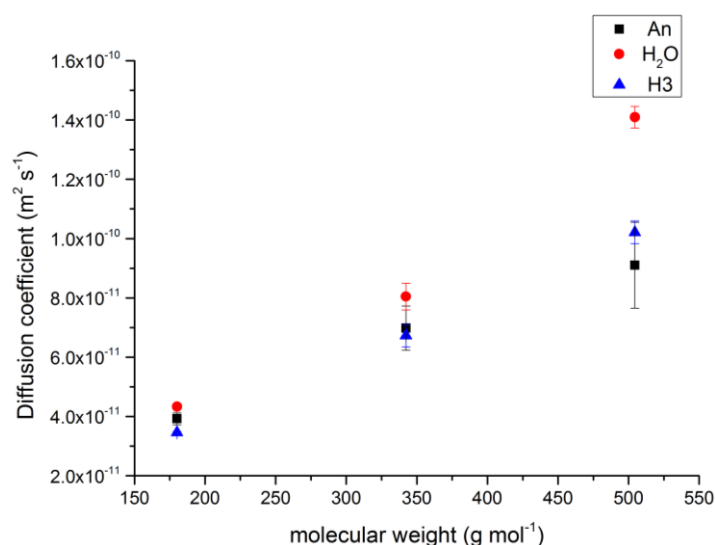


Fig. 2.19 Diffusion coefficients of different protons in $\omega_0=60$ AOT W/O RMs with three different-sizes carbohydrates. This was assessed using a *ledbpgpes2s* pulse sequence.¹²¹ The error bars belong to the error of the fitting.

Table 2.9 Data obtained from the relaxation and diffusion ordered NMR spectroscopy studies for solutions of carbohydrates in AOT W/O RMs. T_1 was assessed by *t1iresgp*; T_2 was assessed by presaturated CPMG for $\omega_0=60$ and CPMG for $\omega_0=20$; DOSY was acquired with *ledbpgpes2s* for $\omega_0=60$ and with *dstebpgp3s* for $\omega_0=20$. Diffusion coefficients (D) is displayed in $m^2 s^{-1}$.

ω_0	sugar	An		H ₂ O				H3		
		T_1 (s)	D ($m^2 s^{-1}$) $\times 10^{-10}$	T_1 (s)	T_2 (s)	τ_c (ns)	D ($m^2 s^{-1}$) $\times 10^{-10}$	T_1 (s)	T_2 (s)	D ($m^2 s^{-1}$) $\times 10^{-10}$
20	Glucose	ND	ND	3.58	0.25	1.60	0.87	0.42	0.02	0.97
	Cellobiose	1.45	ND	2.75	0.29	1.29	0.98	0.41	0.03	0.85
	Cellotriose	1.30	ND	3.62	0.26	1.59	0.93	ND	0.03	0.76
60	Glucose	2.49	0.39	5.74	0.34	1.78	0.43	0.42	0.02	0.35
	Cellobiose	1.76	0.70	5.86	0.33	1.83	0.80	0.42	ND	0.67
	Cellotriose	1.36	0.91	4.92	0.22	2.25	1.41	0.46	ND	1.02

The effect observed in the diffusion coefficients at $\omega_0=60$ while increasing carbohydrate size is identical to the one that occurs with the decrease in the amount of water encapsulated, as can be identified from Table 2.3. This hints that i.e. D-(+)-Cellotriose has a significant effect in the type and size

of aggregate that AOT forms in isooctane. Therefore, using the convection compensated sequence, the diffusion for water protons was assessed in order to investigate the size of these reverse micelles (Table 2.10).

Table 2.10 Diffusional data for water in carbohydrate solutions in AOT W/O RMs. This was obtained using a *dstebgp3s* pulse sequence to determine the hydrodynamic radius, employing the viscosity described in Table 2.1.

ω_0	carbohydrate	$D_{\text{H}_2\text{O}}(\text{m}^2 \text{s}^{-1})$	r_h (nm), H ₂ O
20	D-Glucose	8.68×10^{-11}	5.3
	D-Cellobiose	9.84×10^{-11}	4.7
	D-Cellotriose	9.26×10^{-11}	5.0
60	D-Glucose	4.08×10^{-11}	11.3
	D-Cellobiose	4.25×10^{-11}	10.9
	D-Cellotriose	5.20×10^{-11}	8.9

The effect in terms of size is not significant when $\omega_0=20$ aggregates are considered. These yield a larger size for water than that previously determined for when only water molecules were inside the droplets (Table 2.3), but that is similar in range. However, the same cannot be said for $\omega_0=60$ RMs. There is a trend with increasing solute size (Fig. 2.20) and this corresponds to a decrease in aggregate size that is quite significant. With these data it is possible to affirm that larger solutes can lead to a deformation in the micelle structure. This is supported by the observation of precipitation after several days of the preparation of the samples in the large micellar solutions. This means that possibly the issue at hand is not only the change in size but in shape. If that is the case then the Stokes-Einstein equation must be modified and fitted to other models, such as ellipses or oblates.¹²² However, in such shapes, it would be possible that the radius observed would be larger (since it could be the largest component). Therefore, it is likely that carbohydrates have a cosurfactant effect in the formation of reverse micelles. This can result in the formation of more micelles with smaller radii.

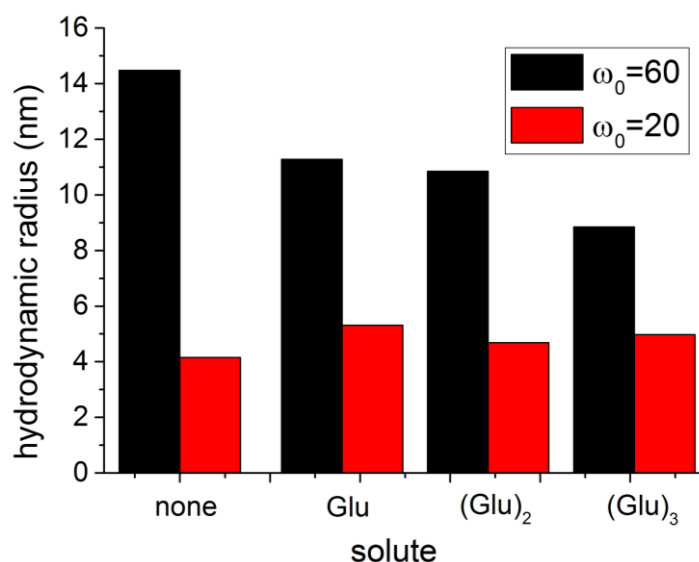


Fig. 2.20 Relation between the hydrodynamic radii from the water diffusion coefficients in $\omega_0=20$ and $\omega_0=60$ AOT W/O RMs with three different-sized carbohydrates and without solute.

Since the number of solutes used is not enough to more accurately evaluate the fitting of the data, this will not be done. Nevertheless, one last question concerning the actual micelles remains, how stable are they in these conditions? This was answered by plotting the diffusion coefficients of water in $\omega_0=60$ W/O AOT solutions containing D-(+)-Glucose against the diffusion times employed (Fig. 2.21).

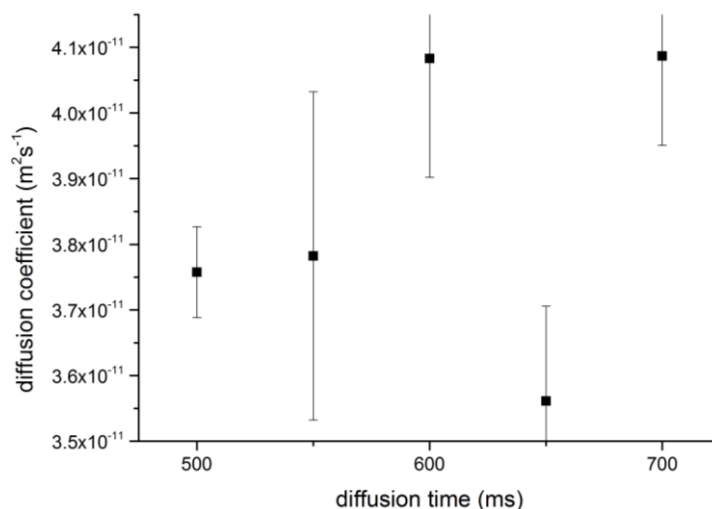


Fig. 2.21 Plot between water diffusion coefficient and time allowed for diffusion in the AOT W/O solution with $\omega_0=60$ and D-(+)-Glucose as a solute, studied by *dstebgp3s*. The error bars belong to the error of the fitting.

Much alike what was previously observed for regular W/O microemulsions, no considerable alterations are observed. Hence it is considered that, at least when this is the solute no exchange processes are observed. It is then considered, that with higher solute sizes, there can be a preferential interaction with the micelle or between the molecules themselves that can lead to some sort of stacking, and eventually lead to a different shape.

So far, the focus has been more on the influence that the carbohydrates employed in this study have on the structure of the RMs in which these are dissolved. But how are the solutes affected? In order to assess this, relaxation studies have been performed.

CPMG data (T_2) did not allow to observe the carbohydrate nuclei, even employing water suppression through presaturation. However, the line broadening previously observed indicate a shorter T_2 than in bulk water. The same is seen for the water molecules. However, if compared to RMs with identical amount of water, the process of spin-spin relaxation is quicker. The dissolved sugar molecules definitely affect viscosity and the dynamics of the system.

There is also a decrease in the spin-lattice relaxation of anomeric protons relatively to the result in bulk water (Table A.2). The correlation between it and the size of the oligomer dissolved in the RMs is somewhat expected, since there is an increase in size (Fig. 2.22).

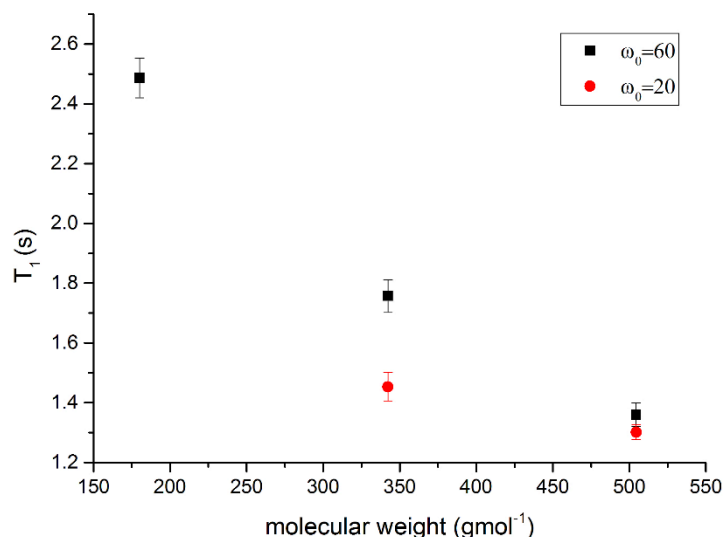


Fig. 2.22 Spin-lattice relaxation times of the anomeric protons of three different-sized carbohydrates in $\omega_0=20$ and $\omega_0=60$ AOT W/O RMs.

The process is likely favoured by the packed environment in which these molecules are dissolved. This clearly affects the dynamics of these carbohydrates, leading to quicker relaxation. This is the opposite of what is intended, but certainly this is due to the attempt of incorporating these molecules in $\omega_0=60$ RMs, which already are on the verge of not forming stable reverse microemulsions. At a smaller micellar size the dynamic alterations observed are less significant.

Finally, it was also attempted to understand how the dynamics of water was affected in these systems by determining its correlation time (Table 2.9). Comparing to the correlation time of water (Table A.2) in a 50mM D-(+)-Glucose solution there is a decrease in these experiments, except for the $\omega_0=60$ solution bearing D-(+)-Cellotriase, which was already proved by diffusion measurements to have a behaviour that is different from the remainder. Since the reduction of the correlation time is the main advantage of using RMs in NMR this is a positive result. Nevertheless, this is higher in these solutions than for equivalent water concentrations without a solute. This can be due to an increase in the aggregate size. According to (18) this is plausible, although it seems more likely that the main effect that must be controlled to achieve lower correlation times is viscosity.

2.2. Application of the NMR methodology to W/CO₂ microemulsions

As was previously mentioned, AOT is insoluble in scCO₂.¹²³ Nevertheless carbon dioxide has an influence on the aggregation of this surfactant.^{124,125} It has also been described that AOT can be dissolved in supercritical CO₂ by adding 7.5 % ethanol as a cosurfactant.¹²⁶ Furthermore other alcohols can be employed for the same task.^{38–40} In this study, the effects of carbon dioxide on the aggregation of AOT will be approached, both while dissolved in water or to assess its ability to form RMs in the supercritical phase.

2.2.1. Influence of CO₂ in AOT aggregation

In order to assess the influence of carbon dioxide on the aggregation of AOT in aqueous solution, HP-fluorescence studies were conducted. For that purpose the probe utilized was Nile red, which has been shown to be solvatochromic in the instance of micellar aggregation occurring.^{127–129} A concentration of probe of 2×10^{-6} M in solutions of 8 mM and 30 mM aqueous solutions of AOT. These were studied at both 25° C and 40° C, as depicted in Fig. 2.23, because to achieve the supercritical phase the temperature must be above 30.97° C.

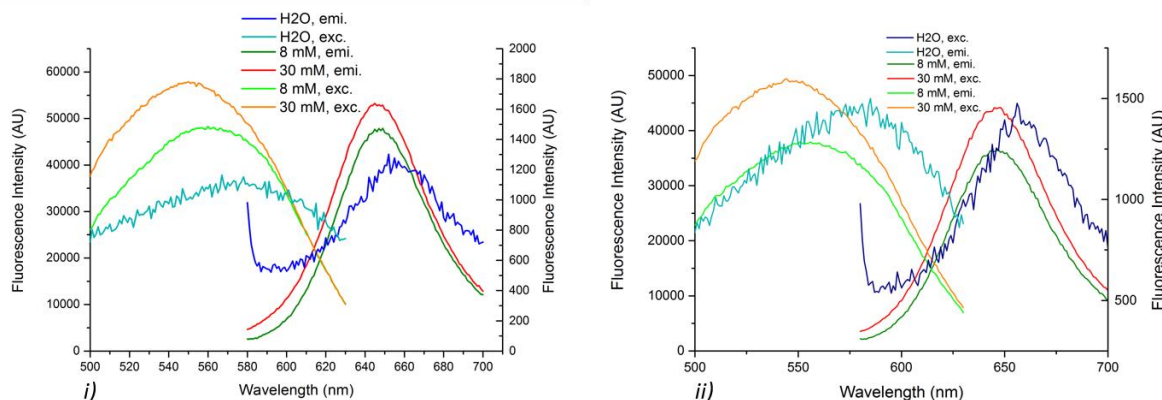


Fig. 2.23 Emission (emi.) and excitation (exc.) spectra at 25° C (i) and at 40° C (ii) of Nile red in water, and aqueous solutions of AOT, 8mM and 30 mM. Excitation spectra were followed at the maximum emission wavelength. Right y axis – spectra in water; left y axis – remaining samples.

The difference in wavelengths registered is not highly significant for these samples, however it is in accordance with previous literature data and it allowed to conduct further studies studies.¹²⁷

A high pressure study was conducted up to a pressure of approx. 64 bar, to study the influence of carbon dioxide in aggregation. This might have a meaning not only to development of CO₂-philic surfactants but, more than that, to CO₂ capture. These results were acquired at 40° C for the 30 mM solution, and are depicted in Fig. 2.24.

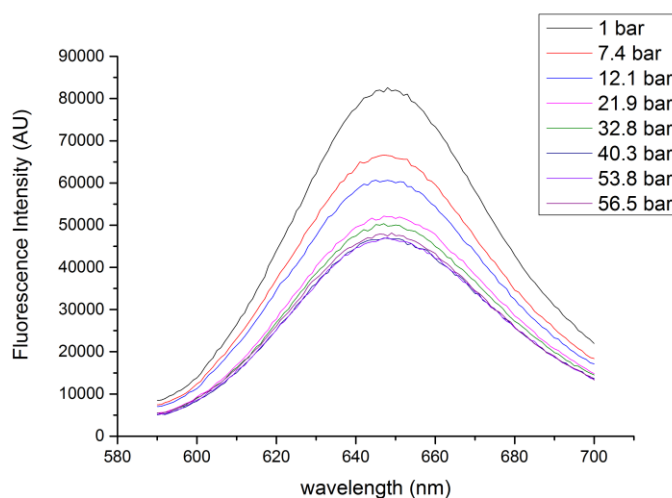


Fig. 2.24 Fluorescence spectra of Nile red in aqueous 30 mM AOT solutions with increasing pressure.

An evolution on emission with the increase in pressure was found, which is in agreement with the literature.¹³⁰ The results obtained for the samples yielded little variation of the maximum emission wavelength. However, a significant variation is observed if the intensity of emission is plotted *versus* the pressure in the system (Fig. 2.25).

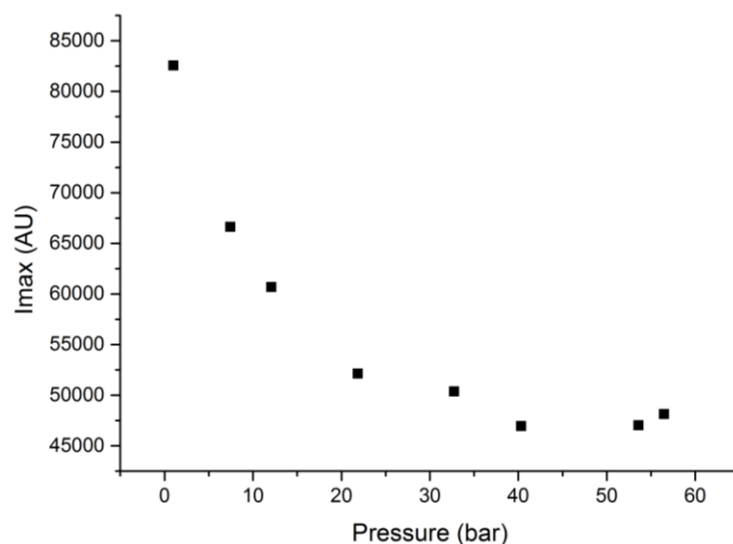


Fig. 2.25 Variation of the intensity of emission of an aqueous AOT Nile red solution with an increase in pressure.

This might be an indication of, either a change in aggregate type up to 30 bar or acidification of the system. This might, however be an interesting system to test novel designed surfactants. It appears that the intensity reaches a plateau, which might correspond that a new form of aggregates was reached.

From all the spectra acquired, the intensities at the maximum emission wavelength (λ_{max}) were gathered. These data are presented below in Table 2.11.

Table 2.11 λ_{max} for the emission of the different samples with $[NR] = 2 \times 10^{-6}$ M in study at 25° C and 40° C.

Solution\ Temperature (° C)	25	40
[AOT]=8 mM	649 nm	647 nm
[AOT]=8 mM; HP	-	641 nm, up to 40 bar
Water	652 nm	656 nm

Even though the variation with gas intake is not very significant, nevertheless a blue shift is observed, if comparing this to a solution of Nile red in water and even water in an aqueous AOT medium. This might indicate that a more nonpolar environment is attained, or it might be due to the water acidification. This methodology allows to observe that even though AOT is not soluble in carbon dioxide, its aggregation is influenced by its presence. Nevertheless more complex fluorescence experiments, such as those employing Förster Resonance Energy Transfer (FRET) can be employed to more

accurately assess the formation of W/CO₂ microemulsions.¹³¹ This is suggested as a future study, though.

2.2.2. Assessment of W/CO₂ microemulsions using NMR spectroscopy

This project has the ultimate goal of observing through NMR spectroscopy large biomolecules encapsulated in W/CO₂ reverse micellar systems. However, to get there it is first necessary to understand whether or not such aggregates are obtained in scCO₂ by NMR spectroscopy. Furthermore the goal is to apply the previously acquired knowledge to understand the size and dynamics of the existent aggregates. For that purpose, a solution of AOT, water and ethanol as a cosurfactant has been employed at different CO₂ pressures.¹³² The experiments were performed above the critical point of CO₂ (30.97° C and 73.74 bar). All were conducted at 40° C (313.15 K), each at a different pressure, depicted in Table 2.12, alongside with the density and viscosity for pure CO₂ at the same pressure and temperature.

Table 2.12 Density and viscosity data for the different CO₂ pressures at 313.15 K used during this work. Mass of carbon dioxide determined from the Peng-Robinson equation.¹³³ Remaining information determined using NIST online tool.¹³⁴

Pressure (bar)\Properties	m _{CO₂} (g)	Density (g/ml)	Viscosity (cP)
93.7	0.51	0.562	0.0412
96.2	0.53	0.594	0.0443
97.3	0.54	0.606	0.0454
118.6	0.66	0.714	0.0580
130.7	0.70	0.745	0.0623
141.4	0.72	0.766	0.0655
142.0	0.73	0.767	0.0657
151.7	0.75	0.783	0.0682

The composition of the system was AOT, water and ethanol as a cosurfactant. Since only 0.1% of the volume was ethanol, according to literature it was assumed that solvent properties are those of supercritical carbon dioxide, thus the data in Table 2.12 corresponding to pure carbon dioxide was used.¹³⁵ 0.002% of water was let inside the reactor and a ω_0 of 3.7 was used.

The first approach towards studying this system is to acquire its ¹H NMR spectrum. The spectrum of AOT, with ethanol and water at 40.0° C and 142.0 bar of CO₂ with the respective assignment is presented in Fig. 2.26.

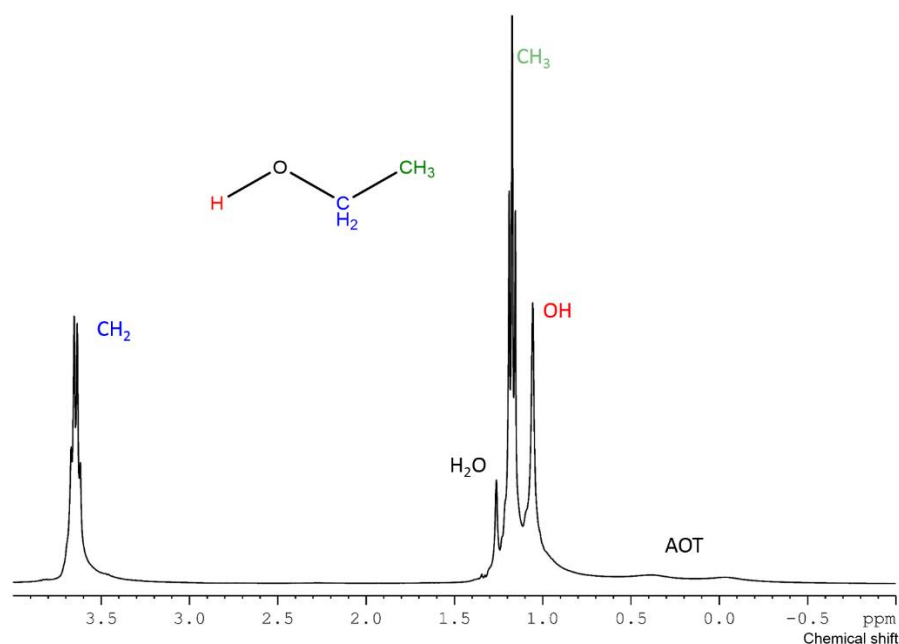


Fig. 2.26 ^1H NMR spectrum of AOT, H_2O and ethanol in scCO_2 ($T=40.0^\circ\text{C}$ and $P=142.0\text{ bar}$) with the assignment of the components.

The first observation concerning the spectrum in Fig. 2.26 is that it displays a degree of anisotropy that has been obtained throughout these studies. This might be due to the nature of the system, consisting of aggregates in scCO_2 , or to some degree of heterogeneity.

Now concerning structural identification, the ethanol alkyl chain peaks are easily identifiable, due to location and multiplicity. A broad peak with low intensity can be found at high field. This is likely to be due to AOT which is in low concentrations and likely aggregated, which is in agreement with the observation. Finally, there are two peaks identified as water and ethanol, but to assign these it was necessary to acquire $^1\text{H},^1\text{H}$ -NOESY spectrum, as shown in Fig. 2.27 (this belongs to a 118.6 bar pressure spectrum, but the issue is the same at all pressures attempted, therefore the information obtained is applicable to the remainder of the spectra).

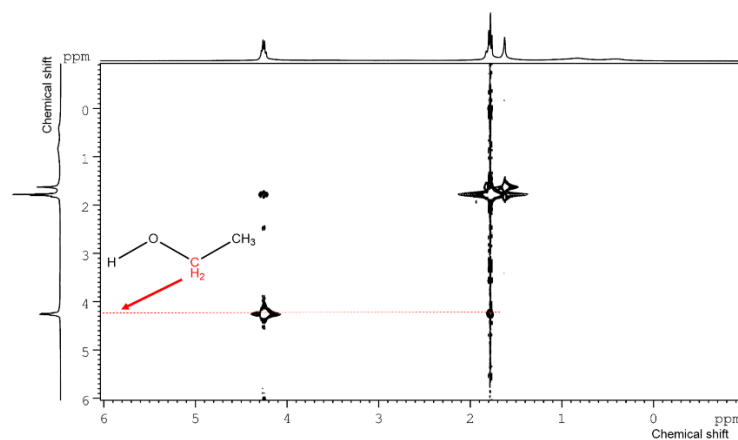


Fig. 2.27 $^1\text{H},^1\text{H}$ -NOESY spectrum of the AOT mixture in scCO_2 ($T=40.0^\circ\text{C}$; $P=118.6\text{ bar}$). The cross relaxation line of the ethanol methylene peak is highlighted.

Through this spectrum alone it is essentially possible to observe that the methyl and methylene groups of ethanol have cross relaxation and that there is exchange between the two OH nuclei, but these remain unidentified. Therefore, the cross relaxation from the ethanol methylene group was extracted and its 1D spectrum is presented in Fig. 2.28.

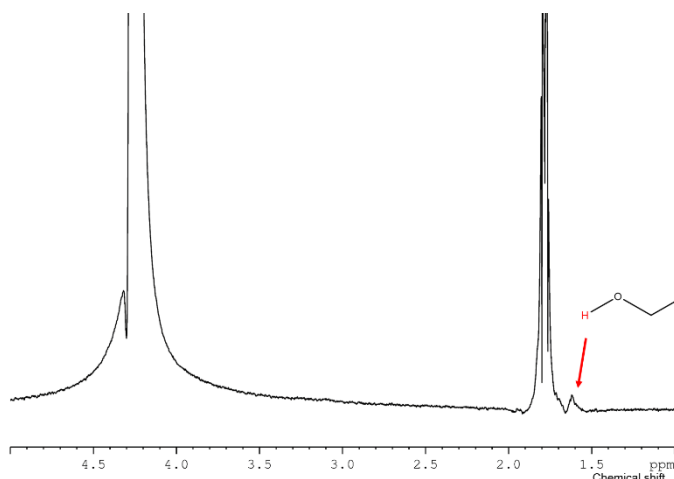


Fig. 2.28 1D projection (extracted from Fig. 2.27) of the NOE spectrum excited at the methylene peak of ethanol.

From Fig. 2.28 it is possible to observe that the phase of the cross relaxation between methylene and itself is positive. This corresponds to an exchange peak. The contact with the ethanol methyl protons has the same phase, as does the one with the hydroxyl group at higher field. No cross peak with the other hydroxyl protons is detected. It is then concluded that the only hydroxyl group that can be exchanging, even if weakly, with the ethanol methylene is the one belonging to the same molecule. Therefore from here on the assignment found in Fig. 2.26 will be applied to all spectra. The data obtained through 1D ¹H spectra is depicted in Table 2.13. The chemical shifts were determined by using the ethanol methyl group as a reference. This was proved as a good approach by using TMS in some samples.

Table 2.13 Observables (obs) taken from 1D ¹H NMR spectra for the AOT mixture in scCO₂, at 40° C at different pressures. The methyl group of ethanol has a constant chemical shift displacement because it was used as a reference.

P(bar)\ ¹ H obs	CH ₂ , EtOH		H ₂ O		CH ₃ , EtOH		OH, EtOH		AOT	
	$\Delta\delta$ (ppm)	$\nu_{1/2}$ (Hz)	$\Delta\delta$ (ppm)	$\nu_{1/2}$ (Hz)	$\Delta\delta$ (ppm)	$\nu_{1/2}$ (Hz)	$\Delta\delta$ (ppm)	$\nu_{1/2}$ (Hz)	$\Delta\delta$ (ppm)	$\nu_{1/2}$ (Hz)
93.7	3.656	16.61	1.249	15.54	1.172	16.83	1.120	14.14	ND	ND
96.2	3.656	17.01	1.262	18.61	1.172	16.27	1.125	12.62	ND	ND
97.3	3.656	16.38	1.233	13.99	1.172	16.35	1.085	10.89	-0.049	223.37
118.6	3.654	16.56	1.218	8.91	1.172	15.54	1.017	8.27	0.216	158.56
130.7	3.653	12.54	1.224	8.31	1.172	15.07	1.013	8.07	0.334	179.96
142.0	3.653	16.91	1.262	7.43	1.172	15.37	1.056	8.84	0.382	169.71
151.7	3.652	11.98	1.276	11.25	1.172	15.46	1.077	8.91	ND	ND

First of all we shall address what is expected. In this case if there is simply a linear trend with the increase in pressure this means that the protons are simply being affected by the solvent density (which is directly affected by the increase in pressure, as can be seen in Table 2.12). This would mean that an alteration only due to solvation by scCO₂ would be occurring. Obviously, if the starting system is already a RM then this sort of trend would be expected, because it would show something alike the variation of water content. It is expected though that a pressure of at least 100 bar would be necessary to attain microemulsions with AOT.¹³² Therefore it is expected that the lower pressures applied will lead to a different sort of aggregate than the larger ones. Something alike an inversion of the evolution or a plateau would therefore be expected for the formation of RMs, or something resembling such systems.

Observing Table 2.13 and Fig. 2.29 it is possible to witness a constant evolution of the chemical shift displacements of the ethanol methylene protons with the increase in pressure, while the linewidth at half height does not have any clear sort of effect. AOT becomes more shielded at higher pressures, which might hint that it is being solubilized or, most likely, interacting more strongly with water. The AOT linewidths are deemed as unreliable, since it has a broad and low sensitive peak. Whereas the ethanol methyl protons show an inflection from 130.7 bar on. This might indicate an alteration in the structure present in solution. This is further addressed in light of the variations in the hydroxyl groups, depicted in Fig. 2.29.

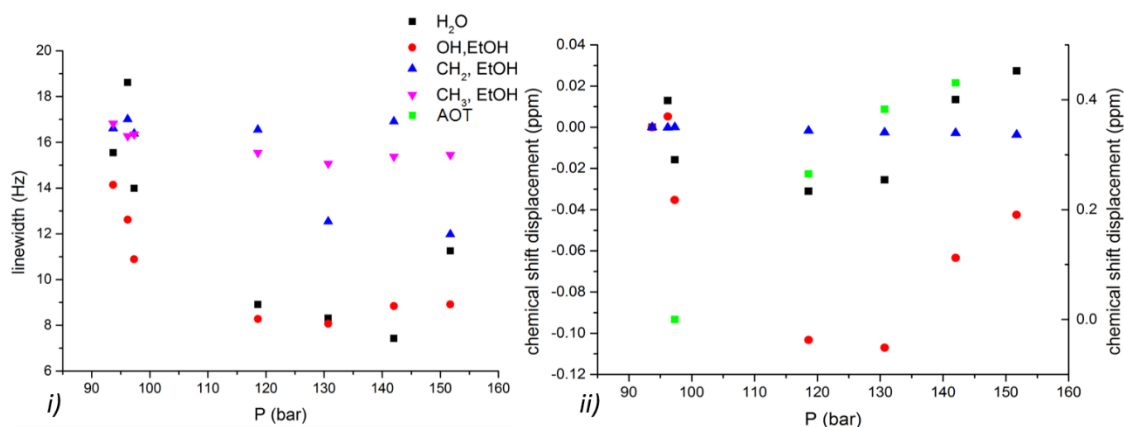


Fig. 2.29 Relation between half-height linewidth (i), chemical shift displacement, using the lowest pressure point as a zero (ii) and the pressure of the system bearing AOT and water, at 40.0° C. The methyl group of ethanol was used as a chemical shift reference and is therefore not depicted. In ii) the right y axis corresponds to AOT, whereas the left y axis corresponds to the remainder nuclei.

In Fig. 2.29 it is possible to identify that at lower pressures the chemical shift or linewidth is approx. at its maximum for this study, reaching then a minimum between 120 and 130 bar and then both observables start to increase again. Both hydroxyl groups have the same sort of behaviour through these studies, which might indicate identical environments. No consistent variation of the alkyl protons of ethanol is observed, which indicates that its solubilization process is not significantly influenced by the increase in density. It was not possible to determine the linewidth of AOT due to low sensitivity. Now, focusing on i), at lower pressures the linewidth is higher and it quickly decreases towards sharper lines and then again increasing. This is observed for both hydroxyl groups and it can be due to a solubilization of the molecules with the increase in pressure, until a plateau is reached. After the pressure required to

dissolve the solutes is reached then aggregation may start to occur, which can explain the increase in linewidth observed. The sort of behaviour observed in the chemical shift displacements (*ii*) of the hydroxyl protons is identical to the one previously described. Since the dissolution in a nonpolar environment can lead to deshielding what is observed in Fig. 2.29 at lower pressures can also be explained in this fashion, as does the deshielding at higher ones, since it corresponds to the constitution of a tighter water pool that is encapsulated. It was also possible to obtain the displacements of AOT chemical shifts at several pressures (the fact that it was not possible at every condition might indicate either insolubility at lower pressures as aggregation at higher ones). These have a steady increase alongside pressure of carbon dioxide, which can be related to the formation of water pools, thus a more polar medium surrounding it.

All of the above observations suggest that at pressures below 100 bar likely the system is not homogeneous, or at least not all the systems components are solubilized. This is reached around 120 bar and above 130 bar there are indications that a microemulsion is reached.

2.2.2.1. Homogeneity assessment of W/CO₂ microemulsions

NMR is not an optical spectroscopy, hence it is not as standard as in other techniques to understand whether or not there is phase separation or heterogeneity. This can be indirectly observed through shimming effects, however a more quantitative way to assess it is desirable. This is possible to do if one uses the main underlying principle to magnetic resonance imaging (MRI) that is spatial encoding.¹³⁶ The technique described from here on is slice selective NMR,^{137,138} and it may be useful to approach nonhomogeneous systems.¹³⁹ This is achieved by the use of pulsed field gradients, much alike DOSY.¹⁴⁰ The application of a gradient throughout a sample gives rise to frequency encoding according to spatial location (as it is demonstrated in (19) (B_z is the magnetic field of a specific spin and G_z is the gradient strength), each spin's frequency will depend on the local gradient).

$$B_z = B_0 + G_z \quad (19)$$

This divides the tube in different frequency encoded slices, with a frequency variation per unit of length, $\Delta\nu$ that relies on the gradient strength and the gyromagnetic constant (γ), as shown in (20).

$$\Delta\nu = \gamma G_z \quad (20)$$

If alongside this PFG one applies a selective pulse (either for excitation or refocusing purposes), which is a shaped pulse with small bandwidth (BW) comparing to a hard pulse,¹⁴¹ a slice of a certain thickness (Δz) is obtained, as demonstrated in . By varying the offset at which this shaped pulse excites is centred, it is possible to image the NMR tube (as depicted in Fig. 2.30).

$$\Delta z = \frac{BW}{\Delta\nu} \quad (21)$$

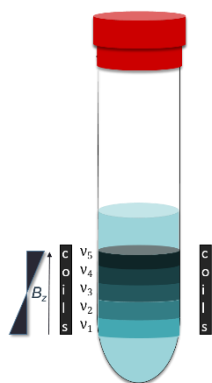


Fig. 2.30 Schematic representation of the NMR slice selection procedure.

This type of NMR technique has been already shown to be useful to approach the diffusion of carbon dioxide into an ionic liquid phase, by the means of ¹³C slice selective spectra throughout a certain period of time.¹⁴² It may allow to understand whether or not the micellar phases dispersed in scCO₂ are evenly distributed or there is a phase separation. A rotating frame imaging technique has already been applied for this purpose.⁶⁷ However, this requires a specific probe while the technique employed from here on can be conducted in a standard liquids spectrometer with a standard probe.

For the ¹H slice selective spectra, the tube was split into 11 0.9 mm slices. A sequential increment of the offset of the selective pulse was set in order to have 1.2 mm differences between each thus ensuring that no spatial overlapping would occur. Since ¹³C is less abundant 3.7 mm slices have been employed in its slice selective spectra, split apart by 4.7 mm. In this case 4 spectra were acquired. A demonstration of the application using both ¹H and ¹³C NMR slice selective pulse sequences to an AOT solution in 93.7 bar of carbon dioxide at 40.0° C is demonstrated in Fig. 2.31.

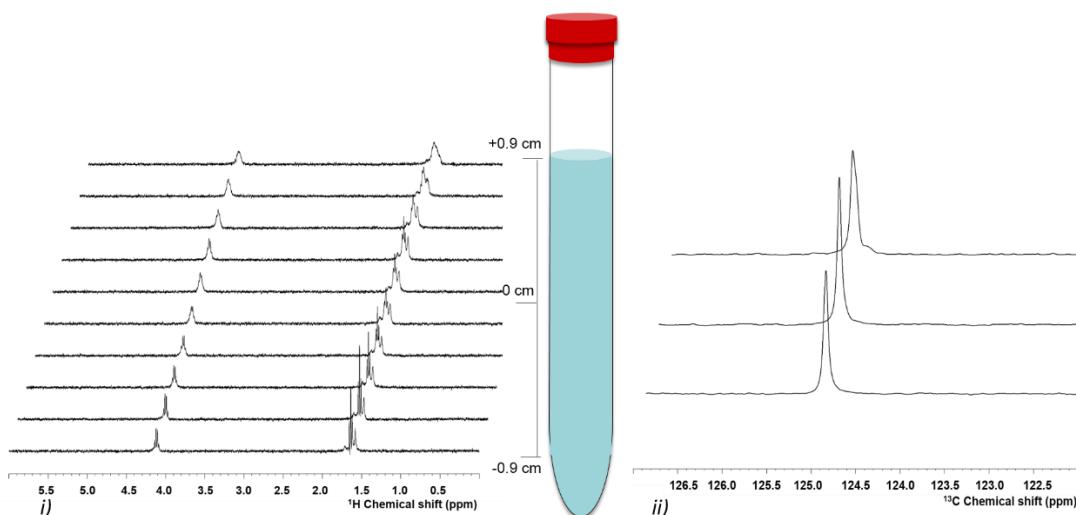


Fig. 2.31 ¹H (i) and ¹³C, displaying only the CO₂ signal (ii) slice selective spectra for a solution of AOT with ethanol and water in 93.7 bar of CO₂ at 40.0° C.

While imaging this system on the z axis, different outcomes can be expected. If a biphasic system is obtained, it is likely that two clearly distinct spectra are obtained from each phase, just alike what Kozminski demonstrated.¹³⁷ If some sort of nonhomogeneous system exists then different chemical

shifts or linewidths can be obtained, due to different local environments. However, if there is a clearly homogeneous solution then identical spectra ought to be obtained at each slice.

By observing Fig. 2.31 one can conclude that the ¹H NMR spectrum maintains itself approx. constant at bottom slices. However, it is observable that at the upper end of the tube there is line broadening that can be due to a different environment in that section. The ¹³C signals have a growing intensity from the bottom (not only the lowest section that is at the bottom of the coils and therefore has necessarily less intensity but also the following one displays this phenomenon) to the top of the tube. This is a way of understanding that the system does not have a homogeneous distribution of the solvent. This is in agreement with the previous observations through the one-dimensional NMR observables (section 2.2.2) that indicated that at lower pressures the system does not form stable aggregates.

Therefore, this procedure was also attempted at a higher pressure as is depicted in Fig. 2.32, for a pressure of 151.7 bar.

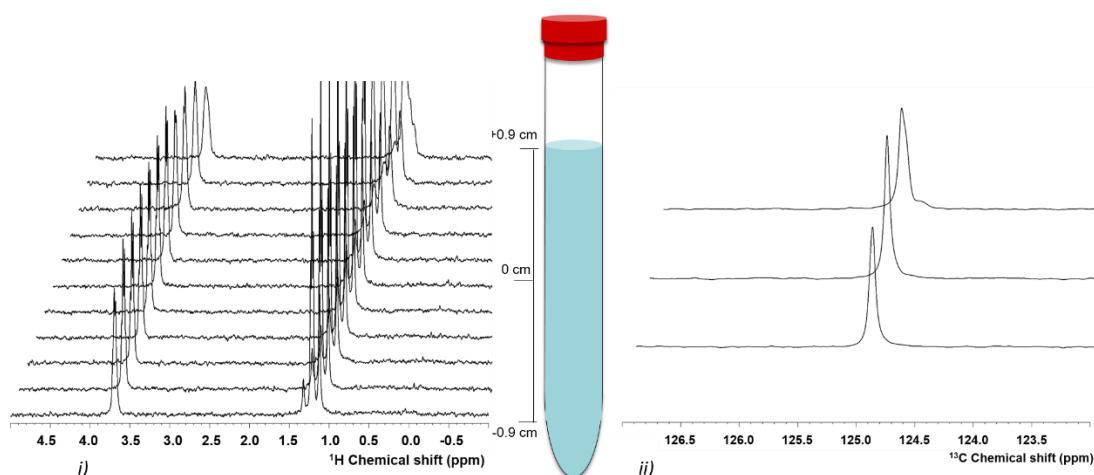


Fig. 2.32 ¹H (i) and ¹³C, displaying only the CO₂ signal (ii) slice selective spectra for a solution of AOT with ethanol and water in 151.7 bar of CO₂ at 40.0° C.

The ¹H spectra demonstrate that only at the top of the tube is possible to observe an increase in linewidth, as before. Something identical to what was seen before at a lower pressure is also observed in the case of carbon dioxide. Nevertheless, the intensities are more even throughout the tube. Still, it is likely that no complete homogeneous was attained, which might be due not only to the nature of the surfactant but most likely to technical issues with the mixing of the sample.

From all these data it is possible to observe that since only approx. 10 µl of sample were used, it would not be possible to obtain ¹H spectra throughout the different slices if there was a clear biphasic system. Thus it was possible to conclude that at least a dispersion of the sample components in the solvent was obtained. And it was confirmed that the sample is approx. evenly distributed, whereas the same was not always observed for carbon dioxide.

2.2.2.2. Diffusion of W/CO₂ microemulsions

Alike what was done for reverse micellar systems dispersed in an isooctane phase, diffusion coefficients were assessed using diffusion ordered NMR spectroscopy. The results from the experimental data are presented in Table 2.14.

Table 2.14 Diffusional data obtained from W/CO₂ microemulsions at different pressures of carbon dioxide. The diffusion coefficient of ethanol is the average between the diffusion coefficients of its methyl and methylene proton peaks and the error corresponds to its standard deviation.

P (bar)\D	D_{EtOH} (m ² s ⁻¹)	D_{H_2O} (m ² s ⁻¹)	$D_{OH, EtOH}$ (m ² s ⁻¹)	D_{AOT} (m ² s ⁻¹)
93.7	(3.01±0.06) x10 ⁻⁸	3.93 x10 ⁻⁸	3.51 x10 ⁻⁸	ND
96.2	(2.61±0.01) x10 ⁻⁸	3.34 x10 ⁻⁸	2.83 x10 ⁻⁸	ND
118.6	(1.68±0.01) x10 ⁻⁸	1.98 x10 ⁻⁸	1.77 x10 ⁻⁸	1.41 x10 ⁻¹⁰
130.7	(1.53±0.03) x10 ⁻⁸	2.26 x10 ⁻⁸	1.57 x10 ⁻⁸	ND
142.0	(1.37±0.03) x10 ⁻⁸	1.86 x10 ⁻⁸	1.51 x10 ⁻⁸	ND
151.7	(1.44±0.01) x10 ⁻⁸	1.92 x10 ⁻⁸	1.46 x10 ⁻⁸	ND

The data presented in Table 2.14 show that the diffusion coefficients observed for this system are considerably faster than those observed in a regular oil phase (Table 2.3). This is due to supercritical CO₂ being considerably less viscous than a regular organic solvent. The evolution of the diffusion coefficients at different pressures is displayed in Fig. 2.33.

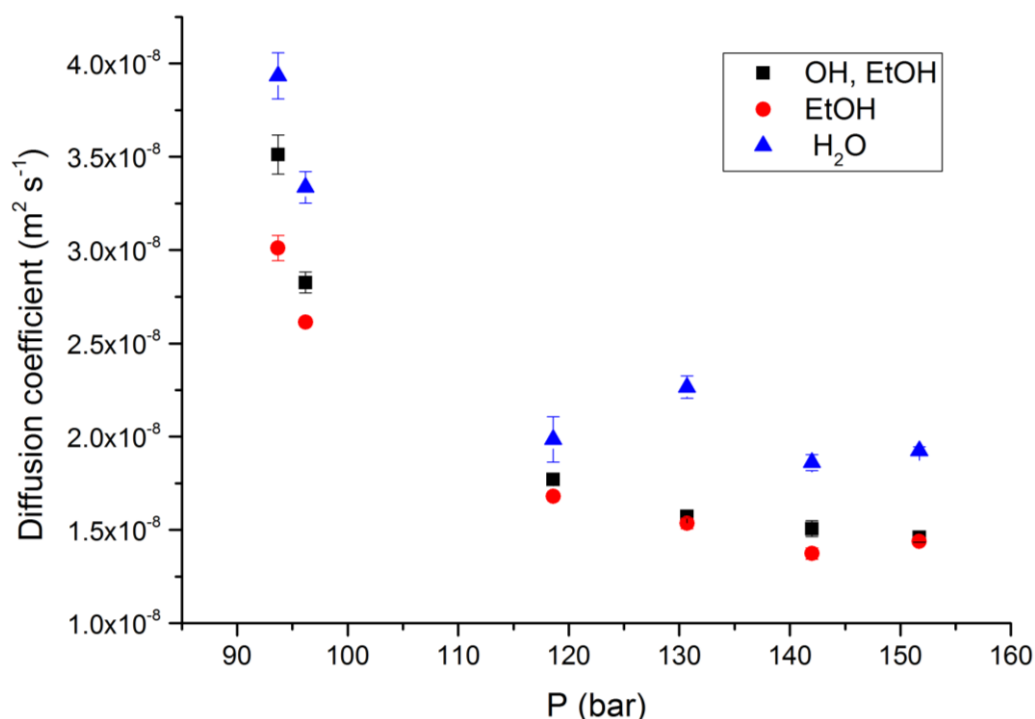


Fig. 2.33 Plot between diffusion coefficients of the components in the AOT, ethanol, water in scCO₂ mixture, at 40.0° C. The error bars belong to the error of the fitting.

Approx. the same trend is observed for every proton. An initial decrease in diffusion occurs until ~120 bar after which a plateau is reached. Alike what was previously discussed, this might be due to an

increase in solubility. Aggregation is likely to occur, and that would lead to a larger, slower diffusing system. Furthermore, it is possible to observe that even though water has a behaviour identical to that of ethanol, even though NOE data evidences that the hydroxyl protons of these two molecules are exchanging (Fig. 2.27), the hydroxyl proton of ethanol resembles more to the remainder of its molecule than to water. This can obviously be related to size, but it can also be due to water being entrapped in RMs. Nonetheless, the diffusion coefficients obtained are one order of magnitude faster than those previously obtained for two RM systems in scCO₂.^{22,65} Nevertheless, in the literature, the variation of diffusion coefficient with an increase in pressure is identical to the one obtained higher for higher pressures. Xu *et al*²² also state that the observed diffusion of water will be larger than the one inside the micelles, because there is water diffusing in carbon dioxide and trapped inside the micelles, as shown by (22), in which D_{water/CO_2} is the diffusion of water in CO₂, f_A is the fraction of water dissolved in the CO₂ continuous phase and D_{ME} is the microemulsion diffusion that is the same as the surfactant.

$$D_{water} = f_A D_{water/CO_2} + (1 - f_A) D_{ME} \quad (22)$$

The diffusion of water in carbon dioxide at different pressures has been described in the literature and at different temperatures.¹⁴³ It was not described at 40° C, but it was at 35° C, at supercritical conditions. This is an approximation to the conditions used in this work, in order to understand the amount of water diffusing in the SCF phase. Therefore, the data from the literature was plotted as shown in Fig. A.9 and equation (25) to relate D_{water/CO_2} and the pressure of the system. This was used with the data of Table 2.14 for the pressure of 118.6 bar and the fraction of water in carbon dioxide determined was 0.62, thus only 38% of water is entrapped in the reverse micellar system. Naturally, this is not completely accurate, it is just an indication of how much water can be inside the microemulsions. Also, the data show that the diffusion is likely to be higher at a higher temperature. Therefore the amount of water in RMs should be slightly higher than the one estimated. Nevertheless this shows that most of the aqueous phase would not be trapped, but dispersed in carbon dioxide, perhaps mediated by ethanol since these have identical diffusional behaviours. Since the diffusion of the reverse micelle corresponds to the one of the surfactant the hydrodynamic radii of the aggregate cannot be measured from the diffusion of water. This must be done through the AOT diffusion coefficient, which was only obtained at one pressure. By using (3) and the viscosity for this pressure from Table 2.12 an r_h of 26.7±10.8 nm is obtained. According to the chemical shift and linewidth observations, it is likely that at these conditions, a stable microemulsion was not formed, thus this might even be an indication of widely polydisperse aggregates. Therefore it was chosen not to use the previously devised scaling factor (10). This approach shall be repeated in the future with a higher amount of surfactant and also by getting the diffusion data of water in CO₂ at 40° C. This is nevertheless a good way to understand that water inside micelles in scCO₂ has a fast dynamics. Due to the order of magnitude of the diffusion coefficient of AOT and the behaviour of water, the data indicates that reverse micelles are possibly being formed, even though it was only possible to determine a wide size range. Furthermore, a slice selective DOSY experiment, which has already been described,¹⁴⁴ can also be a good way to assess whether or not there are

different sorts of aggregates and systems throughout the tube due to heterogeneity, which section 2.2.2.1 confirmed to be occurring in some situations.

2.2.2.3. Dynamics of RMs in scCO₂ studied by NMR

The previous chapter has already indicated that the dynamics of water in RMs in scCO₂ is a subject of significant relevance. Alike what was done for AOT W/O microemulsions, relaxation parameters were assessed for the different components of the mixture, and the results are gathered in Table 2.15.

Table 2.15 Spin-lattice relaxation data for the mixture of AOT, H₂O and ethanol in scCO₂ at 40° C and at different pressures.

P(bar)\T ₁ (s)	T _{1(CH₂), EtOH} (s)	T _{1(D₂O)} (s)	T _{1(CH₃), EtOH} (s)	T _{1(OH), EtOH} (s)	T _{1(AOT)} (s)
96.2	2.07	1.22	2.51	1.69	ND
97.3	2.08	ND	ND	2.46	0.44
118.6	2.95	2.26	3.41	2.35	0.52
130.7	2.16	2.04	3.04	1.96	0.49
142.0	3.41	2.79	4.25	2.54	0.59
151.7	2.66	2.08	3.14	2.25	ND

Reasonably larger relaxation times were obtained for the different components of this mixture, which are identical to the ones obtained for AOT W/O RMs (Table 2.5), which indicates a somehow similar behaviour. The graph of the evolution of spin-lattice relaxation times with the increase in pressure is depicted in Fig. 2.34.

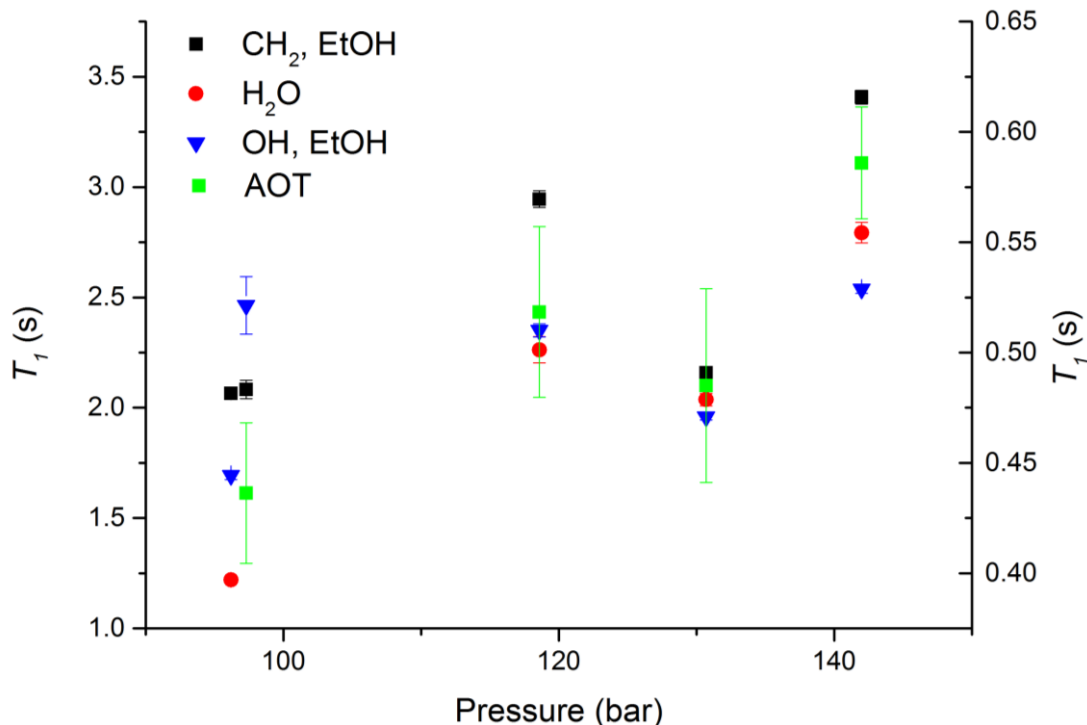


Fig. 2.34 Relation between the spin-lattice relaxation time of the mixture components at 40° C and different pressures. The right y axis is the AOT scale, whereas the left one is used for the remainder of the protons. The error bars belong to the error of the fitting.

From Fig. 2.34 it can be seen that T_1 increases with an increase in pressure, even though this does not occur in a linear fashion. While increasing pressure, the viscosity of the system increases, as demonstrated in Table 2.12. Alongside the increase in viscosity, also the correlation time increases (18). It is then observed that T_1 is increasing with the increase of τ_c , which indicates that this system is behaving according to a large molecular regime (Fig. 1.8). This is one more information to add to the hypothesis of the formation of aggregates, and at some point of reverse micelles.

As previously mentioned, the ultimate goal of this project is to encapsulate large biomacromolecules in W/CO₂ in order to study them by NMR spectroscopy. Hence, a final attempt was made to test this system for encapsulation. An aqueous saturated solution of D-(+)-Glucose (lower concentrations would not provide sufficient sensitivity and these were successfully tested in D₂O, Fig. A.10) was dispersed in CO₂ alongside AOT and ethanol as a cosurfactant, in the conditions previously used, at 141.4 bar at 40° C. The results obtained from the experiment in scCO₂ medium are depicted in Fig. 2.35.

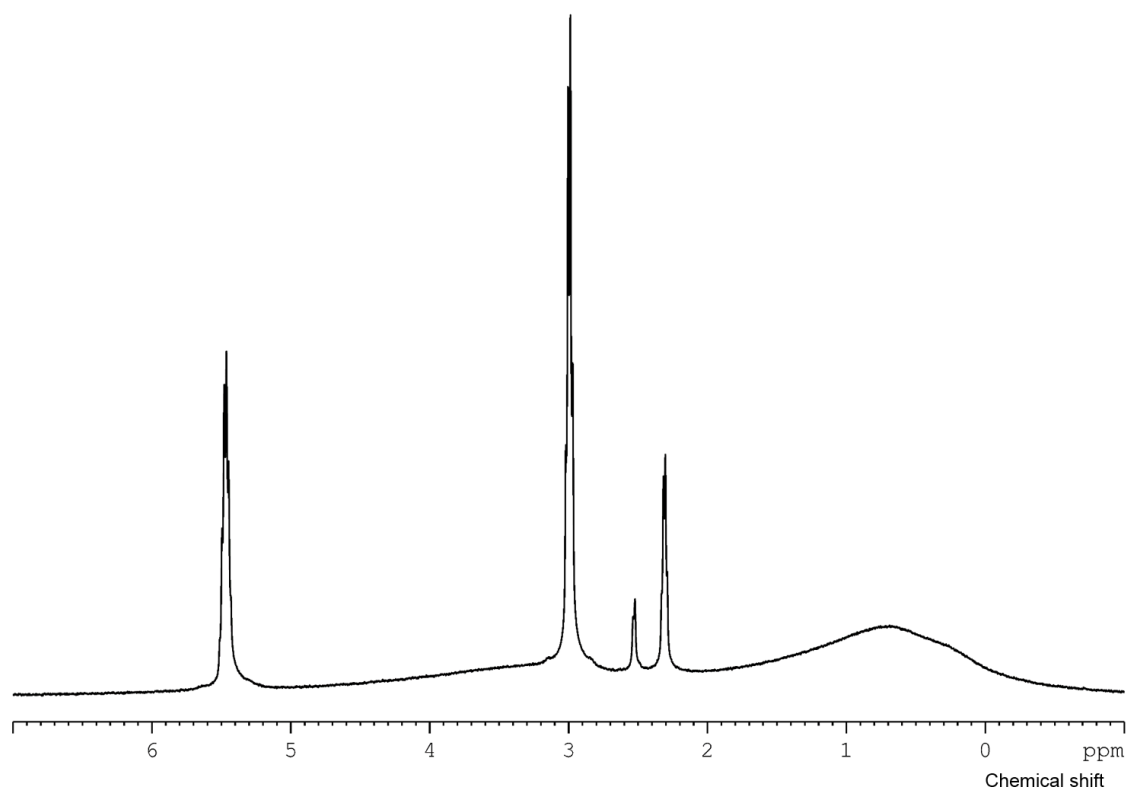


Fig. 2.35 ¹H NMR spectrum of a saturated D-(+)-Glucose solution in a solution of AOT, ethanol and water dispersed in supercritical carbon dioxide at 141.4 bar at 40.0 °C.

As it is easily noted, the spectrum does not have high resolution presenting very broad signals. This is probably due to the fact that the mixture was not homogeneous. Also, no D-(+)-Glucose peaks can be identified. It is likely that the peak close to 1 ppm belongs to AOT, however the solute is not identifiable. Furthermore, it is probable that the mixture did not form a RM, because of its clear

heterogeneity. Therefore a reasonable explanation is that the high concentration of carbohydrate is affecting the stability of the RM, alike what was observed in section 2.1.3.

In order to achieve this sort of experiments, it is probable that a higher amount of water and/or surfactant are needed. It is also likely that a more CO₂-philic surfactant has to be used. In this work, a possible candidate for this task was synthesized, however it was not possible to test it yet. Nevertheless, it was possible to attain a methodology that is useful in assessing W/CO₂ microemulsions.

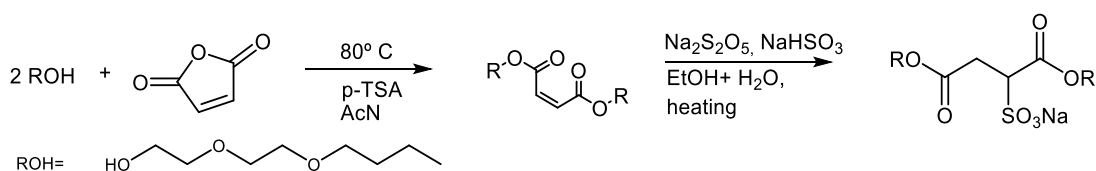
2.3. Experimental section

2.3.1. Chemicals

In this work the following chemicals were used: maleic acid (Matheson, Coleman & Bell), triethylene glycol monomethyl ether (Fluka, 97%), diethylene glycol monobutyl ether (Fischer Lab.), triethylene glycol monomethyl ether (Aldrich, 95%), Sodium 1,4-bis(2-ethylhexyl) sulfosuccinate (Sigma Aldrich, 98%), tetramethylsilane (euriso-top), sulfuric acid (J.T. Baker, ACS grade), anhydrous sodium sulfate (Fisher Scientific, ACS grade), boron trifluoride diethyl etherate (Sigma Aldrich, redistilled), maleic anhydride (Alfa Aesar, 98%), sodium bisulfite (Fisher Scientific, ACS grade), sodium metabisulfite (Sigma Aldrich, 97%), p-toluene sulfonic acid monohydrate (Acros), Nile red (Aldrich), deuterium oxide (euriso-top, 99.85% D), ethanol absolute, (Sigma Aldrich), D-(+)-Glucose (Scharlau, extra pure), D-(+)-Cellobiose (Fluka, >99%) D-(+)-Cellotriase (Megazyme, ~95%), isooctane, filtered (Merck, p.a.) and MilliQ water. The liquids were employed without further purification, while the solids were dried under vacuum. Furthermore, carbon dioxide was supplied by Air Liquide with purity above 99.998%.

2.3.2. Synthetic procedures

The development of AOT-based surfactants was attempted through several methodologies. Essentially, Scheme 1 shows one of the approaches attempted. The other ones use maleic anhydride (maleic acid was also tried) as a starting material. Several catalysts were employed for reaction's the first step, such as sulfuric acid, boron trifluoride diethyl and p-toluenesulfonic acid (p-TSA). The best results were provided by p-TSA.



Scheme 1 Synthetic procedure to obtain an AOT-based surfactant.

The synthesis was conducted according to a literature protocol.¹⁴⁵ 800.0 mg (8.16 mmol) of maleic anhydride were dissolved in 4 ml (23.84 mmol) of diethylene glycol monobutyl ether, with 500 µl of acetonitrile. 1.015 g (6.12 mmol) of p-TSA added as a catalyst. The reaction was kept under nitrogen atmosphere and vacuum cycles were performed. The mixture was heated to 80° C overnight. It was followed via TLC using an eluent composed of ethyl acetate and methanol (8:2) and revealed by UV

light and iodine. When the spot of the product was already significant the reaction was stopped. It was evaporated over vacuum. Then it was cooled under ice and neutralized with a saturated solution of sodium carbonate. The organic layer was extracted with dichloromethane, which was then dried with anhydrous magnesium sulfate. The solvent was evaporated under vacuum, 412.50 mg (12.5 %) of a yellow oil were obtained. This was analysed via ¹H NMR spectroscopy and utilized in the next step.

369.3 mg (0.91 mmol) of the product were dissolved in 4.1 ml of ethanol, to which a 4.5 ml of water solution with 182.6 (1.37 mmol) of sodium bisulfite and 272.2 mg (1.37 mmol) of sodium metabisulfite was added. The mixture was kept under nitrogen atmosphere and heated and stirred for 5 hours. This was followed by NMR spectroscopy. The reaction was stopped when the sulfonate adjacent protons appeared and the double ones disappeared. The mixture was evaporated and a mixture of ethanol and water was used to precipitate the undesired salts, which were filtered. The light yellow solid was then dried, having 100.3 mg (2.7 %) been obtained (which probably was not entirely pure). This was analysed via ¹H and ¹³C NMR spectroscopy.

¹H NMR (400 MHz, D₂O): δ (ppm) = 4.37 – 4.09 (m, 5H), 3.62 (m, 14H), 3.44 (d, 4H), 3.04 (m, 4H), 2.85 (m, 2H), 1.42 (q, 4H), 1.23 (q, 4H), 0.79 (t, 6H).

2.3.3. Physicochemical studies of W/O microemulsions

For the W/O microemulsion assays, a solution of AOT in isooctane with a concentration of 0.1 M was prepared by dissolving 1.1116 g in 25 ml of isooctane. To prepare the RMs, the solutions described in Table 2.16 were prepared by adding water (9:1, D₂O:H₂O) to a certain volume of the isooctane solution of AOT.

Table 2.16 Experimental amounts of the solution of AOT in isooctane and water added to prepare the different solutions used in this study.

ω_0	$V_{\text{isooctane}}$ (μl)	V_{water} (μl)
1	1996.4	3.6
5	1982.2	17.8
10	1964.6	35.4
20	1930.5	69.5
30	1897.5	102.5
40	1865.7	134.3
50	1834.9	165.1
60	1805.1	194.9

To prepare the RM solution bearing carbohydrates, the proportions of isooctane and water (in this case with a carbohydrate) as the ones described in Table 2.16 were added to prepare the $\omega_0=60$ and $\omega_0=20$ solutions. But first 50 mM solutions of carbohydrates were prepared. 45.7 mg of D-(+)-Glucose were dissolved in 5 ml of 9:1, D₂O:H₂O. The same was done for the remaining sugars, but by adding 51.5 mg of D-(+)-Cellobiose to 3 ml of water with the same composition, and 8.8 mg of D-(+)-Cellobiose to 348.9 μl of the same water solution. After the preparation, all samples were under ultrasound radiation for approx. 10 minutes and were filtered.

2.3.3.1. DLS measurements

All Dynamic Light Scattering experiments were performed at 25.0 ° C on a Nano Particle analyzer, SZ-100-Z (Horiba Scientific) at a 90° angle, equipped with a DPSS (Diode Pumped Solid-state - $\lambda = 532$ nm , 10 mW) laser.

A cumulant analysis was performed to extract the size of the particles. Each experiment was conducted on average for 180 seconds. Each sample was measured at least three times to perform an average and to determine the standard deviation

2.3.3.2. NMR experiments

All NMR spectra were acquired on a Bruker Avance III 400 spectrometer equipped with a multinuclear direct detection probehead (BBO), a temperature control unit, and a pulse gradient unit capable of producing magnetic field pulsed gradients in the z direction of 56.0 G cm⁻¹ operating at 400.15 MHz for hydrogen, and 100.61 MHz for carbon. Temperature was set and stabilized using the spectrometer hardware. All NMR studies of W/O microemulsions were conducted at 25° C.

¹H NMR spectra (taken with zg30) were acquired with 64k time domain points over a spectral window of 8223.68 Hz (20.5514 ppm), centered at 2471.09 Hz (6.175 ppm) and with 32 scans and 2 dummy scans per FID. Relaxation delays between of 1 second were used. Typical 90 degree pulse lengths were, as an example, 11.60 μ s. In order to perform chemical shift measurements, all spectra were referenced by the peak of nucleus A belonging to isooctane, set at 1.7117 ppm, which corresponds to its chemical shift in CDCl₃ (Fig. A.1).

In order to obtain ¹H solvent suppressed spectra were acquired using an excitation sculpting routine (zgesgp).¹⁴⁶ This was done by the aid of a sine (Sinc1.1000) shaped pulse with a length of 3.6 μ s and centered at the frequency of the CH₂ and CH₃ peaks of isooctane with 64 scans and 4 dummy scans per FID, with a relaxation delay of 10 s.

Diffusion measurements were performed using the stimulated echo sequence using bipolar sine gradient pulses and eddy current delay before the detection (ledbpgp2s).¹⁰³ And with dstebpgp3s (using also double stimulated echo for convection compensation).¹⁰⁴ Typically, in each experiment 16 spectra of 16K data points were collected, with usual values for the duration of the magnetic field pulse gradients (δ) of 6 ms and time allowed for diffusion of 400 ms to 600 ms, and an eddy current delay set to 5 ms. The gradient recovery time was 200 μ s. The sine shaped pulsed gradient (g) was incremented from 5 to 95 % of the maximum gradient strength in a linear ramp. This was conducted for 8 and 16 scans for the first and second pulse sequences mentioned respectively. To determine the diffusion coefficients, the spectra were first processed in the F2 dimension by standard Fourier transform and baseline correction with the Bruker Topspin software package (version 3.2). The diffusion coefficients are determined by exponential fitting of the data belonging to individual columns of the 2D matrix using DOSY Toolbox.¹⁴⁷ In order to obtain solvent suppression, ledbpgpes2s,¹²¹ with excitation sculpting was applied, using the same parameters as before and the ones from the previously acquired zgesgp.

Spin-lattice relaxation times (T_1) were obtained by the inversion recovery pulse sequence. In order to estimate T_1 , 1D inversion recovery pulse sequences were acquired, in which τ_{null} was estimated. The relaxation delays were set to 10 s. Typically 20 spectra, with τ values between 100 ms and 5 s, were acquired with 14k data points. The spectra were first processed in the F2 dimension by standard Fourier transform and baseline correction with the Bruker Topspin software package (version 3.2). The relaxation times were determined by using the relaxation analysis routine of Bruker Topspin and then fitted to an exponential equation (11) using OriginPro 9. A solvent suppression was also implemented and used, via an excitation sculpting scheme, t1iresgp,¹⁴⁸ using the same parameters as the inversion recovery scheme and as zgesgp for the solvent suppression purposes.

Spin-spin relaxation times (T_2) were obtained by the CPMG pulse sequence. The relaxation delays were set to 10 s. Typically 30 slices were taken at variable repetitions of spin echoes, with τ values between 5 ms and 6 s, were acquired with 32k data points. The evolution time, d2, was set at 1 ms. The spectra were first processed in the F2 dimension by standard Fourier transform and baseline correction with the Bruker Topspin software package (version 3.2). The relaxation times were determined by using the relaxation analysis routine of Bruker Topspin and then fitted to an exponential equation (12) using OriginPro 9. In order to obtain the solvent suppressed spectra, a presaturation CPMG pulse sequence was implemented and applied.¹⁴⁹

2.3.4. Physicochemical studies of W/CO₂ microemulsions

The samples for the high pressure experiments were prepared by dissolving 13.5 mg of AOT in 100 μ l of ethanol and 2 μ l of water (in the same isotopic composition). To the high pressure tube, 10 μ l of this solution were added. In some experiments 2 μ l of TMS were also added.

For the fluorescence studies, a stock solution of 2×10^{-4} M of Nile red was prepared in ethanol to avoid decomposition in water. This was diluted to 2×10^{-6} M in a 8 mM and 30 mM AOT aqueous solution.

2.3.4.1. HP fluorescence experiments

Emission and excitation spectra were obtained on a Photon Technology International Fluorimeter (SYS 2459) with Felix 32 software for data analysis (linked to a personal computer) and a 150 W high-pressure xenon lamp. 0.2 mm, and 0.4 mm slits were used in this study in a quartz cuvette. For the high pressure the studies were conducted with 5 mm, 10 mm slits.

In order to conduct pressure studies, a stainless steel cell with three quartz windows was employed. Temperature was set up using four cartridge electric heating elements and a rheostat in a system. Temperature was monitored by an Omega HH503 microprocessor thermometer connected to a J-K-T thermocouple. High pressure generators (Model: 50-6-15; Pressure rating: 15,000 psi; capacity per stroke: 20 mL), valves and tubings were purchased from High Pressure Equipment Company (HIP), Pennsylvania. The 0-25000 psi pressure gauge was purchased from McDaniel Controls, Inc.¹⁵⁰ The pressure chamber has a 16 cm³ volume and the samples were placed inside it using a pyrex cuvette. 8

mM and 30 mM solutions Nile Red in AOT were analysed by room pressure fluorescence and the 8 mM was studied by HP fluorescence.

2.3.4.2. HP NMR experiments

The HP NMR spectroscopy experiments were conducted in a 5 mm zirconia tube with a titanium valve purchased from Daedalus Innovations, LLC. The volume of the setup used to prepare the samples and to acquire NMR spectra was 1.011 ml. All NMR spectra were acquired on a Bruker Avance III 400 spectrometer equipped with a temperature control unit, and a pulse gradient unit capable of producing magnetic field pulsed gradients in the z direction of 56.0 G cm⁻¹, operating at 400.15 MHz for hydrogen and 100.61 MHz for carbon. Upon the pressurization of each sample, the tube was stirred and left to equilibrate for approx. 2 hours.

¹H NMR spectra using identical parameters as those described at section 2.3.3.2. In order to obtain better spectra in these conditions, a 1D CPMG routine was employed with 10 μs echo time. This was performed in a similar way to the 1D experiments described, but with a relaxation delay of 10 s. The chemical shifts are referenced by the methyl peak of ethanol, set at 1.1721 ppm.

The relaxation experiments were also conducted in an identical way to section 2.3.3.2, as were DOSY, but employing a diffusion time of 25 ms and a pulse of 800 μs.

Two dimensional nuclear Overhauser effect spectra were acquired with 32k points in the direct dimension (t₂) and 256 increments in the indirect dimension (t₁) with 2 scans per increment. A spectral window of 2801.1 Hz (7.0 ppm) centered at 1016.4 Hz (2.540 ppm) was identical in both dimensions. The relaxation delay was set to 8 s and mixing times of 300 ms were employed. The phase was corrected using the 1D spectra obtained through NOESY.

¹³C NMR spectra were acquired with zgpg30 pulse scheme, with a relaxation delay set to 2 s. These were acquired with 64k time domain points over a spectral window of 24038.5 Hz (238.885 ppm), centered at 10060.8 Hz (99.991 ppm) and with 512 scans and 4 dummy scans per FID.

In order to obtain ¹H slice selective spectra, a single spatially encoded pulsed-field gradient echo, se-SPFGE¹³⁸ pulse sequence was implemented and used. Besides typical ¹H NMR acquisition parameters, a gradient strength of 5 G cm⁻¹ was commonly applied, alongside a Reburp.1000 selective inversion pulse with a length of 2.32 ms to encode 2000 Hz. The offset of this pulse was sequentially incremented by 2500 Hz from the low offsets (corresponding to the bottom of the tube) to the higher ones (corresponding to the top of the tube).

Identical procedures were conducted to acquire ¹³C slice selective spectra, but by employing a 90 degree slice selective excitation, zgpg,¹⁴² which was implemented in the NMR spectrometer. A gradient strength of 5 G cm⁻¹ was commonly applied, alongside a sinc (Sinc1.1000) selective excitation pulse with a length of 803 μs to encode 2000 Hz. The offset of this pulse was sequentially incremented by 2500 Hz from the low offsets (corresponding to the bottom of the tube) to the higher ones (corresponding to the top of the tube).

3. NMR STUDIES OF THE PROCESS OF GELATION OF LMOGS

3.1. Proof of concept NMR studies to follow the formation of LMOG-based gels

The properties of gels formed by LMOGs have been vastly approached in the literature.¹⁵¹ In this work, the focus is exclusively on the formation of the gel from a solution state. The study is focused on the gelation time, the time interval between of reaction and a constant storage modulus (G' , which corresponds to the gel point).¹⁵² To determine this, NMR spectroscopy will be employed. However, several techniques can and have been employed to assess this property. The ultimate goal is not really to obtain a numerical value (which might differ inside an NMR tube and a wider vial, due to surface effects) for the time necessary to form the gel network, but to assess the dynamics involved in the formation of such network. Therefore, the already mentioned DOSY methodology is going to be employed. Its use in the studies of gels has been addressed in section 1.2.1. Only work that followed the gelation process employing diffusion order spectroscopy was found.⁸⁹ In such paper, this technique is not used to study the formation of a LMOG gel, but a gel from casein.

In the Weiss group, low molecular mass organogelators (LMOG) have been widely studied, through different techniques, ranging from SANS to rheology.^{76,153} One of the structural templates for the development of these molecules is HSA (Fig. 1.10). In this work, the focus will be around such molecules. In order to understand whether or not the plan outlined could be executed, a gelator with a large time of gelation was first studied. This was Ni(DODA)₂, which can be found in Fig. 3.1. Previous visual observations indicated that its e gelation would take more than one hour.

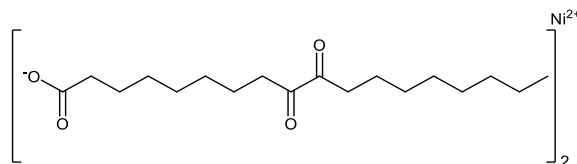


Fig. 3.1 Chemical structure of Ni(DODA)₂

The fact that this molecule has nickel in it, which is paramagnetic, may be complicated for its NMR analysis. A ¹H NMR spectrum in toluene-d₈ was acquired, as depicted in Fig. 3.2.

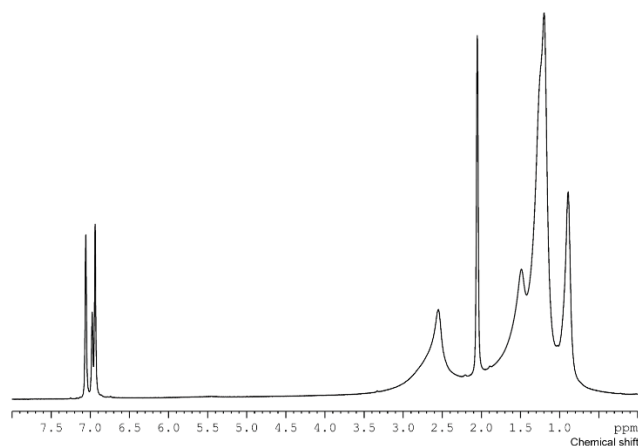


Fig. 3.2 ¹H NMR spectrum of Ni(DODA)₂ in toluene-d₈, 5.0 wt%.

It is possible to observe that the protons at higher fields (the exception is the one at approx. 2.0 ppm that belongs to toluene) are significantly broadened. It is likely that this is due to the paramagnetic effect, rather than exclusively from aggregation. However an attempt was made to conduct DOSY experiments and these are depicted in Fig. 3.3.

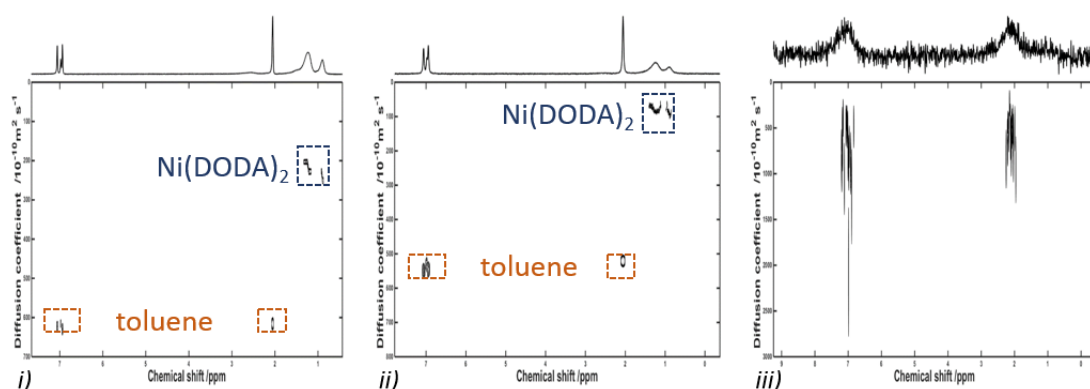


Fig. 3.3 ¹H DOSY spectra of Ni(DODA)₂ (5.0 wt% in toluene-d₈). $t=48$ min (i); $t=78$ min (ii); $t=\infty$ (iii).

The spectra in Fig. 3.3 show that the solvent and the gelator have clearly different diffusion coefficients, it is also noticeable that the former is larger, which is natural, given that even in gel state the solvent keeps some motion. In *i*) there are initially two regimes for the gelator, while from a point on this collapses (*ii*). This is likely related to the aggregation process, which forms different-sized clusters throughout time. It is probable that from a point on a more homogeneous is formed and only the small-sized aggregates are observed through NMR. A spectrum was acquired at infinite time, just to assure that a gel was formed, which was clear both visually and through this liquid state NMR experiment (Fig. 3.3).

The process of gelation was followed throughout time and the DOSY data were plotted (Fig. 3.4).

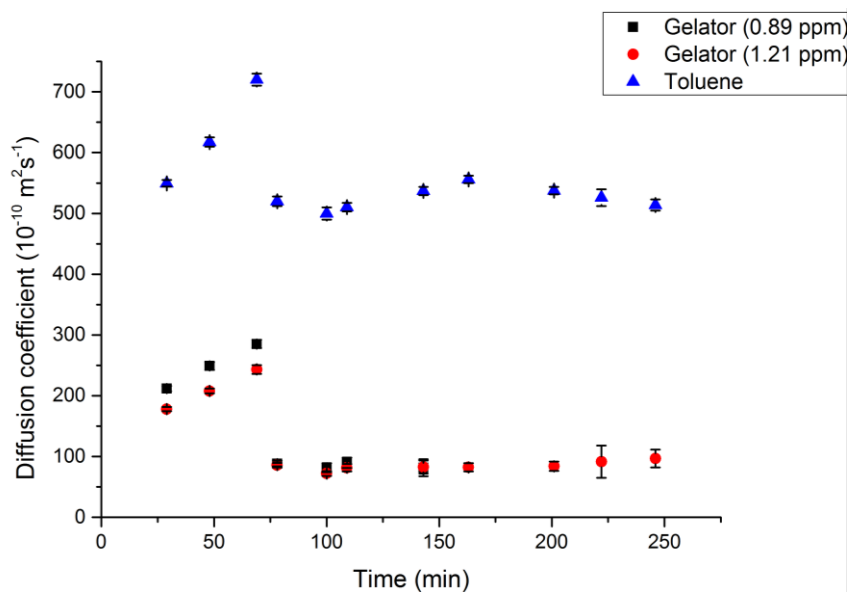


Fig. 3.4 Representation of the diffusion coefficient of $Ni(DODA)_2$ (5 wt% in toluene- d_8) over time. The error bars belong to the error of the fitting.

In Fig. 3.4 two regimes for the gelator (in this case observed at two different chemical shifts) are depicted in the beginning and from $t=89$ min a plateau is reached. The visual observation of the sample at this point revealed a dense liquid, but not yet a fully formed gel. The increase of diffusion coefficient observed in the beginning of the process is somehow counterintuitive given that the formation of aggregates ought to be occurring. Nevertheless, the same increase is observed for the gelator and for the solvent. Therefore an approach previously used by Brand *et al*⁶⁶ was attempted, in which the ratio between the diffusion coefficients of the gelator and of the solvent is plotted, in this instance over time, as depicted in Fig. 3.5. This ought to eliminate the factor of viscosity in (3), since it is the same system, and only relate the hydrodynamic radius of both components.

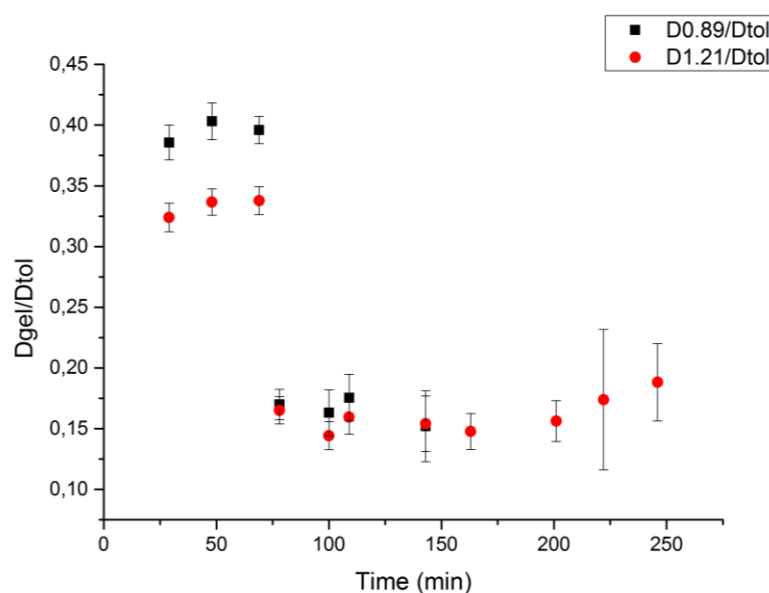


Fig. 3.5 Representation of ratio between the diffusion coefficients of $Ni(DODA)_2$ (5 wt%) and toluene- d_8 over time. The error bars belong to the error of the fittings on this ratio.

It is possible to understand through Fig. 3.5 that the initial increase noted on the diffusion coefficients is approximately equal for the gelator and for toluene, as there is only slight change on the ratio throughout the initial times. It is then thought that the most influencing factor for the increase seen in Fig. 3.4 is the viscosity. However, since Ni(DODA)₂ is forming a network, its diffusion coefficient should become altered, which it does, but in the same way as the solvent. This might indicate that the solvent is involved in the process of gelation, eventually it can be entrapped in the aggregates. Nevertheless, these are mere speculations, since there are not enough data to be certain about a mechanism. Furthermore, due to paramagnetism, this is not the most adequate system to apply in NMR, even though it was useful as a proof of concept towards the use of DOSY to follow the dynamics of gelation.

Afterwards, HSA (depicted in Fig. 1.10) was used as a gelator. The solvent was also toluene-d₈ and first a 2.0 wt% sample was prepared. Visual cues indicated that the gel would be formed in approximately two minutes. This was an experimental problem, since the pulse sequence previously employed would take longer than that the time it takes for the solution to become a gel. Therefore, in order to study this system the One-shot DOSY pulse sequence was attempted, which takes approx. 2 minutes per acquisition.¹⁵⁴ This was then applied to the mentioned mixture, as displayed in Fig. 3.6.

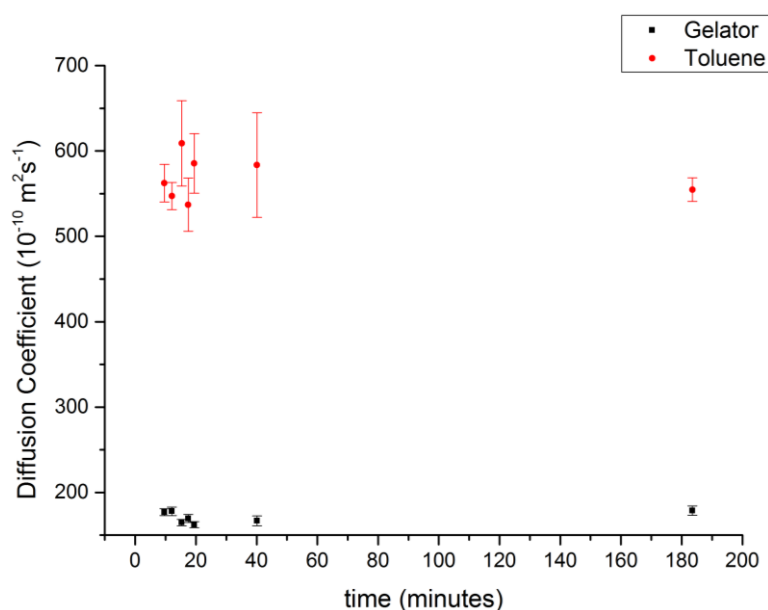


Fig. 3.6 Diffusion coefficients plotted over time for HSA, 2.0 wt% in toluene-d₈. The error bars belong to the error of the fitting.

From the experimental data, an approximately constant evolution with time is observed. This indicates that only the gel phase was observed, being impossible to observe the solution and therefore the process of network formation. In order to slow down the process of gelation one can increase the temperature at which the solution cools down or the concentration of the gelator. The latter was chosen and a 1.0 wt% solution of HSA in toluene-d₈ was prepared and analysed by DLS (Fig. 3.7). Visually, a gel-like structure at this concentration would take 10 or more minutes to form.

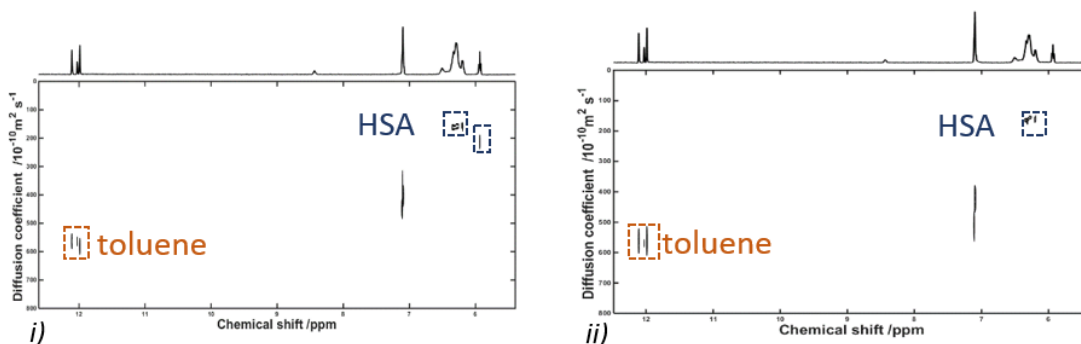


Fig. 3.7 DOSY spectra of HSA (1 wt% in toluene-d₈). $t=5$ minutes and 35 seconds (i); $t=54$ minutes and 20 seconds (ii).

It was then possible to acquire DOSY spectra in which two regimes were found in *i*) (alike what was found in Fig. 3.3) and then just one regime later on (*ii*). This is already enough to understand that two different sorts of environments were observed during the NMR experiments, a solution and a gel (which was visually confirmed) states. Hence the diffusion coefficients were plotted against the time for each measurement (Fig. 3.8), as was the ratio between the diffusion rates of gelator and solvent (Fig. 3.9).

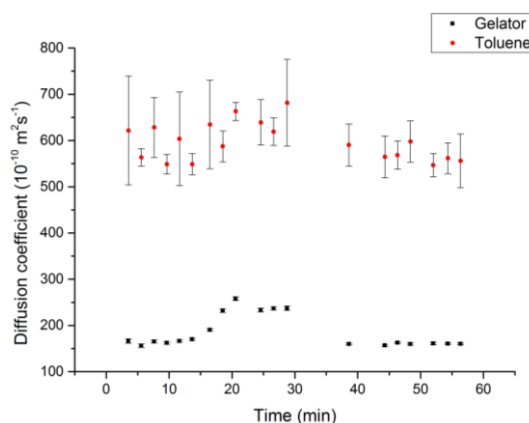


Fig. 3.8 Diffusion coefficients plotted over time for HSA, 1.0 wt%, in toluene-d₈. The error bars belong to the error of the fitting.

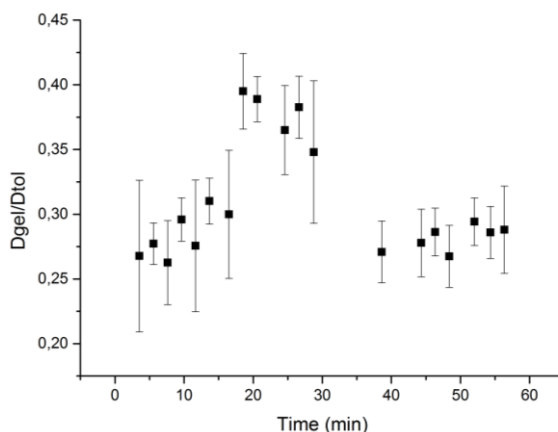


Fig. 3.9 Representation of ratio between the diffusion coefficients of HSA (1.0 wt%) and toluene-d₈ over time. The error bars belong to the error of the fittings on this ratio.

The data obtained revealed that the diffusion coefficient of the gelator increased upon aggregation, but in this turn it remained identical for toluene throughout the evolution of the experiment. This is especially clear by observing Fig. 3.9, in which the ratio increases with the formation of the gel network (the error of the measurement might be an issue, but clearly a trend is observed). Therefore it is not likely that the effect seen in Fig. 3.8 is only due to viscosity changes, the hydrodynamic radius of the HSA is changing over time. In this system it is unlikely that the solvent has a direct influence on the gelation process. Two plateaus are observed and that may be due to different sorts of networks being present at over time. It shall also be noted that the diffusion coefficients in the second plateau, in which the sample is already a gel, is identical to the ones obtained in the solution state. This might be due to, at both stages, essentially composed of monomeric or small oligomeric structures being observed, either diffusing in the bulk or in a more tightly packed gel.

One question still remains: why is there an increase of the diffusion coefficients while gel formation is occurring? These observations are somehow similar to those described in section 1.2.1, from the data of Brand *et al*⁸⁴ and Nonappa *et al*,⁸⁵ in which increases in diffusion rates in the gel phase comparing to the solution state increase. Just alike it was suggested for those studies, this might be due to the an increase of large aggregates over time, which become NMR invisible and only the monomers or small oligomers are being observed, whereas in the beginning average sized aggregates are observed.

In conclusion, these preliminary studies indicate that DOSY is a promising technique towards studying the dynamics of formation of a LMOG-formed gel. It may allow us to understand the solvent role in the aggregation, and to understand kinetics, at a molecular level, having an understanding of hydrodynamic radius. Other NMR experiments, such as relaxation measurements, can be combined with these to assess the site specific influences of aggregation, more relevantly in structurally diverse gelators.

3.2. Experimental section

3.2.1. Chemicals

For the gelator studies, a 5.0 wt% solution of Ni(DODA)₂ in toluene-d₈ was obtained from Mohan Zhang and 1.0 wt% and 2.0 wt% solutions of HSA in toluene-d₈ were obtained from and Dr. V. Ajay Mallia and used as received. For these studies the toluene-d₈ from Aldrich was utilized.

3.2.2. NMR experiments

The NMR spectra were acquired using a Varian INOVA III 400 MHz NMR spectrometer, equipped with a temperature control unit, and a pulse gradient unit capable of producing magnetic field pulsed gradients in the z direction of 22.0 G cm⁻¹ operating at 400.15 MHz for hydrogen.

Diffusion measurements were performed using the stimulated echo sequence using bipolar sine gradient pulses and eddy current delay before the detection (ledbpgp2s) for the Ni(DODA)₂ sample.¹⁰³ And with One-shot DOSY for the HSA samples.¹⁵⁴ Typically, in each experiment 16 spectra of 16K data

points were collected, with usual values for the duration of the magnetic field pulse gradients (δ) of 6 ms and time allowed for diffusion of 400 ms to 600 ms, and an eddy current delay set to 5 ms. The gradient recovery time was 200 μ s. The sine shaped pulsed gradient (g) was incremented from 5 to 85 % of the maximum gradient strength in a linear ramp. Relaxation delays of 5 s and 2 s were employed, respectively. The gradient length was varied from 1.2 ms to 1.5 ms, diffusion delays from 300 ms to 400 ms were used, while gradient stabilization delays of 0.5 ms were put in practice to obtain decays dependent on the diffusion coefficient of the molecules. The Ni(DODA)₂ experiments took 9 minutes or 16 minutes on average, depending on the use of 4 or 8 scans, respectively. The HSA studies took 1 minute and 52 seconds. To determine the diffusion coefficients, the spectra were processed in the F2 dimension by standard Fourier transform and baseline correction with DOSY Toolbox.¹⁴⁷ The diffusion coefficients are determined by exponential fitting of the data belonging to individual columns of the 2D matrix using DOSY Toolbox.

In order to start the gelation process in this work, a temperature trigger was employed. The solvent bearing the gelator molecule is heated to yield a solution phase above its gelation temperature (T_g , which is the minimum temperature required to dissolve the gelator in the solvent) and put in the NMR spectrometer at 25° C and studied over time.

4. CONCLUSIONS AND FUTURE PERSPECTIVES

The core of the project was to develop an NMR methodology for the dynamic and structural characterization of W/CO₂ microemulsions. For this purpose W/O microemulsions formed by AOT in isooctane were first studied. Through DOSY it was possible to determine hydrodynamic radii of the W/O microemulsions in agreement with the literature. The studies determined that stable microemulsions are obtained, in which water has a different behaviour when encapsulated in smaller or larger micelles. In the former, it has a decrease in its NMR relaxation processes, and has a more restricted dynamics, whereas in the latter it displayed a behaviour more alike bulk water. The sizes of the small water pools that lead to rotational motions inside reverse micelles was assessed and determined as approximately 6 Å. This is an estimate that can be related with the size of the shell of molecules bound to the micellar layer, which indicates that interactions with AOT are what influences more significantly the water dynamics. One other conclusion taken from this work is that water dynamics in these reverse micelles is greatly influenced by the microviscosity inside the droplets.

Carbohydrate encapsulation was conducted to characterize the dynamics of RMs and its interaction with solutions. While in small sized droplets ($\omega_0=20$) the solutes do not alter most of the properties of the reverse micelles that contain them. However, when encapsulated in larger micelles ($\omega_0=60$) the hydrodynamic radius determined showed a decrease with molecular size, mostly when D-(+)-Celotriose was the solute. This is a counterintuitive result, since a larger solute being encapsulated results in a smaller-sized micelle. It is therefore likely that its specific interactions might have led to a cosurfactant effect that yields a larger number of RMs with smaller radii.

W/CO₂ microemulsions formed by AOT were analysed via NMR spectroscopy, using the methodology previously developed in isooctane medium, the behaviour indicated that probably at pressures above 130 bar reverse micelles are attained. The homogeneity of the system was assessed by slice selective NMR spectroscopy. It was determined that approximately 60 % of the water was diffusing in the supercritical fluid and only 40 % remained inside the micelles. It was not possible to accurately assess the sizes of the reverse micelles, due to low sensitivity. The system must be optimized for future studies, perhaps by employing larger amounts of AOT and larger ω_0 . One of the future goals is to apply these methods to synthesized surfactants that are more CO₂-*philic* and would allow to determine structure of entrapped molecules in this environment via NMR spectroscopy.

It was also possible to prove that DOSY can be used to study the dynamics of gel formation by LMOGs. From the studies, it is concluded that in the toluene gels of Ni(DODA)₂ and HSA there is a diffusion increase previous to the gel network is completely formed, which may be due to the larger aggregates already formed having a much quicker relaxation and being therefore NMR-invisible. Toluene displayed a behaviour alike Ni(DODA)₂ but different from HSA while the gel formation was occurring. Hence it is thought that it is directly involved in the gel formation of the former but not the latter. This was a proof of concept and still a lot has to be done to fully understand the formation of these networks by NMR, mainly relaxation studies. These will also be used as chromatographic stationary

phases inside NMR tubes, to separate molecules based on size and properties. One other future goal is to devise a strategy to study this process of formation in thixotropic gels, after pressure is released.

A) APPENDIX

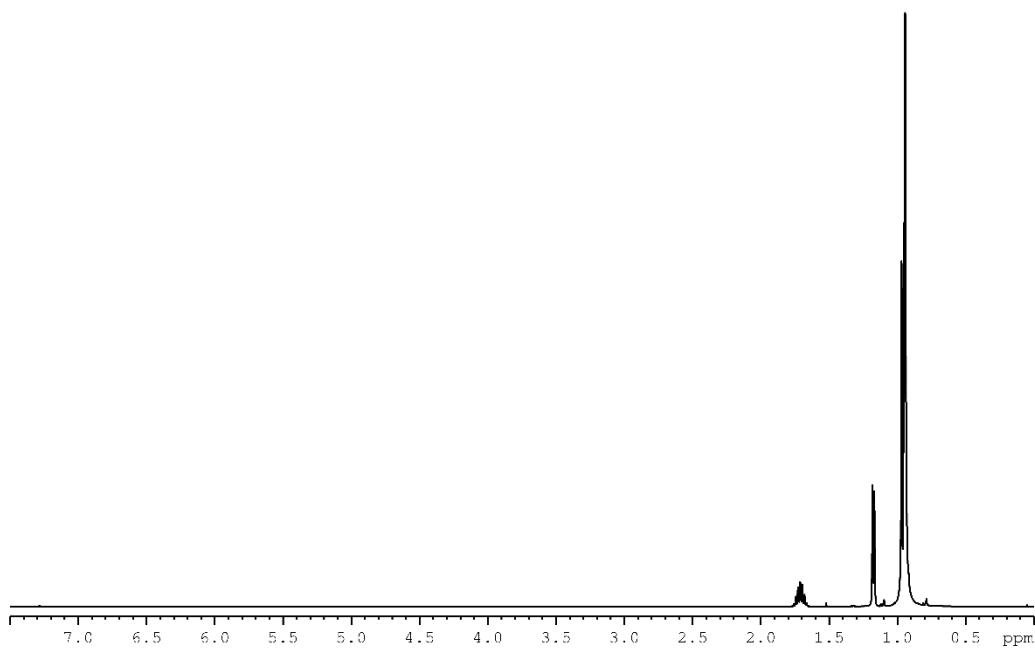


Fig. A.1 ¹H NMR spectrum of isooctane in CDCl₃.

Equation to obtain the correlation time of ¹H relaxed by ¹H at a 9.4 T magnetic field and with T_1/T_2 above 20¹¹²:

$$\tau_c(ns) = 1.531249 + 0.032861 \frac{T_1}{T_2} - 0.000049 \left(\frac{T_1}{T_2}\right)^2 + 0.436269 \times 10^{-7} \left(\frac{T_1}{T_2}\right)^3 - 1.448567 \times 10^{-11} \left(\frac{T_1}{T_2}\right)^4 \quad (23)$$

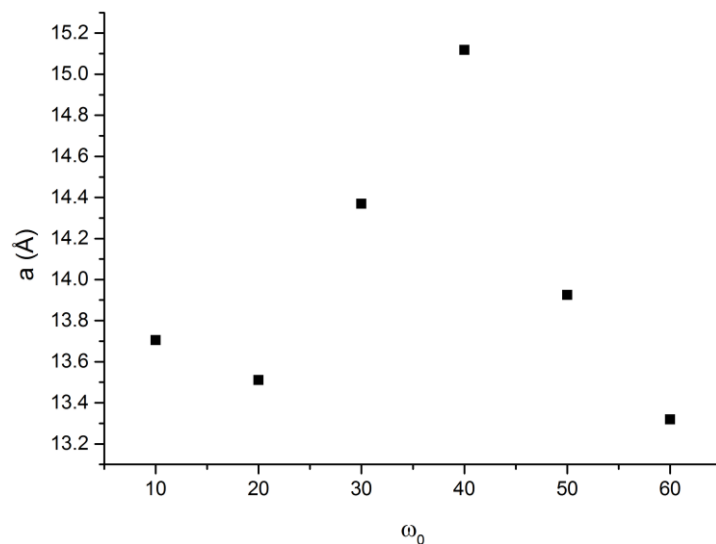


Fig. A.2 Relation between a (radius of the relaxing nucleus) of water protons of W/O AOT reverse micelles and ω_0 .

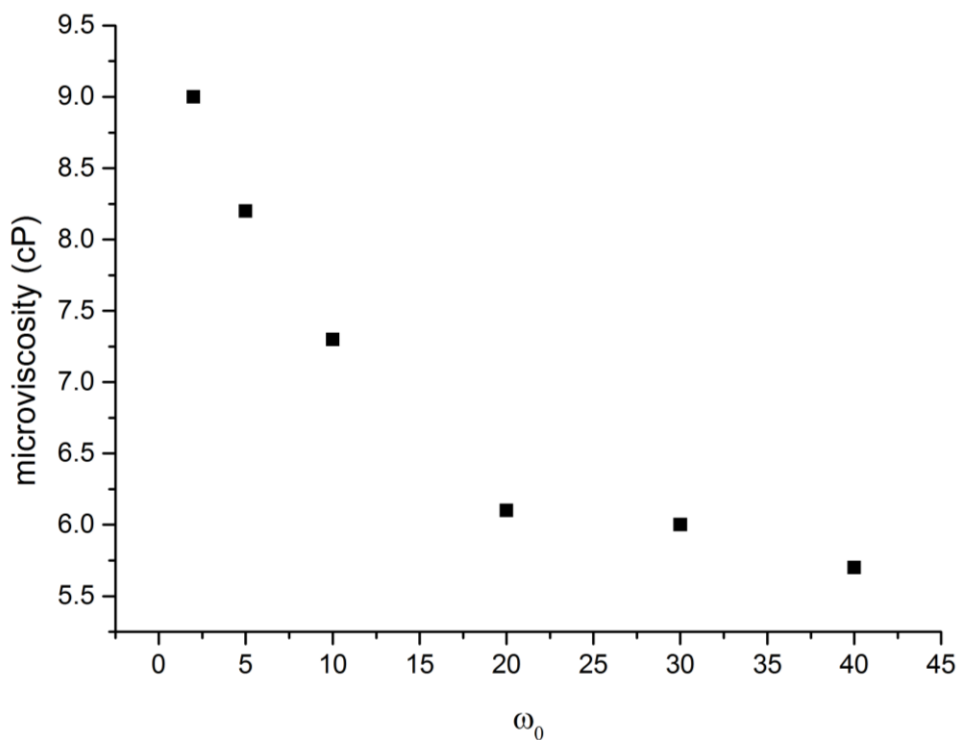


Fig. A.3 Plot between microviscosity and ω_0 in AOT W/O RMs with data from Rafiq et al,¹⁰⁷ which was fitted to obtain (24) with $R^2=0.991$.

$$\eta = 4.09036e^{-\frac{\omega_0}{10.6053}} + 5.63507$$

(24)

Table A.1 Variation of microviscosity ($\mu\eta$) with ω_0 for AOT W/O RMs, taken from Rafiq et al¹⁰⁷ and (24).

ω_0	$\mu\eta$ (cP)
60	5.6
50	5.7
40	5.7
30	6.0
20	6.1
10	7.3
5	8.2
2	9.0

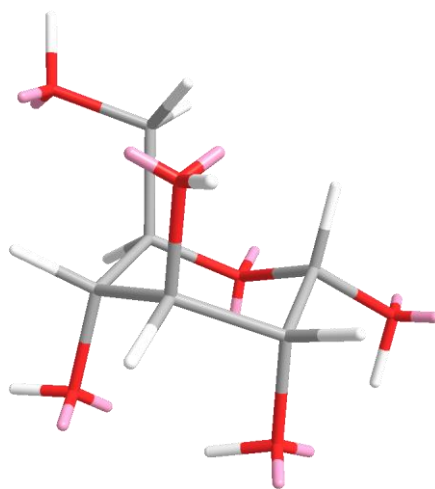


Fig. A.4 Molecular mechanics structure of D-(+)-Glucose obtained using Chem3D Pro 14.0.

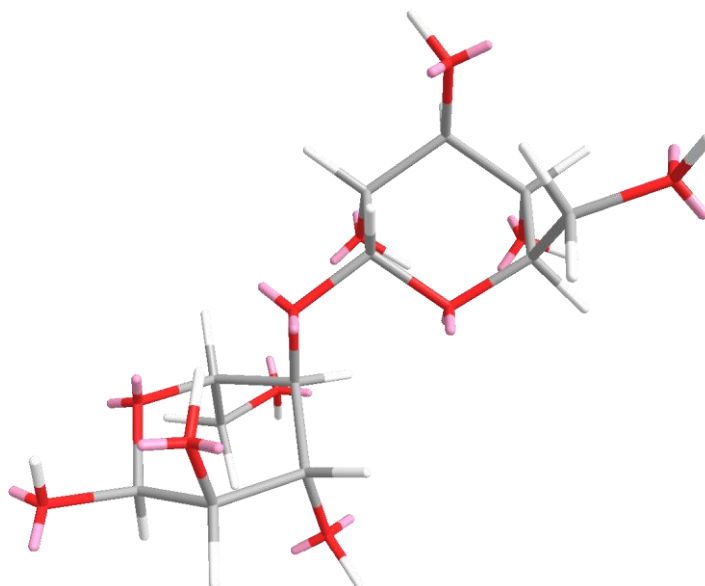


Fig. A.5 Molecular mechanics structure of D-(+)-Cellobiose obtained using Chem3D Pro 14.0.

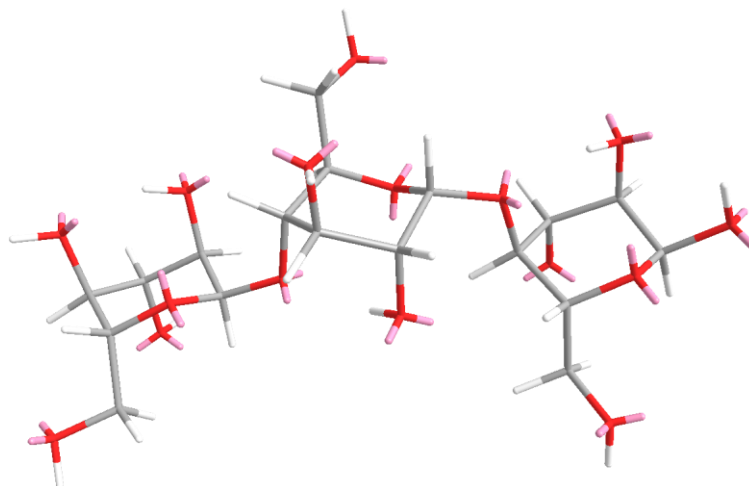


Fig. A.6 Molecular mechanics structure of D-(+)-Cellotriose obtained using Chem3D Pro 14.0.

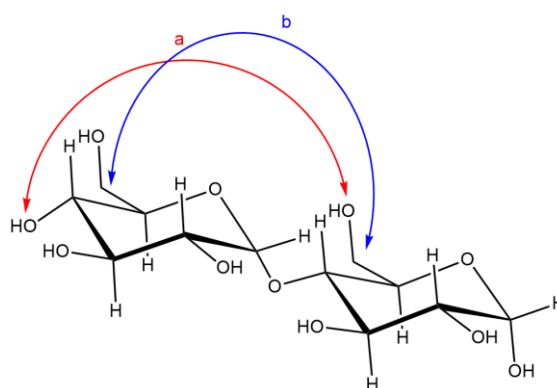


Fig. A.7 Structure of D-(+)-Cellobiose and intramolecular distances determined from molecular mechanics using Chem3D Pro 14.0. $a=10.278 \text{ \AA}$; $b=10.385 \text{ \AA}$.

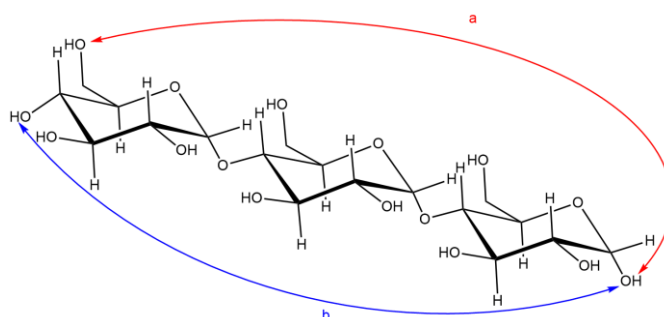


Fig. A.8 Structure of D-(+)-Cellotriose and intramolecular distances determined from molecular mechanics using Chem3D Pro 14.0. $a=14.581 \text{ \AA}$; $b=13.738 \text{ \AA}$.

Table A.2 ¹H NMR chemical shift, line width and relaxation data summary obtained for a D-(+)-Glucose 50mM solution in D₂O. An is the proton adjacent to the anomeric carbon in the sugar molecule.

	$\Delta\delta$ (ppm)	$\nu_{1/2}$ (Hz)	T_1 (s)	T_2 (s)	τ_c (ns)
An	5.1346	6.018	3.33	0.49	1.04
H ₂ O	4.6984	3.882	5.25	0.27	1.92

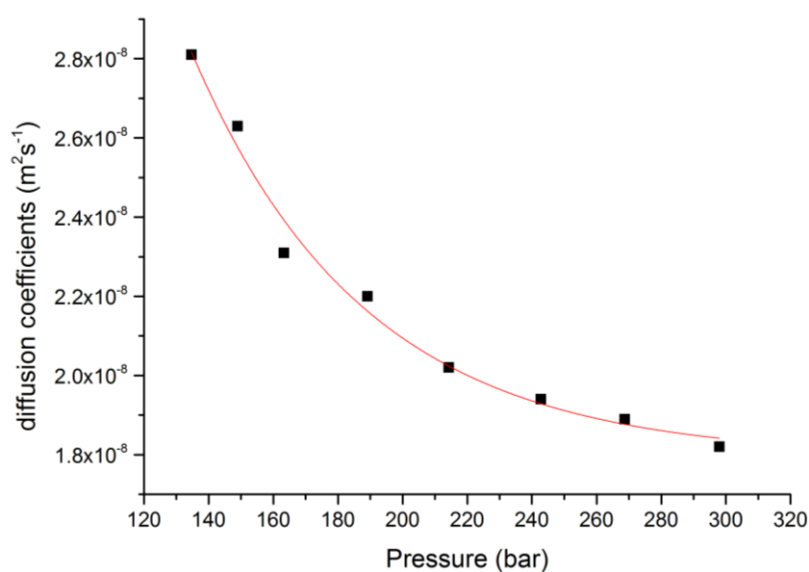


Fig. A.9 Diffusion coefficients of water in carbon dioxide at 35° C at different pressures. Data extracted from Xu et al.¹⁴³ The equation for the trendline of the exponential fitting is (25) and was obtained with a $R^2=0.98$.

$$D_{\text{water}/\text{CO}_2} = 1.28 \times 10^{-7} e^{-\frac{p}{53.3515}} + 1.79 \times 10^{-8}$$

(25)

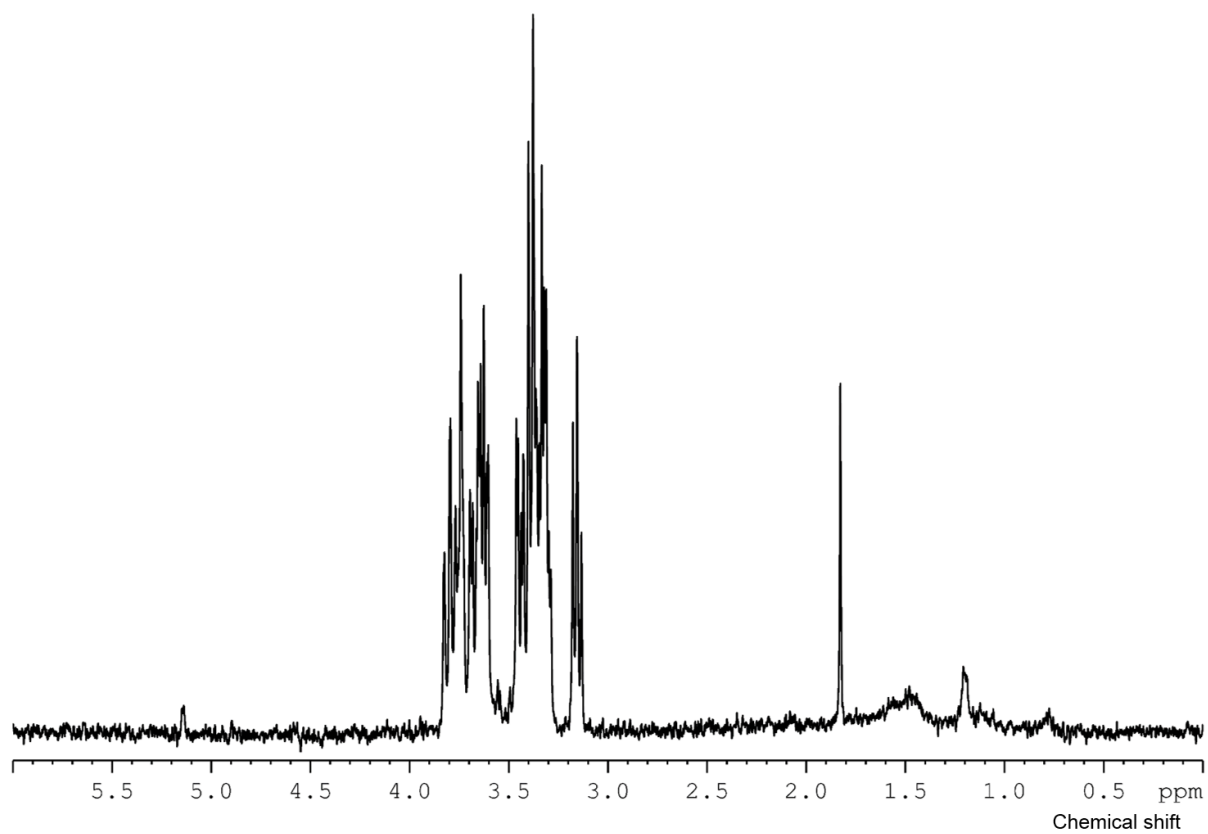


Fig. A.10 Solvent suppressed ¹H NMR spectrum of saturated D-(+)-Glucose diluted in a D₂O volume similar to the one in the HP tube.

5. REFERENCES

- (1) Dlugokencky, E.; Tans, P. NOAA/ESRL (www.esrl.noaa.gov/gmd/ccgg/trends/), last accessed in 25/08/2015.
- (2) Yu, K.; Curcic, I.; Gabriel, J.; Tsang, S. *ChemSusChem* **2008**, *1*, 893.
- (3) Dibenedetto, A.; Angelini, A.; Stufano, P. *J. Chem. Technol. Biotechnol.* **2014**, *89*, 334.
- (4) Beckman, E. J. *J. Supercrit. Fluids* **2004**, *28*, 121.
- (5) Poling, B. E.; Prausnitz, J. M. *The Properties of Gases and Liquids*, 5th ed.; McGraw-Hill, 2001.
- (6) <http://cnx.org/contents/cd1205e1-8edd-4b12-aff5-ecdbdfdf4fc@2/Carbon-Dioxide> last seen in 13/09/2015.
- (7) Hanrahan, J. P.; Ziegler, K. J.; Galvin, J. P.; Holmes, J. D. *Langmuir* **2004**, *20*, 4386.
- (8) Raveendran, P.; Ikushima, Y.; Wallen, S. L. *Acc. Chem. Res.* **2005**, *38*, 478.
- (9) Drake, B. D.; Smith, R. L. *J. Supercrit. Fluids* **1990**, *3*, 162.
- (10) Raveendran, P.; Wallen, S. L. *J. Phys. Chem. B* **2003**, *107*, 1473.
- (11) Tafazzoli, M.; Khanlarkhani, A. *J. Supercrit. Fluids* **2007**, *40*, 40.
- (12) Raveendran, P.; Wallen, S. L. *J. Am. Chem. Soc.* **2002**, *124*, 12590.
- (13) Smith, P. G.; Dhanuka, V. V.; Hwang, H. S.; Lim, K. T.; Johnston, K. P. *Ind. Eng. Chem. Res.* **2007**, *46*, 2473.
- (14) Zhang, H.; Li, R.; Su, B.; Xing, H.; Yang, Y.; Ren, Q. *J. Chem. Eng. Data* **2012**, *57*, 1991.
- (15) Ma, S.; Wu, Y.; Hurrey, M. L.; Wallen, S. L.; Grant, C. S. *J. Phys. Chem. B* **2010**, *114*, 3809.
- (16) Reynolds, L.; Gardecki, J. A.; Frankland, S. J. V.; Horng, M. L.; Maroncelli, M. *J. Phys. Chem.* **1996**, *100*, 10337.
- (17) Kauffman, J. F. *J. Phys. Chem. A* **2001**, *105*, 3433.
- (18) Eastoe, J.; Gold, S. *Phys. Chem. Chem. Phys.* **2005**, *7*, 1352.
- (19) Czajka, A.; Hazell, G.; Eastoe, J. *Langmuir* **2015**, *31*, 8205.
- (20) Lide, D. R. *CRC Handbook of Chemistry and Physics*, 88th ed.; CRC Press, 2007.
- (21) Drohmann, C.; Beckman, E. J. *J. Supercrit. Fluids* **2002**, *22*, 103.
- (22) Xu, B.; Lynn, G. W.; Guo, J.; Melnichenko, Y. B.; Wignall, G. D.; McClain, J. B.; Desimone, J. M.; Johnson, C. S. *J. Phys. Chem. B* **2005**, *109*, 10261.
- (23) Hilf, J.; Schulze, P.; Frey, H. *Macromol. Chem. Phys.* **2013**, *214*, 2848.
- (24) Sagisaka, M.; Kudo, K.; Nagoya, S.; Yoshizawa, A. *J. Oleo Sci.* **2013**, *62*, 481.

- (25) Mohamed, A.; Trickett, K.; Chin, S. Y.; Cummings, S.; Sagisaka, M.; Hudson, L.; Nave, S.; Dyer, R.; Rogers, S. E.; Heenan, R. K.; Eastoe, J. *Langmuir* **2010**, *26*, 13861.
- (26) Mohamed, A.; Ardyani, T.; Sagisaka, M.; Ono, S.; Narumi, T.; Kubota, M.; Brown, P.; James, C.; Eastoe, J.; Kamari, A.; Hashim, N.; Md Isa, I.; Abu Bakar, S. *J. Supercrit. Fluids* **2015**, *98*, 127.
- (27) Cooper, A.; Londono, J.; Wignall, G.; McClain, J. B.; Samulski, E. T.; Lin, J. S.; Dobrynin, A.; Rubinstein, M.; Burke, A. L. C.; Fréchet, J. M. J.; Desimone, J. M. *Nature* **1997**, *389*, 368.
- (28) Hankel, R. F.; Rojas, P. E.; Cano-Sarabia, M.; Sala, S.; Veciana, J.; Braeuer, A.; Ventosa, N. *Chem. Commun.* **2014**, *50*, 8215.
- (29) Liang, C.; Liu, Q.; Xu, Z. *ACS Appl. Mater. Inter.* **2014**, *6*, 6898.
- (30) Everett, D. H. *Basic Principles of Colloid Science*; Royal Society of Chemistry, 1988.
- (31) Everett, D. H. *Pure Appl. Chem.* **1972**, *31*.
- (32) Kilikian, B. V.; Bastazin, M. R.; Minami, N. M.; Gonçalves, E. M. R.; Junior, A. P. *Brazilian J. Chem. Eng.* **2000**, *17*, 133.
- (33) Eicke, H.-F. *Top. Curr. Chem.* **1980**, *87*, 85.
- (34) Luisi, P. L.; Giomini, M.; Pileni, M. P.; Robinson, B. H. *Biochim. Biophys. Acta* **1988**, *947*, 209.
- (35) Laia, C.; Brown, W.; Almgren, M.; Costa, S. *Langmuir* **2000**, *16*, 465.
- (36) Bartscherer, K. A.; Minier, M.; Renon, H. *Fluid Phase Equilib.* **1995**, *107*, 93.
- (37) Yee, G. G.; Fulton, J. L.; Smith, R. D. *Langmuir* **1992**, *8*, 377.
- (38) Hutton, B. H.; Perera, J. M.; Grieser, F.; Stevens, G. W. *Colloids Surf., A* **2001**, *189*, 177.
- (39) Hutton, B. H.; Perera, J. M.; Grieser, F.; Stevens, G. W. *Colloids Surf., A* **1999**, *146*, 227.
- (40) Liu, J.; Ikushima, Y.; Shervani, Z. *J. Supercrit. Fluids* **2004**, *32*, 97.
- (41) Zhang, J.; Han, B. *Acc. Chem. Res.* **2013**, *46*, 425.
- (42) Eastoe, J.; Paul, A.; Nave, S.; Steytler, D. C.; Robinson, B. H.; Rumsey, E.; Thorpe, M.; Heenan, R. K. *J. Am. Chem. Soc.* **2001**, *123*, 988.
- (43) Cássio, F.; de Góes, L.; Pereira, T.; da Rocha, S.; Bazito, R. In *12th European Meeting on Supercritical Fluids*; 2010.
- (44) Keiper, J. S.; Simhan, R.; DeSimone, J. M.; Wignall, G. D.; Melnichenko, Y. B.; Frielinghaus, H. *J. Am. Chem. Soc.* **2002**, *124*, 1834.
- (45) Adkins, S. S.; Chen, X.; Nguyen, Q. P.; Sanders, A. W.; Johnston, K. P. *J. Colloid Interface Sci.* **2010**, *346*, 455.
- (46) Sagisaka, M.; Narumi, T.; Niwase, M.; Narita, S.; Ohata, A.; James, C.; Yoshizawa, A.; Taffin de Givenchy, E.; Guittard, F.; Alexander, S.; Eastoe, J. *Langmuir* **2014**, *30*, 6057.
- (47) Sagisaka, M.; Iwama, S.; Yoshizawa, A. *Langmuir* **2012**, *28*, 10988.

- (48) Bongartz, N.; Patil, S. R.; Stubenrauch, C.; Blunk, D. *Colloids Surf., A* **2012**, *414*, 320.
- (49) Sagisaka, M.; Fujii, T.; Koike, D.; Yoda, S.; Takebayashi, Y.; Furuya, T.; Yoshizawa, A.; Sakai, H.; Abe, M.; Otake, K. *Langmuir* **2007**, *23*, 2369.
- (50) Adkins, S. S.; Chen, X.; Nguyen, Q. P.; Sanders, A. W.; Johnston, K. P. *J. Colloid Interface Sci.* **2010**, *346*, 455.
- (51) Eastoe, J.; Gold, S.; Rogers, S.; Wyatt, P.; Steytler, D. C.; Gurgel, A.; Heenan, R. K.; Fan, X.; Beckman, E. J.; Enick, R. M. *Angew. Chemie Int. Ed.* **2006**, *45*, 3675.
- (52) Dupont, A.; Eastoe, J.; Murray, M.; Martin, L.; Guittard, F.; Taffin de Givenchy, E.; Heenan, R. K. *Langmuir* **2004**, *20*, 9953.
- (53) Dupont, A.; Eastoe, J.; Martin, L.; Steytler, D.; Heenan, R. K.; Guittard, F.; Taffin de Givenchy, E. *Langmuir* **2004**, *20*, 9960.
- (54) Liu, J.; Han, B.; Wang, Z.; Zhang, J.; Li, G.; Yang, G. *Langmuir* **2002**, *18*, 3086.
- (55) Stone, M.; da Rocha, S.; Rosicky, P. J.; Johnston, K. P. *J. Phys. Chem. B* **2003**, *107*, 10185.
- (56) Sagisaka, M.; Hino, M.; Oasa, J.; Yamamoto, M.; Yoda, S.; Takebayashi, Y.; Furuya, T.; Yoshizawa, A.; Ochi, K.; Otake, K. *J. Oleo Sci.* **2009**, *58*, 75.
- (57) Da Rocha, S.; Harrison, K.; Johnston, K. *Langmuir* **1999**, *15*, 419.
- (58) Acharya, D. P.; Hartley, P. G. *Curr. Opin. Colloid Interface Sci.* **2012**, *17*, 274.
- (59) Niessen, H. G.; Woelk, K. In *In situ NMR Methods in Catalysis*; 2007; Vol. 276, pp 69–111.
- (60) Stahla, M. L.; Baruah, B.; James, D. M.; Johnson, M. D.; Lvinger, N. E.; Crans, D. C. *Langmuir* **2008**, *24*, 6027.
- (61) Maitra, A. *J. Phys. Chem.* **1984**, *88*, 5122.
- (62) Law, S. J.; Britton, M. M. *Langmuir* **2012**, *28*, 11699.
- (63) Wong, M.; Thomas, J. K.; Nowak, T. *J. Am. Chem. Soc.* **1977**, *99*, 4730.
- (64) Schwartz, L. J.; DeCiantis, C. L.; Chapman, S.; Kelley, B. K.; Hornak, J. P. *Langmuir* **1999**, *15*, 5461.
- (65) Nagashima, K.; Lee, Jr., C. T.; Xu, B.; Johnston, K. P.; DeSimone, J. M.; Johnson, C. S. *J. Phys. Chem. B* **2003**, *107*, 1962.
- (66) Thurecht, K. J.; Hill, D. J. T.; Whittaker, A. K. *J. Supercrit. Fluids* **2006**, *38*, 111.
- (67) Fremgen, D.; Smotkin, E. *J. Supercrit. Fluids* **2001**, *19*, 287.
- (68) Blakey, I.; Thurecht, K. J.; Whittaker, A. K. *Chem. Commun.* **2010**, *46*, 2850.
- (69) Kowalewski, J.; Mäler, L. *Nuclear Spin Relaxation in Liquids: Theory, Experiments, and Applications*; CRC Press, 2006.
- (70) Shi, Z.; Peterson, R. W.; Wand, A. J. *Langmuir* **2005**, *21*, 10632.

- (71) Valentine, K. G.; Mathies, G.; Bédard, S.; Nucci, N. V.; Dodevski, I.; Stetz, M. A.; Can, T. V.; Griffin, R. G.; Wand, A. J. *J. Am. Chem. Soc.* **2014**, *136*, 2800.
- (72) Horn, W. D. Van; Ogilvie, M. E.; Flynn, P. F. *J. Am. Chem. Soc.* **2009**, *131*, 8030.
- (73) Nucci, N. V.; Valentine, K. G.; Wand, A. J. *J. Magn. Reson.* **2014**, *241*, 137.
- (74) George, M.; Weiss, R. G. *Acc. Chem. Res.* **2006**, *39*, 489.
- (75) Abdallah, D. J.; Weiss, R. G. *Adv. Mater.* **2000**, *12*, 1237.
- (76) Mallia, V. A.; George, M.; Blair, D. L.; Weiss, R. G. *Langmuir* **2009**, *25*, 8615.
- (77) Mallia, V. A.; Butler, P. D.; Sarkar, B.; Holman, K. T.; Weiss, R. G. *J. Am. Chem. Soc.* **2011**, *133*, 15045.
- (78) Mallia, V. A.; Weiss, R. G. *Soft Matter* **2015**, *11*, 5010.
- (79) Tachibana, T.; Mori, T.; Hori, K. *Bull. Chem. Soc. Jpn.* **1980**, *53*, 1714.
- (80) Tachibana, T.; Mori, T.; Hori, K. *Bull. Chem. Soc. Jpn.* **1981**, *54*, 73.
- (81) Terech, P.; Rodriguez, V.; Barnes, J. D.; McKenna, G. B. *Langmuir* **1994**, *10*, 3406.
- (82) Shapiro, Y. E. *Prog. Polym. Sci.* **2011**, *36*, 1184.
- (83) Carrara, C.; Viel, S.; Delaurent, C.; Ziarelli, F.; Excoffier, G.; Caldarelli, S. *J. Magn. Reson.* **2008**, *194*, 303.
- (84) Brand, T.; Richter, S.; Berger, S. *J. Phys. Chem. B* **2006**, *110*, 15853.
- (85) Nonappa; Šaman, D.; Kolehmainen, E. *Magn. Reson. Chem.* **2015**, *53*, 256.
- (86) Brand, T.; Nolis, P.; Richter, S.; Berger, S. *Magn. Reson. Chem.* **2008**, *46*, 545.
- (87) Dama, M.; Berger, S. *J. Phys. Chem. B* **2013**, *117*, 5788.
- (88) Song, J.; Wang, H.; Li, M. *J. Mol. Struct.* **2015**, *1079*, 250.
- (89) Le Feunteun, S.; Ouethrani, M.; Mariette, F. *Food Hydrocoll.* **2012**, *27*, 456.
- (90) Yemloul, M.; Steiner, E.; Robert, A.; Bouguet-Bonnet, S.; Allix, F.; Jamart-Grégoire, B.; Canet, D. *J. Phys. Chem. B* **2011**, *115*, 2511.
- (91) Zhao, Q.; Brenner, T.; Matsukawa, S. *Carbohydr. Polym.* **2013**, *95*, 458.
- (92) García-Aparicio, C.; Quijada-Garrido, I.; Garrido, L. *J. Colloid Interface Sci.* **2012**, *368*, 14.
- (93) De, T. K.; Maitra, A. *Adv. Colloid Interface Sci.* **1995**, *59*, 95.
- (94) Rička, J.; Borkovec, M.; Hofmeier, U. *J. Chem. Phys.* **1991**, *94*, 8503.
- (95) Zulauf, M.; Eicke, H.-F. *J. Phys. Chem.* **1979**, *83*, 480.
- (96) Goffredi, M.; Liveri, V. T.; Vassallo, G. *J. Solution Chem.* **1993**, *22*, 941.

- (97) Pádua, A. A. H.; Fareleira, J. M. N. A.; Calado, J. C. G.; Wakeham, W. A. *J. Chem. Eng. Data* **1996**, *41*, 1488.
- (98) Frank, S. G.; Zografi, G. *J. Colloid Interface Sci.* **1968**, *28*, 66.
- (99) Laia, C.; López-Cornejo, P.; Costa, S. *Langmuir* **1998**, *7463*, 3531.
- (100) Bohidar, H. B.; Behboudnia, M. *Colloids Surf., A* **2001**, *178*, 313.
- (101) Geiger, S.; Eicke, H.-F. *J. Colloid Interface Sci.* **1986**, *110*, 181.
- (102) Stejskal, E. O.; Tanner, J. E. *J. Chem. Phys.* **1965**, *42*, 288.
- (103) Wu, D. H.; Chen, A. D.; Johnson, C. S. *J. Magn. Reson. Ser. A* **1995**, *115*, 260.
- (104) Jerschow, A.; Müller, N. *J. Magn. Reson.* **1997**, *125*, 372.
- (105) Frank, S. G.; Zografi, G. *J. Colloid Interface Sci.* **1969**, *29*, 27.
- (106) Hasegawa, M.; Sugimura, T.; Suzaki, Y.; Shindo, Y.; Kitahara, A. *J. Phys. Chem.* **1994**, *98*, 2120.
- (107) Rafiq, S.; Yadav, R.; Sen, P. *J. Phys. Chem. B* **2010**, *114*, 13988.
- (108) Faeder, J.; Ladanyi, B. M. *J. Phys. Chem. B* **2000**, *104*, 1033.
- (109) Cabrita, E. J.; Berger, S.; Bräuer, P.; Kärger, J. *J. Magn. Reson.* **2002**, *157*, 124.
- (110) Buch, V.; Devlin, J. P. *Water in Confining Geometries*; Springer Verlag, 2003.
- (111) Hauser, H.; Haering, G.; Pande, A.; Luisi, P. L. *J. Phys. Chem.* **1989**, *93*, 7869.
- (112) Carper, W. R.; Keller, C. E. *J. Phys. Chem. A* **1997**, *101*, 3246.
- (113) Riter, R. E.; Willard, D. M.; Levinger, N. E. *J. Phys. Chem. B* **1998**, *5647*, 2705.
- (114) Balasubramanian, S.; Bagchi, B. *J. Phys. Chem. B* **2002**, *106*, 3668.
- (115) Piletic, I. R.; Moilanen, D. E.; Spry, D. B.; Levinger, N. E.; Fayer, M. D. *J. Phys. Chem. A* **2006**, *110*, 4985.
- (116) Moilanen, D. E.; Fenn, E. E.; Wong, D.; Fayer, M. D. *J. Phys. Chem. B* **2009**, *113*, 8560.
- (117) Martinez, A. V.; Dominguez, L.; Małolepsza, E.; Moser, A.; Ziegler, Z.; Straub, J. E. *J. Phys. Chem. B* **2013**, *117*, 7345.
- (118) Desando, M. A.; Lahajnar, G.; Sepe, A. *J. Colloid Interface Sci.* **2010**, *345*, 338.
- (119) Silber, J.; Biasutti, A.; Abuin, E.; Lissi, E. *Adv. Colloid Interface Sci.* **1999**, *82*, 189.
- (120) Greenspoon, N.; Wachtel, E. *J. Am. Chem. Soc.* **1991**, *113*, 7233.
- (121) Balayssac, S.; Delsuc, M.-A.; Gilard, V.; Prigent, Y.; Malet-Martino, M. *J. Magn. Reson.* **2009**, *196*, 78.

- (122) Sandoval, T. E.; Espinoza, L. J.; Guerra, I. A.; Olea, A. F.; Gárate, M. P. *Colloids Surf., A* **2012**, *398*, 17.
- (123) Harrison, K.; Goveas, J.; Johnston, K. P.; O'Rear III, E. A. *Langmuir* **1994**, *10*, 3536.
- (124) Giddings, L. D.; Olesik, S. V. *Langmuir* **1994**, *10*, 2877.
- (125) Li, W.; Yang, Y.; Luo, T.; Zhang, J.; Han, B. *Phys. Chem. Chem. Phys.* **2014**, *16*, 3640.
- (126) Ihara, T.; Suzuki, N.; Maeda, T.; Sagara, K.; Hobo, T. *Chem. Pharm. Bull.* **1995**, *43*, 626.
- (127) Stuart, M. C. A.; Van De Pas, J. C.; Engberts, J. B. F. N. *J. Phys. Org. Chem.* **2005**, *18*, 929.
- (128) Datta, A.; Mandal, D.; Pal, S. K.; Bhattacharyya, K. *J. Phys. Chem. B* **1997**, *101*, 10221.
- (129) Kurniasih, I. N.; Liang, H.; Mohr, P. C.; Khot, G.; Rabe, J. P.; Mohr, A. *Langmuir* **2015**, *31*, 2639.
- (130) Zhai, L.; Zhang, J.; Shi, Q.; Chen, W.; Zhao, M. *J. Colloid Interface Sci.* **2005**, *284*, 698.
- (131) García Sánchez, F.; Carnero Ruiz, C. *J. Lumin.* **1996**, *69*, 179.
- (132) Zhou, Y.; An, X.; Shen, W.; Zhang, Y. *Chinese Sci. Bull.* **2006**, *51*, 1138.
- (133) Peng, D.-Y.; Robinson, D. B. *Ind. Eng. Chem. Fundam.* **1976**, *15*, 59.
- (134) NIST Standard Reference Database 69: NIST Chemistry WebBook, last seen on 5/10/2015.
- (135) Suzuki, K.; Sue, H.; Itou, M.; Smith, R. L.; Inomata, H.; Arai, K.; Saito, S. *J. Chem. Eng. Data* **1990**, *35*, 63.
- (136) Shaka, A.; Freeman, R. In *Advanced Magnetic Resonance Techniques in Systems of High Molecular Complexity*; 1986.
- (137) Kozminski, W. *Pol. J. Chem.* **2000**, *74*, 1185.
- (138) Castañar, L.; Nolis, P.; Virgili, A.; Parella, T. *Chem. Eur. J.* **2013**, *19*, 15472.
- (139) Lauterbur, P. C.; Kramer, D. M.; House, W. V.; Chen, C. N. *J. Am. Chem. Soc.* **1975**, *97*, 6866.
- (140) Parella, T. *Magn. Reson. Chem.* **1998**, *36*, 467.
- (141) Freeman, R. *Prog. Nucl. Magn. Reson. Spectrosc.* **1998**, *32*, 59.
- (142) Allen, J.; Damodaran, K. *Magn. Reson. Chem.* **2015**, *53*, 200.
- (143) Xu, B.; Nagashima, K.; DeSimone, J. M.; Johnson, C. S. *J. Phys. Chem. A* **2003**, *107*, 1.
- (144) Park, K. D.; Lee, Y. J. *Magn. Reson. Chem.* **2006**, *44*, 887.
- (145) Dawar, P.; Raju, M. B.; Ramakrishna, R. A. *Synth. Commun.* **2014**, *44*, 836.
- (146) Stott, K.; Stonehouse, J.; Keeler, J.; Hwang, T.-L.; Shaka, A. *J. Am. Chem. Soc.* **1995**, *117* (10), 4199.
- (147) Nilsson, M. *J. Magn. Reson.* **2009**, *200*, 296.

- (148) Hoffmann, M. M.; Sobstyl, H. S.; Seedhouse, S. J. *Magn. Reson. Chem.* **2008**, *46*, 660.
- (149) Hoffmann, M. M.; Sobstyl, H. S.; Badali, V. A. *Magn. Reson. Chem.* **2009**, *47*, 593.
- (150) Yu, T.; Weiss, R. G. *Green Chem.* **2012**, *14*, 209.
- (151) Terech, P.; Weiss, R. G. *Chem. Rev.* **1997**, *97*, 3133.
- (152) Poolman, J. M.; Boekhoven, J.; Besselink, A.; Olive, A. G. L.; van Esch, J. H.; Eelkema, R. *Nat. Protoc.* **2014**, *9*, 977.
- (153) Mallia, V. A.; Terech, P.; Weiss, R. G. *J. Phys. Chem. B* **2011**, *115*, 12401.
- (154) Pelta, M. D.; Morris, G. A.; Stchedroff, M. J.; Hammond, S. J. *Magn. Reson. Chem.* **2002**, *40*, S147.